MULTI-TONE REPRESENTATION OF ARBITRARY WAVEFORMS AND APPLICATION TO THE ANALYSIS OF NONLINEAR AMPLIFIERS AND FEEDFORWARD LINEARIZERS

A THESIS SUBMITTED TO
THE GRADUATE SCHOOL OF NATURAL AND APPLIED SCIENCES
OF
MIDDLE EAST TECHNICAL UNIVERSITY

BY

AHMET MUTLU

IN PARTIAL FULFILLMENT OF THE REQUIREMENTS
FOR
THE DEGREE OF MASTER OF SCIENCE
IN
ELECTRICAL AND ELECTRONICS ENGINEERING

AUGUST 2005

Approval of the Graduate School of Natural and Applied Sciences

Prof. Dr. Canan Özgen
Director

I certify that this thesis satisfies all the requirements as a thesis for the degree of Master of Science.

Prof. Dr. İsmet Erkmen
Head of Department

This is to certify that we have read this thesis and that in our opinion it is fully adequate, in scope of quality, as a thesis for the degree of Master of Science.

Assoc. Prof. Dr. Simsek Demir
Supervisor

Examining Committee Members

Prof. Dr. Canan Toker (chair) (METU, EEE) _____

Assoc. Prof. Dr. Simsek Demir (METU, EEE) _____

Prof. Dr. Yalçın Tanık (METU, EEE) _____

Assoc. Prof. Dr. Sencer Koç (METU, EEE) _____

Dr. Arslan Hakan Coşkun (ASELSAN) _____

I hereby declare that all information in this document has been obtained and presented in accordance with academic rules and ethical conduct. I also declare that, as required by these rules and conduct, I have fully cited and referenced all materials and results that are not original to this work.

Name, Last Name:

Signature:

ABSTRACT

MULTI-TONE REPRESENTATION OF ARBITRARY WAVEFORMS AND APPLICATION TO THE ANALYSIS OF NONLINEAR AMPLIFIERS AND FEEDFORWARD LINEARIZERS

Mutlu, Ahmet
M.Sc., Department of Electrical and Electronics Engineering
Supervisor: Assoc. Prof. Dr. Şimşek Demir

August 2005, 127 pages

Characterization of nonlinear systems is a challenging task as the output can not be expressed simply in terms of input signal. Therefore, a universal analysis method is essential to simplify this procedure. Modeling of the input signal is a crucial part of such analysis. In this thesis, multi-tone representation is employed to model arbitrary, stochastically not well-defined input signals and thereafter characterize nonlinear systems. In order to verify the validity of multi-tone representation, multi-tone modeling concept is primarily applied to real life amplifier characterization in single amplifier configuration. This experiment demonstrated potential of multi-tone modeling concept in nonlinear system characterization and encouraged application of the concept to analysis of feedforward linearizers, which are complicated systems due to the presence of two nonlinear amplifiers and the requirement of strict amplitude, phase and delay matching within two loops of the circuit. It has been assumed that main and error amplifiers can be modeled with third order AM/AM nonlinearities and there exists

no delay mismatch within the loops. Hence, closed form expressions relating the main and adjacent channel power at the output of the feedforward system to the system parameters are obtained. The developed model is verified by RF and system simulations. As a result, a mathematical handy tool to specify circuit parameters rapidly for optimum linearity performance and efficiency is achieved.

Keywords: Modeling, Multi-tone representation, Feedforward, Linearization.

ÖZ

RASTGELE SİNYALLERİN ÇOK-TONLU GÖSTERİMİ VE DOĞRUSAL OLMAYAN GÜÇ YÜKSELTEÇLERİNE VE İLERİBESLEME DOĞRUSALLAŞTIRICILARINA UYGULAMASI

Mutlu, Ahmet
Yüksek Lisans, Elektrik ve Elektronik Mühendisliği Bölümü
Tez Yöneticisi: Doç. Dr. Şimşek Demir

Ağustos 2005, 127 sayfa

Doğrusal olmayan sistemlerin karakterizasyonu sistem çıkışının doğrudan girişteki işaretin cinsinden ifade edilememesi nedeniyle zorlu bir iştir. Bu nedenle, bu prosedürü kolaylaştıracak genel bir analiz yöntemi gereklidir. Bu gibi analizlerde, giriş işaretinin modellenmesi analizin çok önemli bir parçasıdır. Bu tezde, çok-tonlu gösterim rastgele, stokastik olarak tanımlı olmayan işaretlerin modellenmesi ve daha sonra doğrusal olmayan sistemlerin karakterizasyonu için kullanıldı. Çok-tonlu gösterimin geçerliliğini kanıtlamak için, çok-tonlu modelleme kavramı öncelikle tek kademeli gerçek bir güç yükseltecin karakterizasyonu için kullanıldı. Bu deney, çok-tonlu modelleme kavramının doğrusal olmayan sistemlerin karakterizasyonu alanındaki potansiyelini gösterdi ve bu kavramın, doğrusal olmayan iki güç yükseltecin varlığı ve iki ayrı döngü içinde genlik, faz ve gecikme uyumunun gerekliliği yüzünden karmaşık bir sistem olan ileribesleme doğrusallaştırıcılarına uygulanmasına cesaretlendirdi. Asıl ve hata yükselteçlerinin üçüncü dereceden genlik bozukluğu ile modellenebildiği ve

döngüler içinde gecikme uyumsuzluklarının olmadığı varsayılmıştır. Böylelikle, ileribesleme sisteminin çıkışındaki ana ve yan kanal güç seviyelerini sistem parametrelerine bağlayan kapalı ifadeler elde edilmiştir. Geliştirilen model Radyo Frekansı (RF) ve sistem simülasyonları ile doğrulanmıştır. Sonuç olarak, en uygun doğrusallaştırma performansı ve verimlilik için devre parametrelerini hızlı bir şekilde belirlemeye yönelik kullanışlı bir matematiksel araç elde edilmiştir.

Anahtar kelimeler: Modelleme, Çok-tonlu gösterim, İleribesleme, Doğrusallaştırma

To my parents

ACKNOWLEDGMENTS

I would like to express my sincere gratitude to my thesis advisor Assoc. Prof. Dr. Simsek Demir for his guidance, support and encouragement throughout the study of this thesis. It was a privilege for me to have an outstanding research experience under his supervision.

It is a distinction for me to acknowledge Dr. Hakan Coskun for sharing his experience and technical facilities with me, lighting the way for the concept of this research and his invaluable suggestions and contributions.

I am grateful to ASELSAN Electronics Industries for not only giving me the opportunity to improve my engineering capabilities but also providing me every kind of software, hardware and financial support throughout the progress of this work. It is also my pleasure to express my appreciation to my colleagues who always supported me spiritually and provided me a nice, friendly office atmosphere.

Finally, I would like to deeply appreciate my parents, my sister and Derya Kaya for their endless love, support, encouragement and patience. This thesis would have been impossible without their guidance.

TABLE OF CONTENTS

LIST OF FIGURES

FIGURES

LIST OF TABLES

TABLES

CHAPTER 1

INTRODUCTION

Emerging communication systems employ high order modulation schemes due to increasing importance of spectral efficiency, i.e., the ability to transmit data at the highest possible rate for a given channel bandwidth. In order to increase data rate without affecting the other bits of information, however, frequency filtering is applied to the baseband signal using raised cosine shaped low-pass filters. Typical 2G wireless systems such as Global System for Mobile Communications (GSM) use constant envelope modulation with only the phase of the signal varying with time and were intended to make power amplifier design simpler. 2,5G and 3G wireless systems, however, adopted more complex modulation schemes in order to respond to the growing need for spectral efficiency. As a result of filtering and utilization of high order and multi-carrier modulation schemes like QAM, QPSK and OFDM, RF signals with relatively high peak-to-average ratios evolved. In addition, wireless technology trends claim light, tiny and multi-task devices. As a result, linearity and efficiency of radio frequency power amplifiers became a crucial design issue.

Linear power amplifiers are designed to amplify single/multi-carrier, analog/digital and constant/non-constant envelope signals without adding a significant distortion to the output signal. Linear amplifiers are thus expected to be effectively transparent to the modulation scheme and number of carriers, i.e. they can handle the universality requirement for Universal Mobile Telecommunication Systems (UMTS). A common design conflict is that while spectral efficiency demands a highly linear power amplifier, power efficiency is

maximized when a power amplifier is run as a constant envelope nonlinear element. Therefore, there is a trade off between linearity and efficiency.

Linearity objective can be simply accomplished by “backing off” PA such that it operates away from compression point. So-called Class-A amplifiers have good distortion performance but suffer from low efficiency. Furthermore, because of deep back-off, Class-A amplification is limited in terms of output power capability. This problem can be solved by paralleling the output transistors, but this solution contradicts the constraints of the modern communication systems, which prefer light, tiny and cheap handsets. The current state-of-art, therefore, is to design a linear power amplifier which operates as close to saturation as possible in order to maximize its power efficiency. To achieve this goal various linearization techniques like Feed-forward, Envelope Elimination and Restoration (EER), Predistortion and Linearization with Nonlinear Components (LINC) are employed [1-3]. Among these methods, feedforward linearization is distinctive in terms of linearization and bandwidth. However, analysis of feedforward systems is difficult due to their relatively complex structures. Therefore, it is essential to have analytical tools to predict the final regime of such a complex system. This will allow a designer to optimize system parameters for good linearity and efficiency without much effort.

In this thesis, multi-tone modeling is employed to predict the final performance of a nonlinear system in response to an arbitrary excitation. However, the output of a nonlinear system in response to an arbitrary excitation cannot be given simply as the sum of elementary outputs as in the case of linear systems. The practical consequence of this statement is that the closer the characteristics of the test signal are to those of the excitation expected in practice the closer the prediction of the system’s response to this excitation is. Multi-tone signals, which are easy to create and handle, are employed as test signals. In literature, multi-tone modeling has been investigated and figures of nonlinearity have been calculated for a system excited with multi-tone signals [4-6]. Adjacent Channel Power Ratio (ACPR) measurements of a nonlinear system excited with various multi-tone signals and pseudorandom digital modulation have been compared in [4] and the affect of changing magnitude and phase of multi-tone

signals has been investigated. In [5], phase and magnitude of multi-tone signals are modified to represent ACPR of digitally modulated QPSK signal. The number of tones in a multi-tone signal is varied from 3 to 65 and ACPR simulation results for digitally modulated signal and its multi-tone models are compared. Selection procedure of multi-tone signals is not mentioned. In [6], the order of system nonlinearity has been extended to include fifth order distortion products and figures of merit of nonlinear distortion have been calculated for in-phase or random phase multi-tone excitation. In [7], Coskun proposed multi-tone representation of arbitrary signals with equally spaced, in-phase tones with variable amplitude and applied this representation to analyze delay and phase matched feedforward system. In this thesis, expressions for delay and phase matched feedforward system are extended to include phase mismatches. Parameter selection criteria are defined to select proper multi-tone model. Moreover, the validity of multi-tone concept is verified by applying arbitrary signals and their multi-tone models to real life amplifiers.

The performance of the multi-tone modeling is evaluated by comparing the system's response for multi-tone signals to response for arbitrary real/complex enveloped signals. Real/complex enveloped signals are chosen arbitrary because of the fact that practical systems, in general, are intended to handle information signals, which, by definition are unpredictable. The multi-tone modeling idea is first applied to real amplifiers in single amplifier configuration. Then, the multi-tone modeling is used to analyze the feedforward system in simulation environment using real amplifier SPICE models and system amplifiers.

In Chapter 2, first, the concept of linearity and linearization is going to be discussed, and then popular linearization techniques will be mentioned with emphasis on feedforward and predistortion. In Chapter 3, multi-tone modeling concept will be introduced. Then, this concept will be applied to real life amplifiers in single amplifier configuration. The details of the measurement setup, the properties of the input stimuli and the selection criteria used to select the multi-tone models are also explained in this chapter. In Chapter 4, multi-tone concept is employed to analyze the feedforward system and predict the final

performance of the system in response to an arbitrary input signal. The validity of the model is inspected by comparing the response of the system for the multi-tone signals to the response for various real/complex enveloped arbitrary signals. In Chapter 5, we are going to conclude the results that have been obtained.

CHAPTER 2

LINEARITY AND LINEARIZATION

2.1 Linearity Concept

A perfectly linear power amplifier can be characterized by a constant gain and linear phase over the bandwidth of the input signal. The input-output relationship of such a theoretical amplifier can be expressed as follows:

$$V_{out} = G.V_{in} \tag{2.1}$$

where G is the gain of the amplifier. In practice, however, amplifiers have amplitude dependent gain, nonlinear phase and memory. Hence, the equation (2.1) is modified such that it includes also nonlinearity terms, i.e. the terms that cause the output to deviate from ideal response [1]:

$$V_{out} = G_1 V_{in} + G_2 V_{in}^2 + ... + G_n V_{in}^n \tag{2.2}$$

where G_i are complex. The first term represents linear amplification and higher order terms model nonlinearities in a real life amplifier. If we excite such an amplifier with a single sinusoid the output is composed of boosted replica of input signal and some extra terms at the multiples of the main frequency, harmonics, which can be practically eliminated with a simple low pass filter. However, if the input signal is composed of multiple sinusoids or is a band-limited continuous signal the nonlinearities in the output signal are not only the harmonics but also the side products nearby the fundamental tones or spectral regrowth at the sidebands

around the main bandwidth, respectively. These nonlinearities, which are known as intermodulation distortion (IMD), cannot be eliminated by filtering since they are at the vicinity of the fundamental signal.

IMD is one of the major measures of linearity for a power amplifier and its level depends on transistor technology, input and output matching, bias conditions and input signal level [1, 2, 8]. Figure 2.1 illustrates intermodulation distortion for a third order nonlinear system and it is clear from the figure the expression "intermodulation" comes from the fact that unwanted products occur at $nf_1 \pm mf_2$ where n and m are integers and $n \neq m$. As the input power of the amplifier is increased, IMD increases except at around some point known as "sweet spot" [9], where IMD curve presents an unexpected minimum. In real life systems, two tone IMD is traditionally related to adjacent channel power ratio (ACPR), which is the inband distortion for modulated signals. However, recent studies indicate that relating ACPR to two-tone IMD is, in general, difficult without including somehow the envelope distribution statistics which vastly vary for different modulation schemes [10].

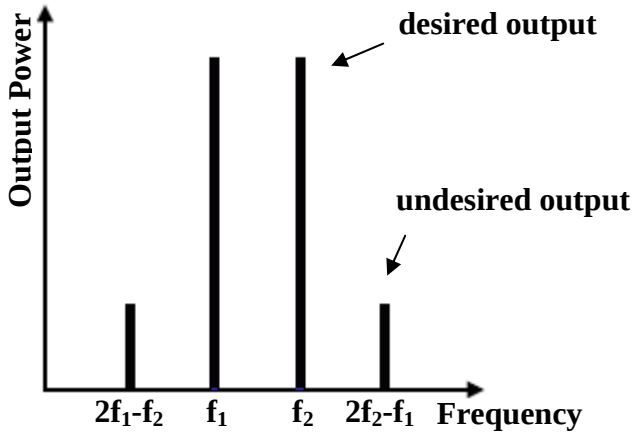

Figure 2.1: Two-tone test creates undesired intermodulation products besides the fundamental tones at the output of a nonlinear device. The figure illustrates this phenomenon for a third order nonlinearity case.

Another commonly used measure of linearity is intercept point, especially third order intercept point (IP3), which is in fact a theoretical point where intermodulation products in question have the same peak power with the fundamental signal. Figure 2.2 illustrates this definition for different orders of

nonlinearity. As the input power is increased IMD increases and finally saturates emphasizing the theoretical nature of intercept point. Sweet spots are also indicated on the same figure.

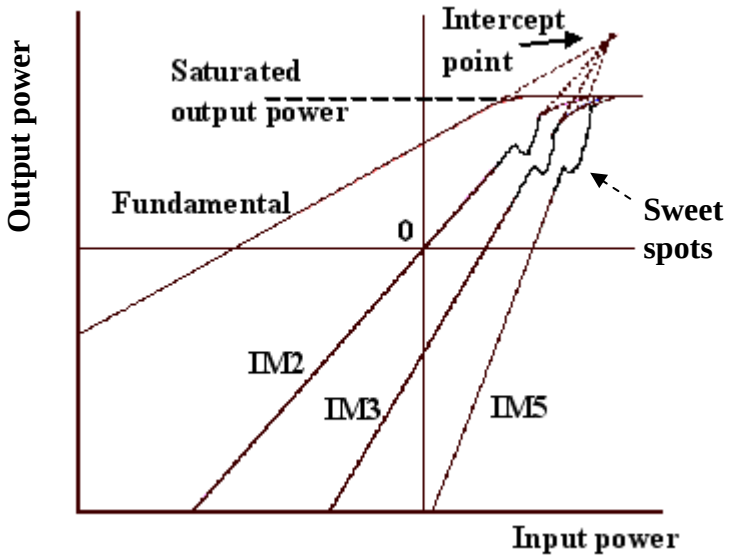

Figure 2.2: Input-output plot of an amplifier illustrates the behavior of linear and nonlinear terms in logarithmic scale at the output of an amplifier. Intercept point (IP) is indicated on figure.

An alternative way of looking at the input-output characteristic of a power amplifier is to treat amplitude and phase distortions separately [1]. This approach results in two separate characteristics with respect to input power, namely AM-AM and AM-PM. AM-AM characteristic relates the output power to the input power and is closely related to IMD. Figure 2.3 illustrates a typical AM-AM plot. Linear region indicates the input power levels where the amplifier exhibits weak nonlinearities, whereas in the nonlinear region the amplifier gain begins to drop and finally amplifier enters compression as the input power is increased. The point where the gain drops 1 dB with respect to the gain at linear region is defined as 1 dB compression point and used interchangeably with IP3 as a measure of nonlinearity. AM-PM characteristic represents the phase variation of the amplifier with respect to input power. Ideally the phase of an amplifier is independent of input power. In practice, however, phase shift introduced by the amplifier can be a function of input power. Thus, any change in input power will modulate phase

causing unwanted phase modulation. AM-PM distortion also causes asymmetry between upperband and lowerband IMD [2].

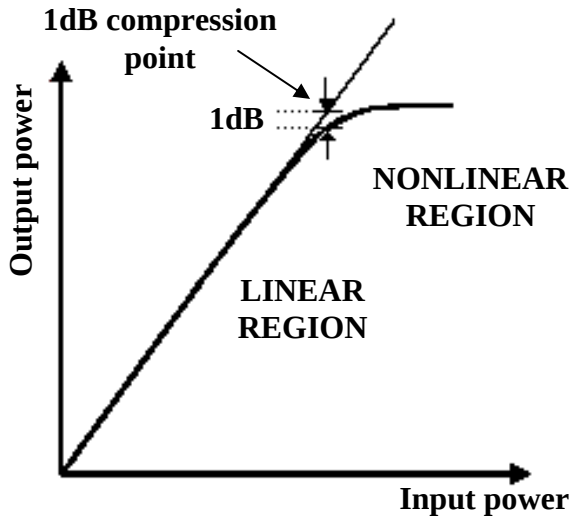

Figure 2.3: AM-AM characteristics of an amplifier. 1 dB compression point is also indicated and used as a figure of merit for linearity.

Another effect that causes IMD asymmetry besides AM-PM conversion is a phenomenon known as memory effect. Memory effect can be defined as combination of bandwidth dependent nonlinear effects. In an amplifier with memory effect, the amplitude and phase of the distortion components (IMD) vary as functions of the modulation frequency or the tone spacing in a two tone signal, and amplitude. Memory effects are of two types; electrical memory effects and thermal memory effects [11, 12]. Electrical memory effects are caused by frequency dependent impedances of signal envelope, fundamental or second harmonic and these affect high modulation frequencies as illustrated in Figure 2.4. Thermal effects though are caused by changes of amplifier characteristics with varying temperature and heat dissipation. These types of memory effects take place at low modulation frequencies up to the megahertz range.

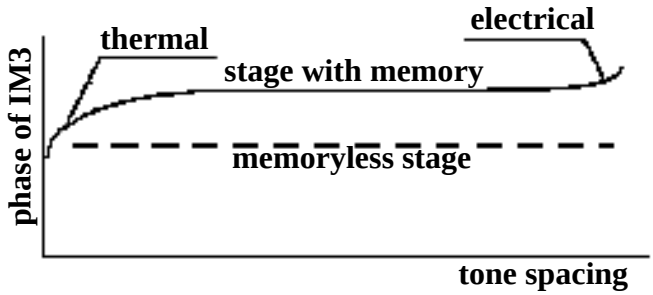

Figure 2.4: Phase of third order intermodulation with changing tone spacing is illustrated. Thermal and electrical memory effects occur at different frequency spacing regions. The case for memoryless amplifier is also included for comparison.

2.2 Types of modulated signals

Modern communication systems use complex modulation schemes for bandwidth efficiency thereby requiring linear amplification. In general, modulation schemes may be classified in two categories in terms of linearity: constant envelope modulation schemes and nonconstant envelope modulation schemes, the latter also known as *linear modulation*. Constant envelope schemes include only phase or frequency variation and do not need linear amplification. Frequency modulation (FM), phase shift keying (PSK), frequency shift keying (FSK) and gaussian minimum shift keying (GMSK) are widely used constant envelope signals.

Linear modulation schemes can be divided into two groups: modulation schemes which modulate only one parameter of a carrier wave and modulation schemes which modulate amplitude and phase together. Amplitude modulation (AM) and M-ary phase shift keying (M-PSK) belong to the first group and M-ary quadrature amplitude modulation (M-QAM) belongs to the latter.

Table 2.1 shows the popular modulation techniques and the respective communication systems employing these techniques. First generation (1G) systems like AMPS employed FSK thereby allowing nonlinear amplification. Similarly, second generation (2G) systems like GSM adopted GMSK. On the other hand, EDGE, which is an enhanced version of GSM used a more spectrally efficient but linear modulation scheme, namely 8-PSK. Third order (3G) systems also employed

QPSK and OQPSK which are linear modulation schemes and require linear amplification.

Table 2.1: Modulation schemes adopted by popular wireless communication standards are tabulated.

Evolution		Standard	Modulation
1G		AMPS	FSK
2G	GSM	GSM	GMSK
		GPRS	GMSK
2.5G		EDGE	8-PSK
3G	UMTS	WCDMA	Q-PSK
	CDMA One	IS-95A	Q-PSK
		IS-95B	Q-PSK
	CDMA 2000	1X	Q-PSK
		1X-EV	Q-PSK
		1X-EVDO	Q-PSK

2.3 Linearization and linearization techniques

Developed second generation and third generation systems allow both speech and data communication. Hence, they are expected to support much higher data rates compared to the first generation and the traditional second generation systems which allow only speech exchange. Furthermore, the merit of spectral efficiency is rapidly growing triggering usage of more complex modulation schemes which contain both amplitude and phase variations. As a result, high linearity amplification and transparency to the modulation scheme and number of carriers became stringency for modern communication systems.

Linear power amplification can be simply achieved by using traditional linear amplifiers, namely Class A or sometimes Class AB amplifiers. The required linearity is obtained by “backing off” the power amplifier. The amplifier is designed such that it can handle peak power of a signal with a very high peak-to-average ratio without distorting the signal. For instance a signal with 6 dB peak-to-average

ratio needs a 400 W linear power amplifier design to produce 100 W average output power. Consequently, either very high power transistor will be used if available or amplification will be achieved by paralleling two or more amplifiers. Both solutions are costly, require very high power transistors, suffer from poor efficiency and need bulky heatsinks. The only way to improve efficiency without trading off linearity much is to employ today very popular techniques of power amplifier linearization.

Linearization is a systematic procedure for reducing a power efficient amplifier's distortion using external circuitry. Linearization allows an amplifier to produce more output power and operate at a higher level of efficiency for a given level of distortion. The theory, principles and techniques of linearization have been evolving since the early days of wireless transmitters. Techniques include feed-forward, predistortion, direct and indirect feedback techniques, envelope elimination and restoration (EER), polar loop, Cartesian loop, and other cancellation methods. System and circuit features that have to be considered include dynamic/static, adaptive/non-adaptive and baseband/RF linearization techniques. In general, there is no 'best' linearization technique. The method used to linearize a power amplifier should be chosen taking into account frequency, modulation method and bandwidth. Contemporary focus of linearization research is on the first two techniques – predistortion and feed-forward - as holding promise for successful adaptation to upcoming advanced wireless communication systems.

2.3.1 Feedforward Linearization

Feedforward linearization technique is the most promising technique which can handle modern wideband multicarrier systems. It is one of the most active technical research topics in recent years. Figure 2.5 illustrates the simplest feedforward system with only essential building blocks included. The system consists of a main amplifier which is inherently nonlinear and an error amplifier which should be highly linear; two phase/delay units which compensate the delay and phase introduced by amplifiers; and four directional couplers which are used to

split (coupler C_1), sample (coupler C_2), subtract (coupler C_3) and combine (coupler C_4) signals at different phases of feedforward linearization process. A two tone signal is employed in order to explain the process and illustrated in Figure 2.5. The two tone undistorted input signal is first split into two paths by a power splitter which is usually a directional coupler (coupler C_1). One of the paths goes to the main amplifier and the other goes to a phase/delay element, which is used to compensate for the main amplifier delay and phase. Main amplifier boosts the two tone signal adding distortion to the output spectra. This distorted signal is sampled by a directional coupler (coupler C_2) and then the sample is compared to the delayed signal coming from the second branch using another coupler (coupler C_3) as a subtractor. The result of this subtraction is a spectrum with only distortion products available and this distortion signal is fed to the error amplifier. Error amplifier is a highly linear gain stage where this distortion signal is boosted without creating extra distortion. Finally the signal at the output of the main amplifier, which is time delayed, is compared and combined at the final coupler stage (coupler C_4), which is used both as a combiner and a subtractor. Finally, the signal at the output of the feedforward linearizer is obtained, which is boosted version of the input signal with ideally no distortion. The first loop of the feedforward system is known as carrier cancellation loop, whereas the second loop is named as error cancellation loop.

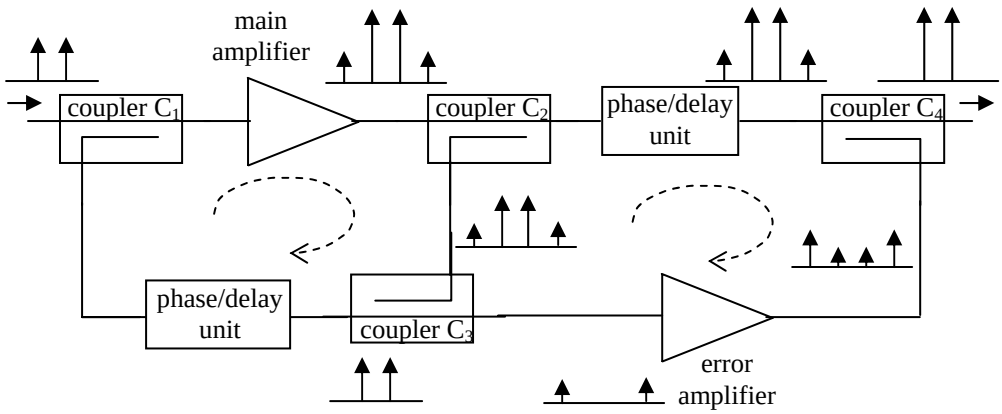

Figure 2.5: A generic feedforward system with its essential building blocks is illustrated. Two tone spectra is employed to demonstrate the principles of feedforward technique.

Feedforward technique is a very popular research topic because of its promising advantages over other linearization techniques. Feedforward systems do not include a feedback system and are ideally unconditionally stable. Moreover, linearity achieved by feedforward systems is rather demanding encouraging research and development of new methods to solve problems encountered in feedforward linearizers. Weaknesses of feedforward system are its poor efficiency, very strict amplitude and phase matching requirement and drift of component characteristics with changing environmental conditions.

Power efficiency of overall feedforward system is a great challenge. There are mainly three components expected to affect the overall power efficiency: main amplifier, error amplifier and main path loss. Main amplifier efficiency is dominant on overall efficiency as expected. Therefore, in practice main amplifier is usually designed as a highly efficient but nonlinear, class-C, amplifier. The error amplifier efficiency is also expected to lessen the overall efficiency because of high linearity requirement. However, the results [3] contradict the expectation, showing that the effect of error amplifier efficiency – provided that its efficiency is not excessively low – is very slight. Therefore, when deciding on the error amplifier the selection criteria are limited to its linearity, gain and phase flatness with frequency, temperature and aging. Main path loss is another effect that lessens the overall efficiency. The loss of couplers used on the main path and especially the loss of the phase/delay element should be considered. Results show that 1 dB additional loss on the main path results in more than 15% degradation in the overall efficiency [3]. Therefore the loss of the main path should be kept at minimum.

The problem of efficiency has been vastly examined and techniques proposed to increase overall efficiency of feedforward linearizers. Main amplifier selection is examined comparing usage of class-C and class-A amplifiers and efficiency improvement with proper selection of output coupler coupling value is illustrated in [13]. Moreover, a linearizer combining predistortion and feedforward techniques in order to increase overall efficiency is proposed [3, 14-16]. This hybrid technique improves efficiency by enhancing linearity of the main amplifier. Also, some original studies employing usage of a series diode linearizer [17] and class-F Doherty amplifier [18] which improve main amplifier linearity are reported. The

affect of loss of main path delay line on overall feedforward system has been investigated in [19]. In [20], a novel method is proposed which uses DSP for the first loop of a feedforward system and removes delay line to improve efficiency.

Another issue in feedforward systems is the strict requirement imposed by the distortion cancellation mechanism; the amplitude and phase matching between the circuit elements must be maintained to a very high degree over the bandwidth of interest. However, the lack of intrinsic feedback path prevents feedforward systems from monitoring its own performance. Hence, it is not that easy to correct for gain or phase changes due to temperature or aging effects. It has been reported that to achieve 25 dB of cancellation, an amplitude error of less than 0.5 dB and a phase error of less than 5˚ would be needed [3]. In order to design a correction circuitry the performance of the feedforward system must somehow be monitored and the parameters of amplifiers and other component adaptively changed. This method has recently gained much interest and most articles concerning feedforward linearization focus on adaptive linearization techniques. The adaptive amplitude and phase compensation circuitry is described in [21] as transparent, fast, broadband, modulation independent, cheap and low power consuming. In [22] a gradient driven adaptive feedforward linearizer with use of DSP is proposed, which uses vector modulators to adaptively change amplitude and phase of the signals in both branches of the linearizer. DSP overcomes inherent problem of mixer DC offsets in vector modulators. In wideband design, it is difficult to maintain good amplitude and phase balance over the entire range of frequencies. A new feedforward amplifier arrangement has been proposed which makes use of phase equalizers to compensate the phase nonlinearity of main and error amplifiers in wideband applications [23]. Another way of compensating amplitude and phase variations again uses adaptive algorithms however make use of a pilot carrier injected to the input of the main amplifier [3, 16, 24]. Pilot carrier vanishes at the output of the feedforward linearizer unless there is an amplitude and phase mismatch. By simply tracking the pilot carrier at the output of the linearizer, feedforward system can be monitored and adaptively normalized. DSP controlled adaptive feedforward amplifiers using pilot carrier and designed for wideband applications has also been reported [25, 26]. Finally, a novel technique of adjusting amplitude and phase for

optimal cancellation performance by monitoring both the amplitude and the phase at the output of the linearizer has been published recently [27]. This technique is applied at the prototyping stage of a real amplifier to decide on parameters of components used in feedforward system.

2.3.2 Predistortion techniques

Predistortion linearization technique involves the creation of a distortion characteristic which is complementary of the amplitude and phase distortion characteristic of the power amplifier. The predistortion linearizer is a cascade of a predistortion circuitry and a nonlinear amplifier as shown in Figure 2.6. Predistorter is designed to distort the signal such that the distortion is just the opposite of that of power amplifier. The result is a linear gain. The predistortion linearization techniques consist of RF/IF predistortion or Baseband predistortion. RF/IF predistorters operate at comparably high frequencies whereas baseband predistortion uses DSP to predistort baseband information before upconversion.

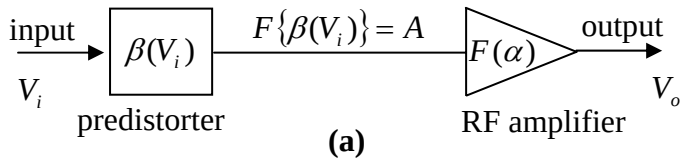

(a)

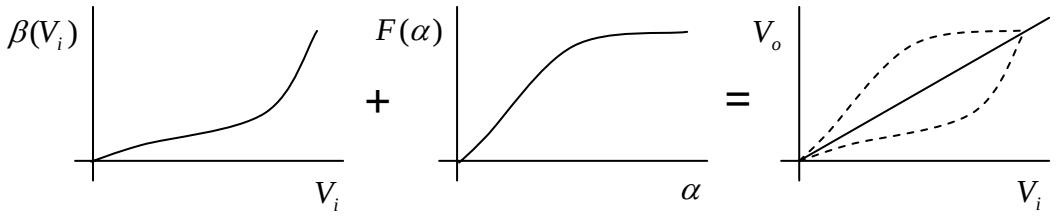

(b)

Figure 2.6: a) A basic predistortion system consists of a predistorter and an RF amplifier. **b)** The distortion characteristic of an ideal predistorter is illustrated. The result of combining predistorter and amplifier is a linear characteristic.

An RF/IF predistorter is placed before the amplifier in RF predistorter and before the upconversion mixer in IF predistorter. In practice, cubic predistortion is widely used instead of higher order predistortion linearization because improvements beyond third order are generally of little benefit [3]. The general form of amplitude characteristic of a power amplifier is compressive; hence a predistorter with expansive form is required to compensate amplifier nonlinearities. The necessary characteristic has been achieved using several techniques. The simplest form is to predistort using nonlinear components such as series diode which improves linearity very slightly but is simple to implement and cheap [3]. Diodes can also be used in anti-parallel diode configuration [3] which is also a simple and effective way of producing third order nonlinearity provided that circuit is input and output matched. Another simple predistorter formed by FET transistor uses the nonlinearity of source-drain channel [3, 28], which resembles the third order nonlinearity required by the predistorter. An alternative method uses piecewise curve-fit of the amplifier transfer characteristics [3, 29]. Implementation of curve-fit predistorters may be based either on attenuator or amplifier configurations. This is a very general form of predistorter because we can approximate any type of nonlinearity by employing enough number of parallel taps; however this technique is inherently very complex.

Predistortion techniques mentioned up to now take only amplitude distortion into consideration. However, phase distortion is also very effective on the distortion cancellation performance of a predistortion system especially when highly nonlinear amplifiers such as class-C are used as RF amplifiers. Techniques which employ two parallel paths and seperately design polynomials for both amplitude and phase characteristics of amplifiers have been reported [30-32]. Consequently, besides amplitude, phase characteristic is also linearized resulting in a better distortion performance.

Similar to the feedforward system, RF predistortion techniques suffer from gain and phase variations due to changing environmental conditions such as temperature. In addition, amplifier characteristics deviate from sample to sample. These facts degrade the performance of predistortion linearizers which already have modest performance compared to feedforward linearizers. To overcome this

difficulty, adaptive predistortion techniques which ensure that amplitude and phase matching can be maintained over the lifetime and operational temperature range of the amplifier have been developed [33-36]. These systems monitor the performance and use a look-up-table to change the predistorter charcteristic whenever the distortion cancellation performance lessens.

After development of digital signal processors (DSP) predistortion techniques adopted use of DSP for adaptively controlling the characteristic of the baseband signal. This technique known as adaptive baseband digital predistortion has become very popular recently. The predistortion linearizer is formed at the baseband and the monitoring of the output is realized by sampling, downconverting and finally converting from analog to digital. The feedback information is studied and if necessary adaptation procedure is initiated; the required amplitude and phase distortion parameters are found from look-up-table and this distortion characteristic is applied to the baseband signal [37-40]. Digital predistortion, however, has a serious drawback, digital-to-analog, analog-to-digital converters and DSP lowers overall power efficiency because of their power requirement which exceeds, in some cases, the power requirement of the power amplifier itself. Moreover, look-up-table must be carefully designed specifically for each modulation, otherwise the response time and size of the system may degrade, [41]. A novel technique of combining look-up-table and polinomial based predistortion to relax requirements of both techniques is proposed in [42].

2.3.3 Other linearization techniques

Feedforward and predistortion linearization are two popular ways of power amplifier linearization. They have their own advantages, requirements and disadvantages. In addition to these well studied techniques there are a majority of other linearization techniques which employ different structures to linearize a power amplifier. In the following discussion feedback oriented linearization techniques, RF synthesis and envelope elimination and restoration will be shortly described.

The Cartesian loop technique is first proposed in 1983 and designed for SSB transmission, but has since been applied to many other techniques such as feedforward. The operational principle is simple. The baseband signal is processed in Cartesian (I and Q) form. The modulation signal is split into quadrature components and fed into differential amplifiers which generate the error signals. The outputs of the differential amplifiers are upconverted to RF. The resultant RF signals are then combined and amplified by nonlinear power amplifier. Cartesian feedback has a serious drawback; it is restricted to narrowband applications compared to feedforward or predistortion [1, 3].

Polar loop feedback is another form of feedback techniques which uses polar representation of complex signal instead of Cartesian representation. The output of the transmitter is sampled and converted to IF. The resulting signal is resolved to polar representation. The rest of the operation is the same as the Cartesian loop transmitter. The technique includes both amplitude and phase characteristics and allows high efficiency class-C type amplifier utilization. As a result, polar loop architecture is gaining interest and some improvements to this technique are proposed [43, 44]. These arrangements allow utilization of DSP and reduce stability constraints in polar loop transmitters. Also, combination of polar loop and other linearization techniques is a promising area of interest [45].

Linear Amplification with Nonlinear Componets (LINC) was first proposed in 1974. The intention of technique is to create a complete linear amplifier with linear input-output relationship, where the intermediate stages of the system could employ highly nonlinear devices. The principle of operation relies on splitting RF signal into two phase modulated constant envelope signals and after amplifying them via nonlinear amplifiers separately recombine the outputs of separate amplifiers using an ideal combiner. The resulting signal is amplified but undistorted replica of the input signal. This technique is inherently suitable to be used at high microwave and millimeter-wave frequencies [3] and has a potential for very high efficiencies. Commercial designs has been newly reported which propose LINC transmitter architectures for software defined radio application [46]. Also, an adaptive architecture to solve the sensitivity problem of LINC transmitters to gain and phase imbalances between the two amplifier branches is proposed [47].

The Envelope Elimination and Restoration (EER) technique was first proposed in 1952. It was originally used at HF amplification of SSB signals. The principle of operation depends on splitting the modulated signal into two branches. In one of the branches, the signal is passed through a limiter to remove amplitude modulation thereby leaving a constant envelope phase modulated signal. This constant envelope signal is then amplified using a nonlinear power amplifier. Meanwhile, an envelope detector detects envelope variations of the input signal, hence creating an amplitude modulated signal in the second branch. Then, this signal is amplified by a highly linear amplifier and the resulting nonconstant signal is used to modulate the collector or power supply of the final RF power stage. As a result, the output signal consists of both amplitude and phase variations with minimum distortion [1, 3]. EER technique is potentially highly linear, efficient and simple to implement.

Table 2.2 tabulates main properties of all linearization systems and techniques mentioned in this chapter. The relative characteristics indicate that each technique has its own advantages and weaknesses. When making a decision on a specific technique, designer should primarily consider what the key requirement of his system is: complexity, efficiency, bandwidth or distortion cancellation performance. All techniques tabulated have found place in different application fields, sometimes in cooperation.

Table 2.2: All linearization techniques of interest are compared in terms of complexity, efficiency, bandwidth and distortion cancellation performance.

Techniques	Complexity	Efficiency	Bandwidth	Performance
Feedforward	High	Moderate	High	High
RF Predistortion	Low	High	Moderate	Moderate
Digital Predistortion	High	Moderate	Moderate	Moderate
Cartesian Feedback	Moderate	High	Narrow	High
Polar Loop	Moderate	High	Narrow	High
LINC	Moderate	High	Moderate	High
EER	Moderate	High	Moderate	High

CHAPTER 3

MULTI-TONE MODELING

Modern communication systems are demanding high data rates and spectral efficiency compelling the adoption of complex linearization techniques such as feedforward linearization. Design and implementation of linearization systems, however, is challenging mostly requiring strict component matching and optimization of several parameters simultaneously. The linearization performance of suchlike systems, therefore, necessitates a careful design including parameter tuning for optimization. Design and simulation tools like Advanced Design System (ADS) and GENESYS have been developed and give the designer a great flexibility. However, these tools are also very complex and not very suitable for rapid optimization. A designer indeed wants to see the effect of each component in his design by just simple calculations. For that reason, analytical tools that characterize nonlinear systems and allow in depth understanding of the system and the system requirements for optimal performance are essential. The characterization of nonlinear RF systems using traditional single-tone and two-tone measurements still represent the industry standard. However, in order to follow the technology trends and meet the new standards' requirements, more involved analysis is needed to sufficiently predict the nonlinear circuit's or system's response in its final operation regime. As a new approach in nonlinear circuit/system characterization, representing today's complex and digitally modulated signals by multi-tones (multisines) has become a significant research subject. Measurement of merits of nonlinearity using multi-tone modeling has been investigated and promising results obtained [4-6]. The subject of this chapter, as well, is multi-tone modeling of

arbitrary stimuli by in-phase equally spaced multi-tones whose number, amplitude and tone spacing can be varied to better predict the nonlinear system's final operation regime. In this chapter, the concept of multi-tone is represented with its characteristic properties first. Then, the parameter selection criteria for multi-tone model are explained. Finally, the multi-tone model is verified using real transistors.

3.1 Multi-tone Concept

Peak-to-average ratio (crest factor) is an important parameter in linear power amplifier design. For a signal carrying information (e.g., a modulated carrier or a multicarrier signal), the total average (P_m) and peak power (P_{pk}) expressions are respectively as follows [1]:

$$P_m = \frac{(V_{1rms})^2 + (V_{2rms})^2 + (V_{3rms})^2 + \ldots}{R} \tag{3.1}$$

and

$$P_{pk} = \frac{(V_{1rms} + V_{2rms} + V_{3rms} + \ldots)^2}{R} \tag{3.2}$$

where V_{irms}, $i = 1,2,3\ldots$, are rms voltages of each sine wave forming the signal and R is the load resistance.

Two-tone signal is the basic of multi-tone analysis and time domain expression of an equal amplitude two tone signal can be written as follows:

$$v_{in}(t) = v\cos(\omega_1 t) + v\cos(\omega_2 t) \tag{3.3}$$

which is equivalent to:

$$v_{in}(t) = 2v\left[\cos\left(\frac{\omega_1 - \omega_2}{2}\right)t\right]\left[\cos\left(\frac{\omega_1 + \omega_2}{2}\right)t\right] \tag{3.4}$$

or

$$v_{in}(t) = 2v\cos(\omega_m t)\cos(\omega t) \tag{3.5}$$

where

$$\omega = \frac{\omega_1 + \omega_2}{2}$$
$$\omega_m = \frac{\omega_1 - \omega_2}{2} \tag{3.6}$$

The envelope peak and average power expressions for the signal in (3.3) are

$$P_{pk} = \left(\frac{2v}{\sqrt{2}}\right)^2 = 2v^2 \tag{3.7}$$

and

$$P_m = 2\left(\frac{v}{\sqrt{2}}\right)^2 = v^2 \tag{3.8}$$

respectively for 1 Ω load resistance. Note that envelope power peak-to-average ratio for the equal amplitude two-tone signal is 3 dB as expected.

It is possible to obtain different envelopes by increasing the number of harmonics of ω_m in (3.5). By increasing the number of tones we can predict the final regime of the system better. Moreover, different peak-to-average ratio and distributions can be easily obtained by changing the number of tones and their amplitude coefficients. In contrast to two tone signal, this gives us a great flexibility in modeling signals with different peak-to-average ratios and characteristics. A general multi-tone signal with the following representation:

$$v_{in}(t) = v\left[\sum_{n=1}^{p} m_n \cos(n\omega_m t)\right]\cos(\omega t) \tag{3.9}$$

has a peak envelope power of:

$$P_{pk} = \left(\frac{v^2}{2R}\right)\left(\sum_{n=1}^{p} m_n\right)^2 \tag{3.10}$$

Mean power for periodic signals with the following form

$$v_{in}(t) = vf(\omega_m t)\cos(\omega t) \tag{3.11}$$

can be computed using the following relationship [2]:

$$P_m = \frac{\omega_m}{2\pi}\int_0^{2\pi/\omega_m} \frac{1}{2}[f(\omega_m t)v]^2\, dt \tag{3.12}$$

Hence mean power for the signal defined in (3.9) is:

$$P_m = \left(\frac{v^2}{4R}\right)\left(\sum_{n=1}^{p} m_n^2\right) \tag{3.13}$$

Combining (3.10) and (3.13) yields us an expression for peak-to-average ratio [2]:

$$\psi = \frac{P_{pk}}{P_m} = 2\frac{\left(\sum_{n=1}^{p} m_n\right)^2}{\left(\sum_{n=1}^{p} m_n^2\right)} \tag{3.14}$$

Different sets of m_n can be chosen to obtain different envelope power distributions for an arbitrary peak-to-average ratio. Note that, maximum envelope peak-to-average ratio of 2p can be obtained for p harmonics. A nonlinear amplifier would be expected to produce different amount of IMD for different envelope power distributions even if their maximum peak to average ratio is same.

3.2 Parameter Selection Criteria

The aim of multi-tone modeling is to mimic the final regime of a nonlinear system which is designed to finally operate under the stimulus of complex digital modulated signals. Hence, the selection of the multi-tone model signals is very critical and should be given the utmost importance. There are mainly four parameters that a designer can use to control the properties of a multi-tone signal: number of tones, spacing between tones, amplitude and phase of the tones. In literature, various combinations of these parameters have been used for nonlinear system characterization. In [5], phase and magnitude of multi-tone signals are modified to represent ACPR of digitally modulated QPSK signal. The number of tones in a multi-tone signal is varied from 3 to 65 and ACPR results for digitally modulated signal and its multi-tone models are compared. This work includes only simulation results for single digitally modulated signal and selection procedure of multi-tone signals is not mentioned. In this thesis, the amplifier nonlinearity is assumed to be of third order and the multi-tone model is confined to in-phase equally distributed (equi-spaced) tones with variable amplitudes. Selection criteria, which are used to find the appropriate multi-tone models for a specific signal, are specified. Moreover, the validity of multi-tone concept is verified by applying arbitrary signals and their multi-tone models to real life amplifiers. The simulation results are also obtained and compared to the measurement results in order to inspect the differences between practical amplifiers and system amplifiers, which are used in simulation environment. Furthermore, the usefulness of multi-tone concept is validated by applying it to a feedforward system, which is relatively complex to analyze.

Peak-to-envelope ratio is an important parameter of the input signal, but it cannot be used alone to design a multi-tone model. An actual digital modulated signal, for instance, cannot be simply modeled with a multi-tone model by just keeping peak-to-average ratios of two signals the same. This approach results in overestimated IMD, since peaks of the representing series of tones drive the amplifier more than the actual signal because of their periodic nature. The model's crest factor, therefore, must be reduced to have a nonlinear effect equivalent to that

of the actual signal. The amount of decrease in the crest factor depends on the system and signal properties; some criteria rather than the crest factor for determining the model signal parameters are required.

One selection criterion would be the distribution of the instantaneous nonlinear power at the output of the main amplifier for a given third-order intercept point (IP3). Assume a system with third order nonlinearity:

$$v_{out} = a_1 v_{in} + a_3 v_{in}^3 \tag{3.15}$$

The power at the output of that nonlinear system will be:

$$P_{out} = \frac{(v_{out})^2}{2} = \frac{(a_1 v_{in} + a_3 v_{in}^3)^2}{2} = \frac{1}{2} a_1^2 v_i^2 + \frac{3}{4} a_1 a_3 v_i^4 + \frac{9}{32} a_3^2 v_i^6 \tag{3.16}$$

where v_i is the envelope of v_{in} . For a third-order nonlinear system, the instantaneous nonlinear power, S, can be expressed as:

$$S = \left| \frac{9}{32} a_3^2 v_i^6 + \frac{3}{4} a_1 a_3 v_i^4 \right| \tag{3.17}$$

where v_i is the instantaneous envelope voltage of the input signal. This expression includes in-band and out-of-band nonlinear terms. Figure 3.1 illustrates the histogram for S for one of the signals we used in this work and its multi-tone model. Note that the number of samples with high S is comparably small; however these few samples are the samples that drive the amplifier into nonlinearity. As S increases, number of samples decreases dramatically for the actual signals, whereas the histogram of the model signals are concentrated at specific points due to their periodicity. Also, maximum value of S, S_{max}, of the model signal is smaller than that of the actual signal.

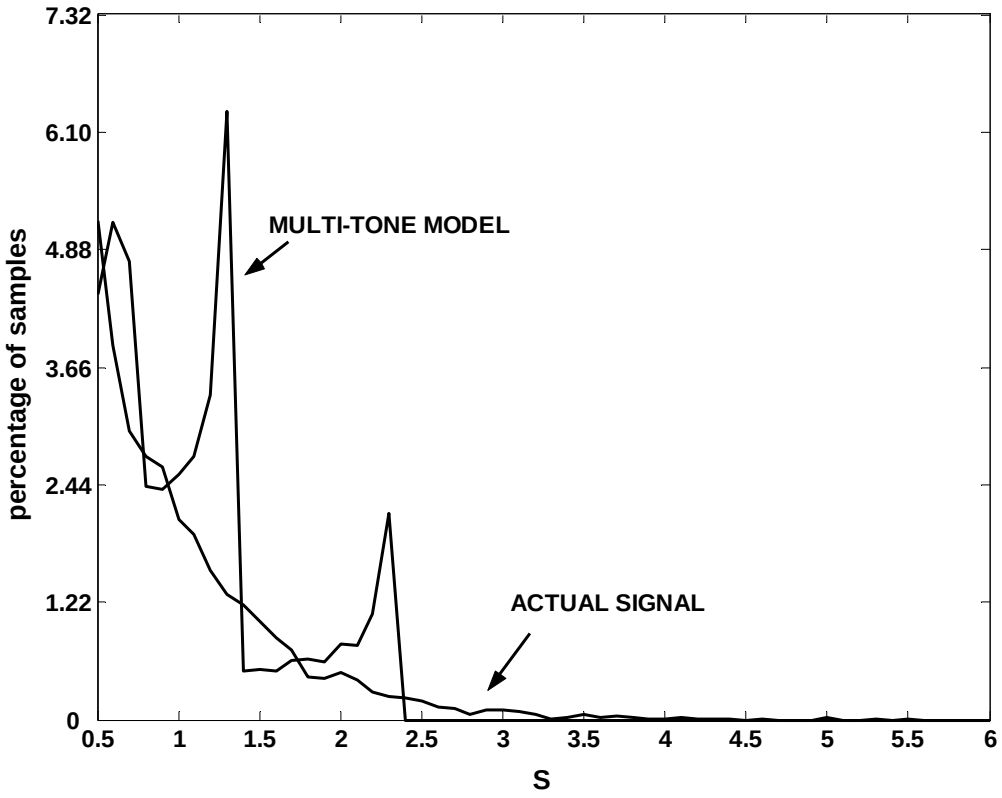

Figure 3.1: The histogram illustrating the distribution of nonlinear terms of a complex arbitrary signal and its multi-tone model. The number of samples of actual signal decreases almost exponentially; whereas, they are concentrated at around specific points for multi-tone model.

Not only the number of peaks, but also the peak value determines the nonlinear products. One shot of high peak level may create an equivalent nonlinear output with repetitive relatively low-level peaks (as in the periodic signal case). Additionally, a constant K can be defined to represent the overall distortion power as follows:

$$K = \sum_i S_i N_i \tag{3.18}$$

where S_i is the histogram index associated with nonlinear power S and N_i is the corresponding number of samples. S reaches to its maximum, i.e., S_{max}, when input voltage is at its peak and its smallest value is zero when the amplifier is completely working in its linear region. K values of the model and the actual signals are

expected to be close to each other, meaning that they both contribute a similar amount of nonlinear power.

An alternative interpretation to K would be the average of the calculated S, which can be assigned to a new parameter M. This parameter is the level of average distortion power. Hence, M can be expressed as:

$$M = \frac{1}{N}\sum_{i} S_i \tag{3.19}$$

where N is the total number of samples. Note that K and M represent the overall nonlinear power, which covers both in-band and out-of-band products.

As usual, if adjacent channel power (ACP) is the basis of comparison between the nonlinearities contributed by the actual and model signals, then only out-of-band products shall be taken into consideration by extracting the in-band distortion. However, both K and M parameters include co-channel (in-band) distortion and are not very suitable for ACP comparison. This requires computing the frequency distribution of the nonlinear power and yields an alternative parameter F, which is defined as follows:

$$F = \sum_{OUT-OF-BAND} \left| FFT(\tfrac{3}{4} a_3 v_i^3, N) \right|^2 \tag{3.20}$$

The N^{th} order FFT of nonlinear term $a_3 v_i^3$ is taken thereby transforming nonlinearities into frequency domain. Then out-of-band frequencies are summed up excluding in-band distortion. Consequently, a figure of measure for ACP comparison is formed.

A designer, in fact, can use all parameters defined here considering the advantages and disadvantages of each. K and M parameters, for instance, are easy to compute and give a coarse idea whether the model is appropriate or not, however, they include in-band distortion besides out of band distortion. The parameter F, on the other hand, is complex to calculate because of FFT operation but gives a better estimate since it includes only out-of-band distortion.

3.3 Application of the model to a real life amplifier

The output of a nonlinear system in response to an arbitrary excitation cannot be given simply as the sum of elementary outputs. The practical consequence of this statement is that the prediction of a system's response to a particular input will be more successful the closer the test input is to the excitation expected in practice. Practical systems are intended to handle information signals, which, by definition are unpredictable. Therefore, the prediction of the system's final response is a difficult task. In this work, actual signals are chosen as arbitrary real and complex enveloped in order to demonstrate that multi-tone modeling can be employed to represent any unpredictable information signal and estimate the response of the system to such arbitrary input signals.

In order to verify multi-tone modeling idea, real enveloped and complex enveloped arbitrary signals and their multi-tone models are created in MATLAB. Actual signals consist of 8192 samples each with every sample arbitrarily chosen using "rand" function. Actual signals are arbitrary in order to demonstrate that multi-tone modeling can be applied to signals with any type of modulation. All signals are then downloaded into an arbitrary signal generator which generated these signals as real time signals. Finally, we used the signals generated by this generator as stimuli for nonlinear amplifiers. The nonlinear amplifiers used in the tests are HMC481MP86 and HMC372LP3 from Hittite Microwave Corporation. The measurements are made at two different frequencies, namely at 1 GHz for HMC481MP86 and 750 MHz for HMC372LP3.

3.3.1 Properties of amplifiers

The HMC481MP86 is a SiGe Heterojunction Bipolar Transistor (HBT) Gain Block MMIC SMT amplifier covering DC to 5 GHz. This Micro-P packaged amplifier is designed to offer typically 20 dB of gain with a +33 dBm output IP3 from 500 MHz up to 1 GHz and can be used up to +21 dBm output power. The

measurements are made for 7 V supply voltage (V_s) at 1 GHz carrier frequency using the evaluation circuit board recommended by Hittite Microwave Corporation. The gain, output IP3 and 1dB compression point measured for this evaluation board at 1 GHz are 19.3 dB, 30.8 dBm and 0 dBm, respectively. IP3 value is obtained from measured IMD value at -20 dBm input power using the following equation:

$$IP3(dBm) = \frac{IMD(dBm/tone)}{2} + P_{out}(dBm/tone) \tag{3.21}$$

where P_{out} is the output power for each tone. The intermodulation distortion products for different input power levels are also measured and given in Table 3.1. Note that fifth order intermodulation products become comparable as input power increases. Figures 3.2 and 3.3 demonstrate AM-AM and AM-PM characteristics of this amplifier at 1 GHz respectively. These plots are obtained using the power sweep property of Agilent PNA series E8801A network analyzer.

Table 3.1: Intermodulation distortion measurement results for HMC481MP86 amplifier. The test is carried with two tones with 1 MHz spacing at 1 GHz carrier frequency.

Input Power (dBm/tone)	**Intermodulation Distortion (dBc)**				**Output Power (dBm/tone)**
	5^{th} order left	**3^{rd}order left**	**3^{rd}order right**	**5^{th} order right**	
-20	-	-62,4	-63	-	-0,4
-18	-	-58,5	-58,8	-	1,6
-16	-	-54,9	-54,9	-	3,5
-14	-	-49,9	-50	-	5,5
-12	-71	-45	-45	-71	7,4
-10	-61,8	-39,4	-39,4	-61,3	9,3
-8	-58	-33,3	-33,2	-58,4	11,0
-6	-44,3	-29,6	-29,7	-44,5	12,7
-4	-32,5	-24,3	-24,5	-31,8	14,0
-2	-30	-16	-16,7	-29,4	14,9

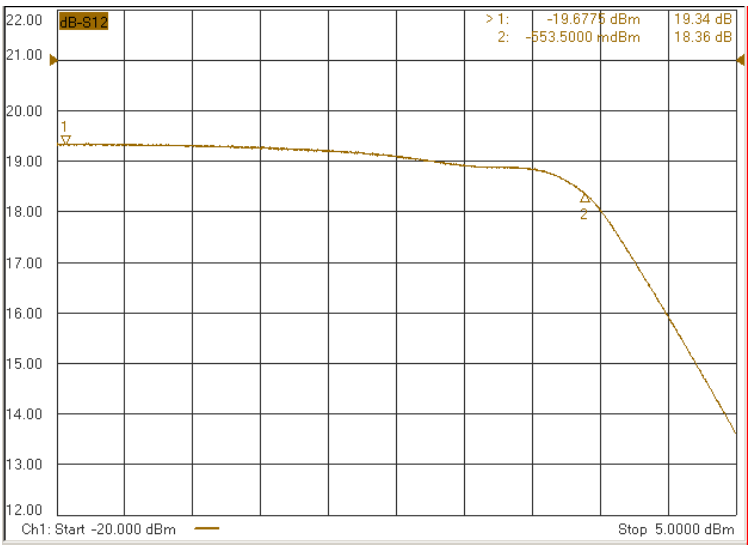

Figure 3.2: AM-AM characteristics of HMC481MP86 amplifier at 1 GHz carrier frequency. The horizontal axis shows the power sweep. Marker 2 indicates the 1 dB compression point of the amplifier.

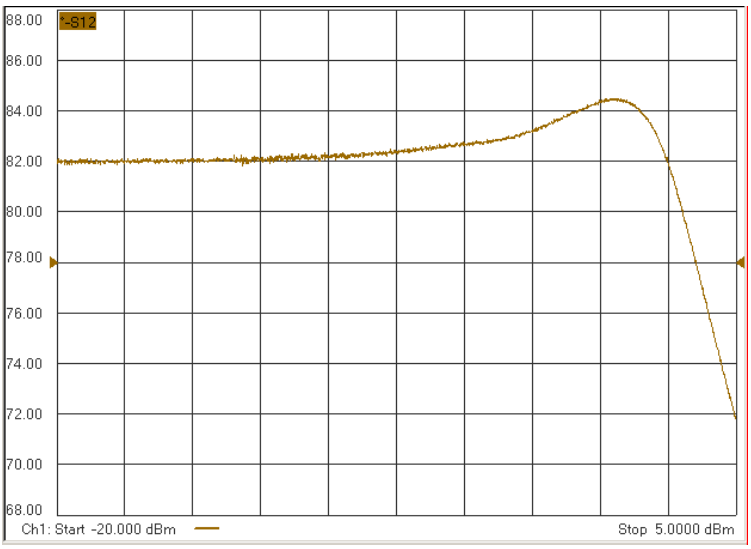

Figure 3.3: AM-PM characteristics of HMC481MP86 amplifier at 1 GHz carrier frequency. The horizontal axis shows the power sweep. The effect of AM-PM becomes significant as amplifier approaches saturation.

The second amplifier, HMC372LP3, is a GaAs PHEMT MMIC Low Noise Amplifier that has been optimized to provide 15 dB gain and +34 dBm output IP3 between 700 and 1000 MHz. The measurements are made for 5 V supply voltage at 750 MHz carrier frequency using the evaluation board recommended by Hittite Microwave Corporation. The gain, output IP3 and 1dB compression point measured for this evaluation board at 750 MHz are 15.6 dB, 35 dBm and 3.4 dBm, respectively. IP3 value is obtained for -20 dBm input power using equation 3.21. The intermodulation distortion products for different input power levels are also measured and given in Table 3.2. Note that fifth order intermodulation products become comparable as input power increases. Figures 3.4 and 3.5 demonstrate AM-AM and AM-PM characteristics of this amplifier at 750 MHz respectively. Gain expansion phenomenon [9, 48], which is sometimes observed around sweet spots, is very obvious in AM-AM characteristics. Around 1 dBm input power, gain expansion takes place and after a peak a sudden gain drop is observed. HMC372LP3 is a more linear amplifier compared to HMC481MP86 but AM-PM affect is much more evident causing sideband asymmetries.

Table 3.2: Intermodulation distortion measurement results for HMC372LP3 amplifier. The test is carried with two tones with 1 MHz spacing at 750 MHz carrier frequency.

Input Power (dBm/tone)	**Intermodulation Distortion (dBc)**				**Output Power (dBm/tone)**
	5^{th} order left	**3^{rd}order left**	**3^{rd}order right**	**5^{th} order right**	
-20	-	-78	-79	-	-4,0
-18	-	-71,6	-75,1	-	-1,9
-16	-	-68,3	-72,7	-	0,1
-14	-	-64.3	-70,4	-	2,1
-12	-	-63.6	-68,8	-	4,2
-10	-	-60.7	-66,5	-	6,1
-8	-78.9	-56.6	-62,7	-77,4	8,2
-6	-71,7	-52	-56,6	-69,4	10,2
-4	-55,9	-43.7	-45,3	-54,8	12,2
-2	-40,7	-29.1	-29,3	-40,6	14,3

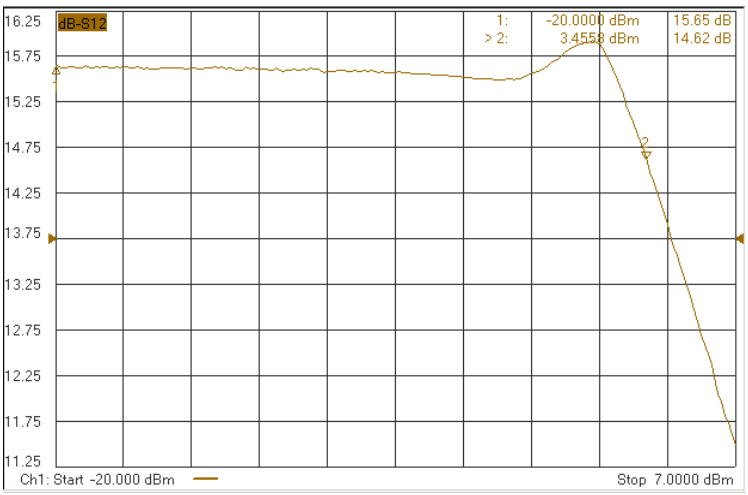

Figure 3.4: AM-AM characteristics of HMC372LP3 amplifier at 750 MHz carrier frequency. The horizontal axis shows the power sweep. Marker 2 indicates 1 dB compression point.

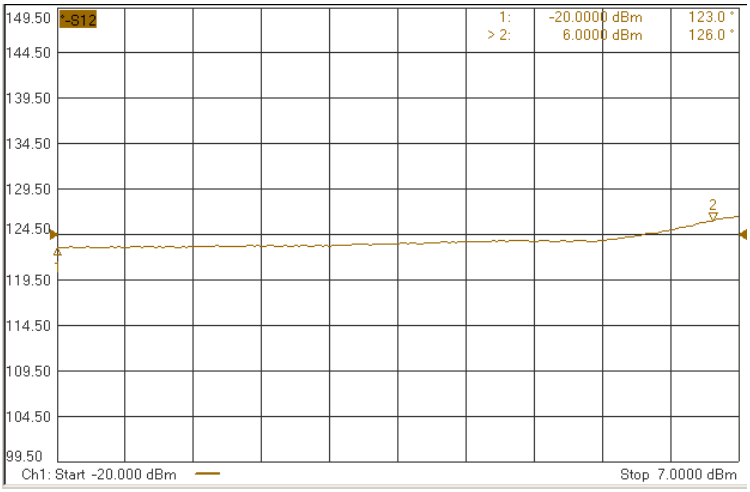

Figure 3.5: AM-PM characteristics of HMC372LP3 amplifier at 750 MHz carrier frequency. The horizontal axis shows the power sweep. AM-PM becomes more effective as amplifier approaches saturation.

3.3.2 Properties of stimuli

The stimuli used in measurements are of two types: *actual signals* and *model signals*. *Actual signals* are real and complex enveloped arbitrary signals formed by "rand" function embedded in MATLAB. *Model signals* are multi-tone signals composed in MATLAB to model the *actual signals*.

There are two signals that we refer to as *actual*, namely, a real enveloped signal and a complex enveloped signal. The real enveloped signal is composed of 8192 samples with sampling frequency of 60 nsecs. The base bandwidth of this signal is 2.5 MHz and it has Ψ of 7.55 dB. The complex enveloped signal is composed of 8192 samples with sampling frequency of 167 nsecs. The base bandwidth of this signal is 900 kHz and it has Ψ of 9.1 dB. Figure 3.6 illustrates instantaneous envelope peak/average histogram of both signals. Note that as peak/average value increases number of samples decreases drastically. The real enveloped and complex enveloped signals at the output of the signal generator are also illustrated in Figure 3.7. The bandwidths of these signals can be easily seen from the graphs.

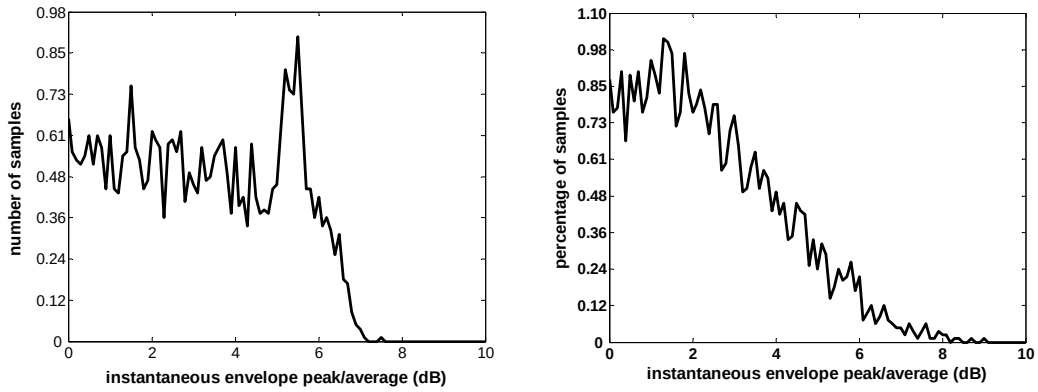

(a) **(b)**

Figure 3.6: Instantaneous envelope peak/average histograms of **a)** real enveloped signal and **b)** complex enveloped signal.

The model signals are multi-tone having the same bandwidth with the actual signal they represent. In this work, each actual signal has been modeled using two multi-tone models. To demonstrate the power of multi-tone modeling we have also included two more multi-tone signals which overestimate and underestimate IMD.

The one which overestimates has a crest factor higher than the model's crest factor and is called ModelHIGH throughout this work. The second one with lower crest factor is referred to as ModelLOW. When deciding on multi-tone models we use the parameter selection criteria previously introduced. The signal generator output for multi-tone models for real and complex enveloped signals are illustrated in Figure 3.8. Equally spaced tones at different frequencies are clearly distinguished. Each model is composed of three tones but when the baseband model is upconverted to RF frequency the tones at image frequencies also come into view. Therefore, each three tone model consists of six tones actually. Tones are evenly spaced over the bandwidth of the actual signal they model and amplitude values are clearly different as a result of different amplitude coefficient selection.

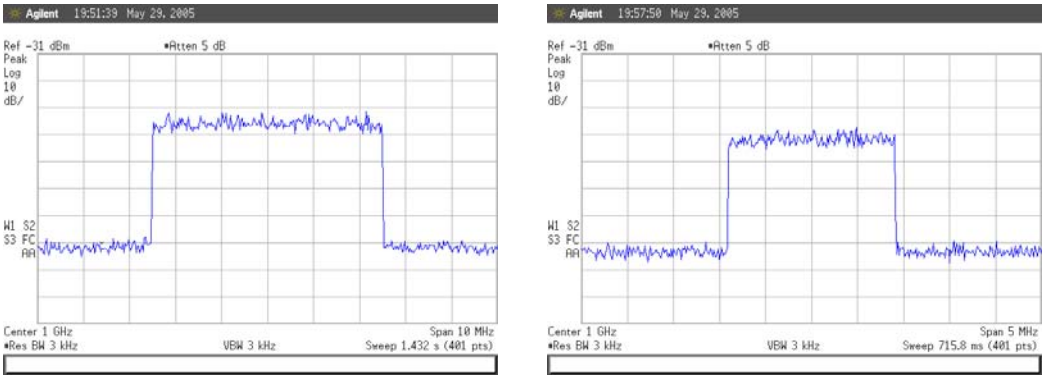

(a) **(b)**

Figure 3.7: Signal generator output for **a)** real enveloped signal and **b)** complex enveloped signal.

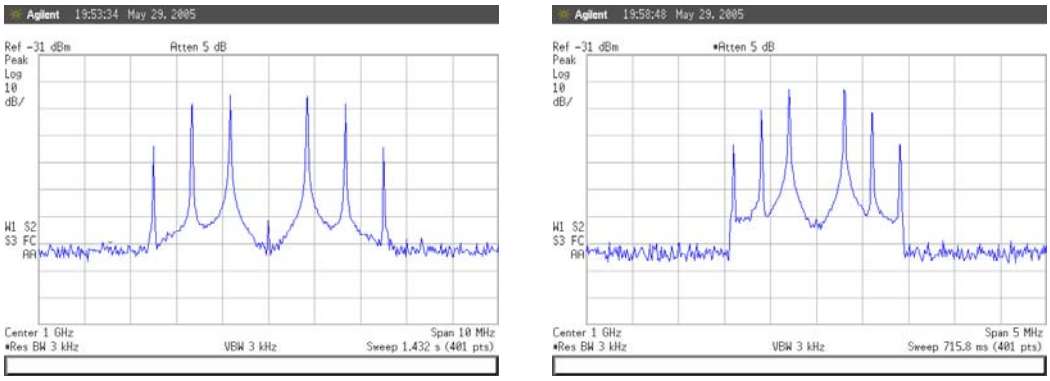

(a) **(b)**

Figure 3.8: Signal generator output for multi-tone model signals for **a)** real enveloped signal and **b)** complex enveloped signal.

3.3.3 Generating the real time stimuli

We prepare the signal in MATLAB in I+jQ form and then seperate its real (I) and imaginary (Q) form and save each into a text file. Then, we scale values of these I and Q vectors into integers lying between 0 and +16383 (see Appendix B). This is a requirement because the DAC used in the signal generator's internal dual arbitrary waveform generator (see Figure 3.9) has 14-bit resolution, allowing up to 16384 quantized voltage levels. Zero voltage is scaled to 8191 and when forming a real enveloped signal (Q in I+jQ is an all zero vector) all entries of Q vector are 8191. The scaled forms are then saved and downloaded into the signal generator via RS-232 interface using a waveform download program supplied by Agilent (see Figure 3.10). This program is an interface between the computer and the signal generator. It adjusts settings for a safe download and then downloads I and Q vectors in text files manually selected by the user.

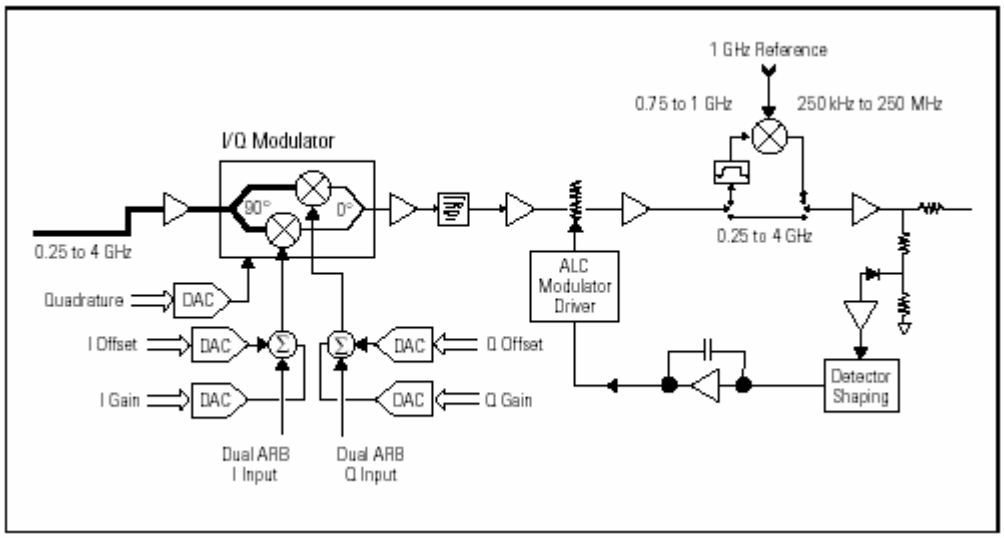

Figure 3.9: Block diagram of the Agilent ESG-D with dual arbitrary waveform generator. I and Q vectors representing the signal to be generated are sent to I/Q modulator where a carrier is modulated and RF signal is created.

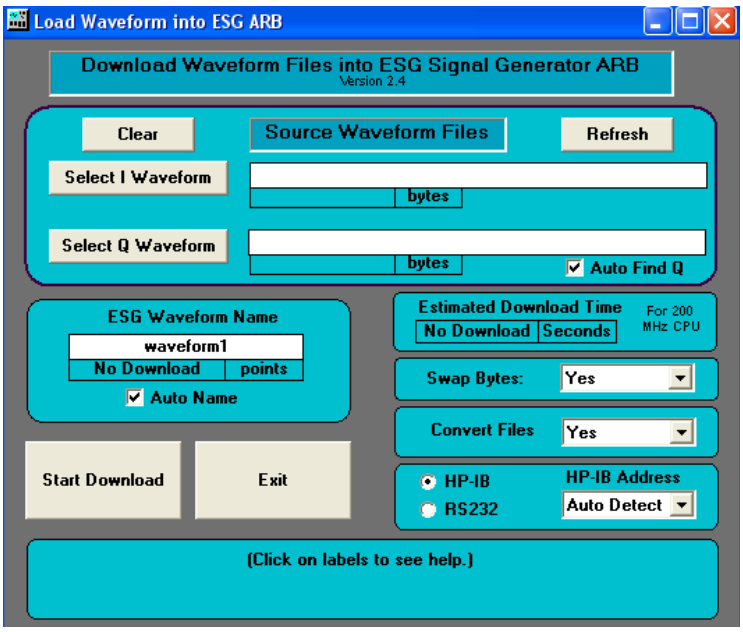

Figure 3.10: ESG-ARB waveform download interface for Agilent ESG-D series signal generators with option UND.

The stimuli prepared in MATLAB are downloaded into Agilent E4433B ESG-D Option-UND signal generator. Figure 3.11 illustrates the signal download phase illustrating each step separately. Either the actual or multi-tone model signal is prepared and scaled in MATLAB and then downloaded into the signal generator via ESG-ARB waveform download interface. This signal generator includes an internal dual arbitrary waveform generator which provides baseband generation for complex RF waveforms. With the capability to drive the ESG-D's I/Q modulator, the internal dual arbitrary waveform generator provides the power to simulate complex, nonstandard, or proprietary modulated RF signals. The generator requires I and Q vectors as input in a specific format in order to generate the waveforms prepared in external simulation tools. Once the baseband signal is downloaded into the signal generator it is saved into the memory with a user defined name and ready to use to generate modulated RF signal.

The sampling frequency of the baseband signal and the proper reconstruction filter must be set manually using the relevant baseband signal menu. There is a bandwidth limitation for the baseband signal; the dual arbitrary waveform generator can generate signals with less than 20 MHz baseband bandwidth. The

signals generated in the signal generator are then, applied to a nonlinear amplifier at a specified frequency and the output of the amplifier is demonstrated and analyzed using Agilent E4402B ESA-E series spectrum analyzer. The criteria used to analyze the problem, namely, the main channel power and the adjacent channel power are measured using the ACP measurement utility of the spectrum analyzer. The only input the analyzer needs is the bandwidth of the main channel and the sidebands which can be easily adjusted by the user.

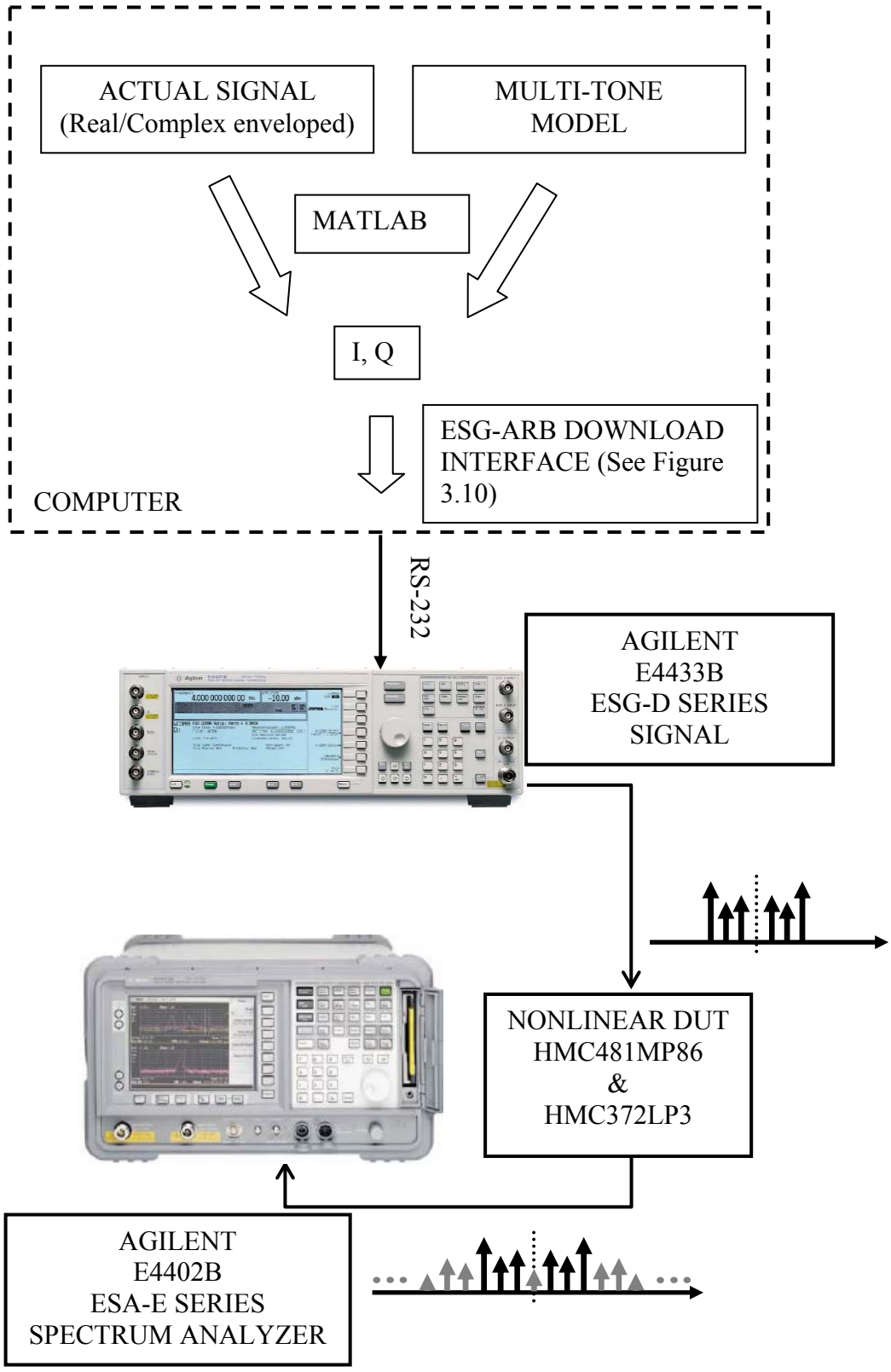

Figure 3.11: The flowchart demonstrating the generation, download and analysis phases of the measurement process.

3.4 Measurement and Simulation Results

This part of the chapter includes the measurement and simulation results for the actual and the multi-tone signals. The measurement results are presented in two parts. First, the results for real enveloped stimulus and for its multi-tone models are illustrated. Next, the results for complex enveloped stimulus and for its multi-tone models are presented. Considering that we have actually two nonlinear amplifiers, both real and complex enveloped signals are used as stimuli to these amplifiers and results for actual signals and one of the multi-tone models are tabulated and illustrated. Simulation results are obtained using system amplifiers in Advanced Design System (ADS) environment. Gain and IP3 values of HMC481MP86 and HMC372LP3, which are measured at 1 GHz and 750 MHz, respectively, are used to specify the characteristics of the system amplifiers. The nonlinearity of the system amplifiers is confined to third order and the power series coefficients which characterize the third order nonlinearity of the amplifiers are evaluated in terms of measured gain and IP3 using the following equations:

$$a_1 = 10^{G/20}$$

$$a_3 = \frac{-2}{3R} 10^{\left(\frac{-IP3}{10}+\frac{3G}{20}\right)} \tag{3.22}$$

where R is the reference impedance of the circuit. The simulation results for high input power, where the terms higher than the third order terms become effective, are obtained for an *effective* IP3, since IP3 can be only defined for weak nonlinear regions of an amplifier. Different from IP3, *effective* IP3 changes with power and is computed by (3.21) for each power level using IMD results of two tone test.

The following two sections present the measurement and simulation results for the real and complex enveloped data. Measurement and ADS results are indicated in the same tables and figures for comparison. More detailed tables and graphics are also given in Appendix A.

3.4.1 Results for real enveloped data

Real enveloped data has a bandwidth of 2.5 MHz and 8192 samples as mentioned before. Figure 3.12 is a screenshot of the spectrum analyzer used in our measurement setup. It illustrates the output of HMC481MP86 at 1 GHz carrier frequency and -8 dBm average input power. Upper and lower sideband distortion

Figure 3.12: Spectrum of the real enveloped signal at the output of HMC481MP86 at 1 GHz carrier frequency for -8 dBm average input power.

can be clearly observed and spectrum analyzer readings of carrier power (main channel power) and upper and lower sideband ACPs are also shown. Moreover, resolution bandwidth (RBW), video bandwidth (VBW), sweep time in microseconds, span of the screen and input attenuation values used when this screenshot is saved are separately indicated. Multi-tone model for this signal is also applied to the same amplifier with the same settings and resulting signal is illustrated in Figure 3.13. Upper and lower sideband distortion is clearly observed but contrary to the sidebands of amplified actual signal, sidebands of amplified

multi-tone signal consist of tones located Δw away from each other where Δw is the separation between fundamental tones. The resulting main channel power and ACP are measured in the same way and results indicated on the display of the spectrum analyzer.

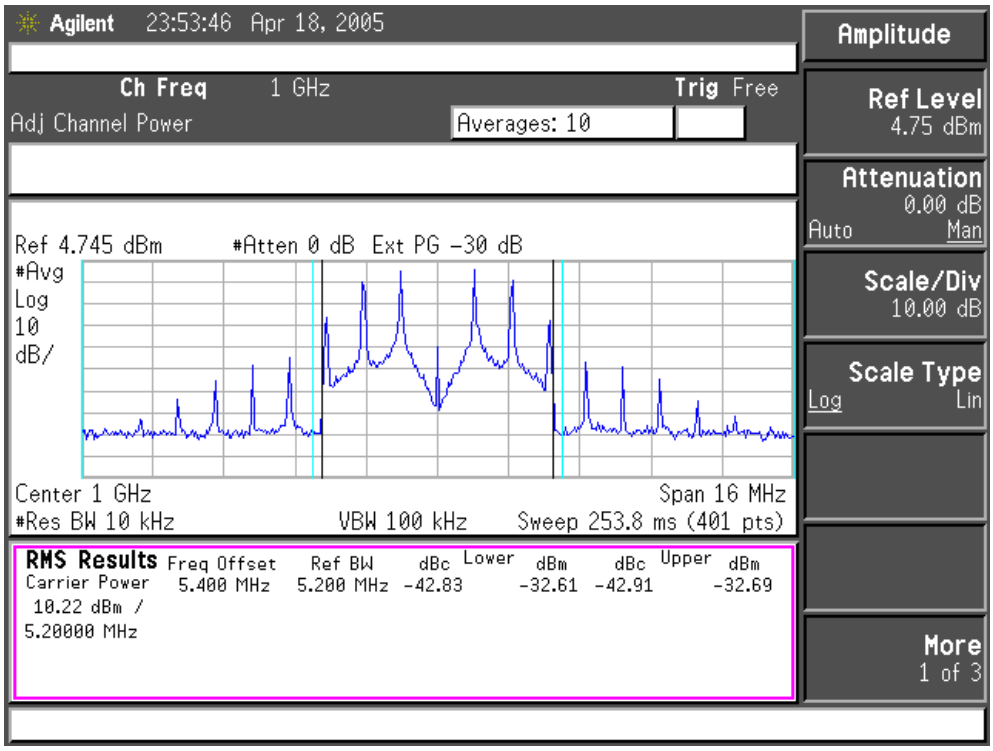

Figure 3.13: Spectrum of the model (m_1=0.9, m_2=0.55, m_3=0.1) for real enveloped signal at the output of HMC481MP86 at 1 GHz carrier frequency for -8 dBm average input power.

The criteria used to decide on multi-tone model signals, Ψ (crest factor), K, M and F are evaluated for each stimulus and Tables 3.3 and 3.4 tabulate these parameters for HMC481MP86 and HMC372LP3, respectively. Parameters are different for each amplifier because the gain and third order intercept points of amplifiers are different. Actual signals can have numerous multi-tone models because there are many multi-tone signals with similar K, M and F parameters. The real enveloped signal (actual signal) is modeled by two different multi-tone models labeled as Model 1 and Model 2. In order to emphasize the importance of parameter selection we have also included a model that overestimates

Table 3.3: Important parameters of the actual and multi-tone signals for HMC481MP86 amplifier. Crest factor (Ψ), K, M and F parameters indicate whether the selected model is suitable or not.

	STIMULI G=19.3, IP3=30.8			**Ψ**	**K (x10^5)**	**F (x10^9)**	**M**
	m_1	m_2	m_3				
	Real enveloped data			7.5	4.48	2.47	54.7
Model 1	0.9	0.55	0.1	6.3	5.13	2.33	62.9
Model 2	0.2	0.55	0.1	6.1	3.78	2.28	46.3
ModelHIGH	1	0.9	0.8	7.7	14.7	8.97	179.9
ModelLOW	0.1	0.1	0.8	4.8	3.07	1.27	37.5

Table 3.4: Important parameters of the actual and multi-tone signals for HMC372LP3 amplifier. Crest factor (Ψ), K, M and F parameters indicate whether the selected model is suitable or not.

	STIMULI G=15.6, IP3=35			**Ψ**	**K (x10^4)**	**F (x10^7)**	**M**
	m_1	m_2	m_3				
	Real enveloped data			7.5	7.03	2.78	8.6
Model 1	0.9	0.55	0.1	6.3	6.90	2.62	8.4
Model 2	0.2	0.55	0.1	6.1	6.60	2.56	8.1
ModelHIGH	1	0.9	0.8	7.7	8.94	10.1	10.9
ModelLOW	0.1	0.1	0.8	4.8	5.19	1.42	6.4

IMD and another one that underestimates IMD and labeled them as ModelHIGH and ModelLOW respectively. Note that as crest factor increases values of K, M and F also increase confirming that distortion increases as the value and number of peaks in a signal are increased. Even though the crest factors of Model 1 and Model 2 are lower than the actual signal, values of parameter selection merits for models are close to those of the actual signal's indicating modeling is successful. This is a result of periodicity of multi-tone models, which drive amplifier more than the actual signal does. Consequently, every multi-tone model will have a lower crest factor than the crest factor of the actual signal.

Table 3.5 shows the output power and IMD in dBm for HMC481MP86. Both measurement and ADS simulation results are tabulated for real enveloped signal and Model 1. A third order nonlinear system amplifier is used to model the amplifier in ADS simulation environment. Figure 3.14 illustrates the measurement and simulation results. Note that measurement and simulation results for actual and model signal are very close as much as measurement and simulation results are evaluated independently. When the measurement results are compared to simulation results, however, we observe that measurement results deviate from simulation, i.e., we cannot measure IMD values smaller than the capabilities of the spectrum analyzer's ACP measurement utility.

Tables 3.6 and 3.15 also demonstrate simulation and measurement results for real enveloped data and one of its multi-tone models (Model1) for HMC372LP3. Interpretations will be similar to those made for HMC481MP86. Measurement results again deviate from simulation results due to the same reason as explained above. If we evaluate measurement and simulation results independently, we observe once more that results for the actual and multi-tone model are consistent.

We have deliberately formed ModelHIGH and ModelLOW to emphasize the importance of parameter selection in multi-tone modeling. Figure 3.16 illustrates the measurement and simulation results for the real enveloped signal, ModelHIGH and ModelLOW. Measurement results deviate from simulation results once more. However, if we evaluate simulation and measurement results separately we see that the model labeled ModelHIGH always overestimates IMD, although the distinction between the actual signal results and ModelHIGH results decreases as input power is decreased. The decrease is more severe in ModelLOW case, such that the actual signal and ModelLOW become undistinguishable for low input voltage. This observation, however, is not valid for ADS simulation results; ModelLOW and ModelHIGH behave as expected as input power is increased. As a result, this figure illustrates that unless model parameters are selected properly, the multi-tone model designed and formed to predict the effect of the actual signal will either over or under estimate the desired results. More detailed measurement and simulation results for all signals are tabulated and illustrated in APPENDIX A.

Table 3.5: Measurement and ADS simulation results for actual and model signals for real enveloped data for HMC481MP86. The parameters of Model 1 are m_1=0.9, m_2=0.55, m_3=0.1.

Input Power (dBm)	Real Enveloped Data & Model 1 (measurement and simulation results in dBm)							
	Actual Signal				Model 1			
	Output Power		IMD		Output Power		IMD	
	Meas.	ADS	Meas.	ADS	Meas.	ADS	Meas.	ADS
-2	14.93	14.00	-8.15	-8.18	15.07	14.07	-8.20	-8.26
-6	11.83	11.78	-25.60	-22.49	11.89	11.73	-25.90	-22.51
-10	8.12	8.24	-38.10	-37.50	8.05	8.22	-38.40	-37.38
-14	4.10	4.35	-46.25	-51.11	4.18	4.34	-46.20	-50.99
-18	0.38	0.38	-54.10	-63.12	0.42	0.37	-53.90	-63.00
-22	-3.57	-3.60	-58.40	-75.10	-3.40	-3.61	-58.15	-74.97
-26	-7.61	-7.59	-62.90	-87.10	-7.66	-7.65	-62.70	-87.11
-30	-11.68	-11.62	-66.10	-99.18	-11.57	-11.60	-65.85	-98.98

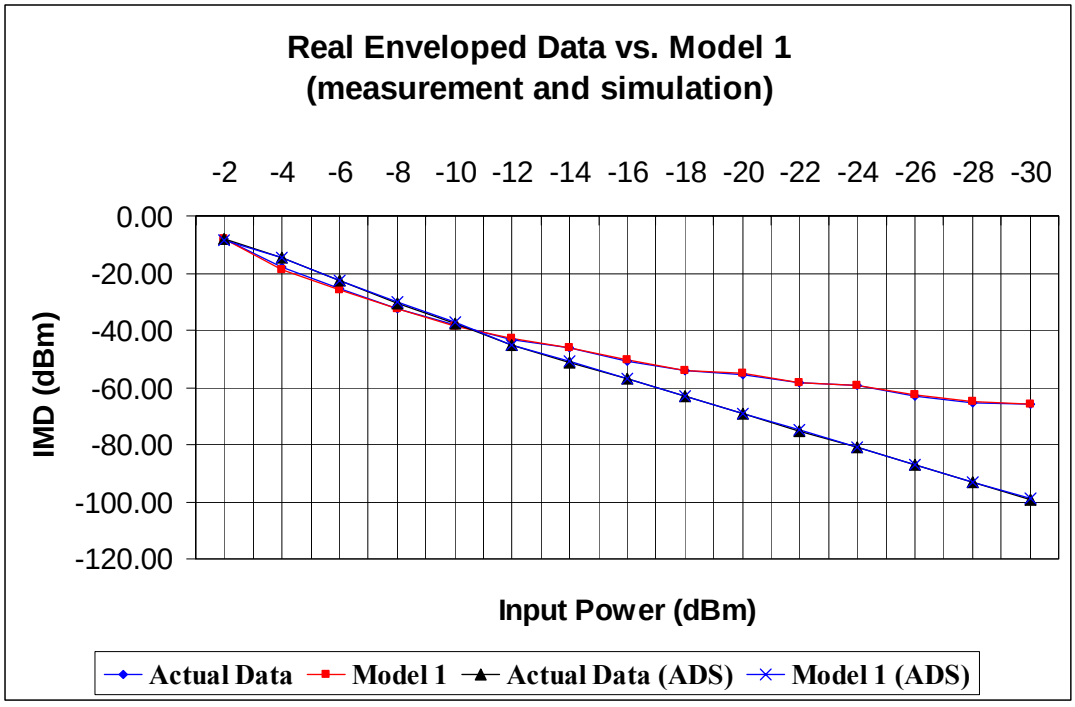

Figure 3.14: Measurement and simulation results for real envelope signal and one of its multi-tone models (Model 1) for HMC481MP86. Simulation results are indicated by ADS expression in parenthesis.

Table 3.6: Measurement and ADS simulation results for actual and model signals for real enveloped data for HMC372LP3. The parameters of Model 1 are m_1=0.9, m_2=0.55, m_3=0.1.

Input Power (dBm)	Real Enveloped Data & Model 1 (measurement and simulation results in dBm)							
	Actual Signal				Model 1			
	Output Power		IMD		Output Power		IMD	
	Meas.	ADS	Meas.	ADS	Meas.	ADS	Meas.	ADS
2	15.72	15.85	-13.15	-15.62	16.00	15.84	-13.90	-15.50
-2	12.57	12.51	-29.30	-33.70	12.82	12.50	-30.80	-33.58
-6	8.76	8.61	-45.30	-46.73	8.78	8.60	-44.90	-46.61
-10	4.54	4.69	-50.60	-58.60	4.70	4.67	-50.05	-58.48
-14	0.47	0.70	-53.80	-70.61	0.53	0.69	-53.65	-70.49
-18	-3.25	-3.30	-59.80	-82.62	-3.33	-3.31	-59.20	-82.50
-22	-7.32	-7.33	-63.80	-94.70	-7.21	-7.34	-63.20	-94.58
-26	-11.71	-11.34	-67.75	-106.73	-11.50	-11.35	-67.20	-106.61
-30	-15.36	-15.29	-70.90	-118.59	-15.18	-15.30	-70.65	-118.48

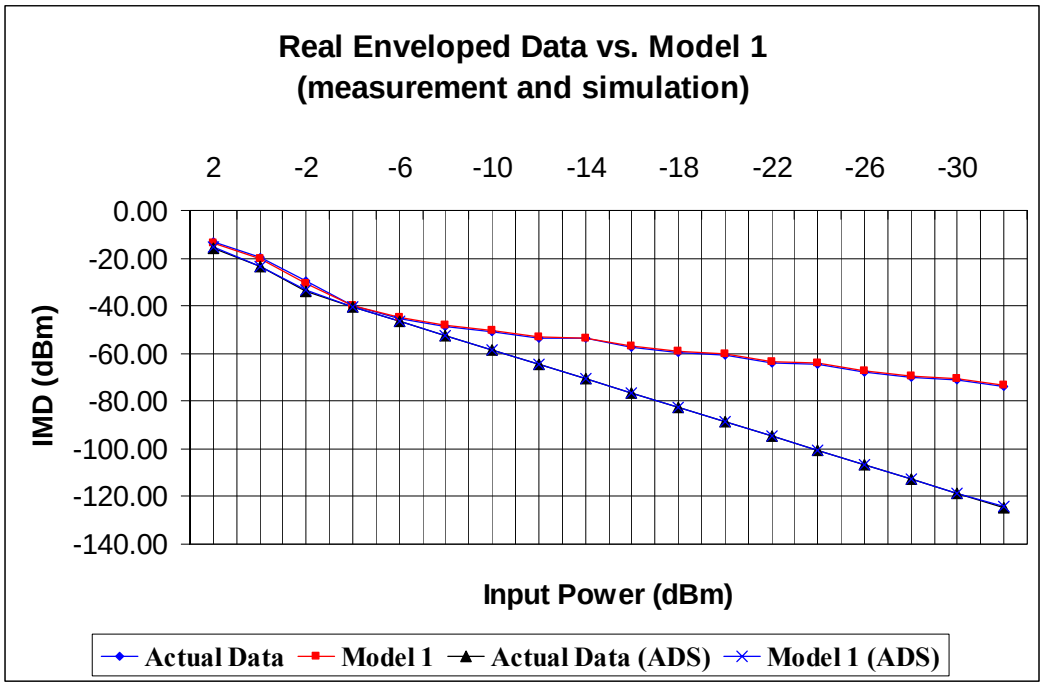

Figure 3.15: Measurement and simulation results for real envelope signal and one of its multi-tone models (Model 1) for HMC372LP3. Simulation results are indicated by ADS expression in parenthesis.

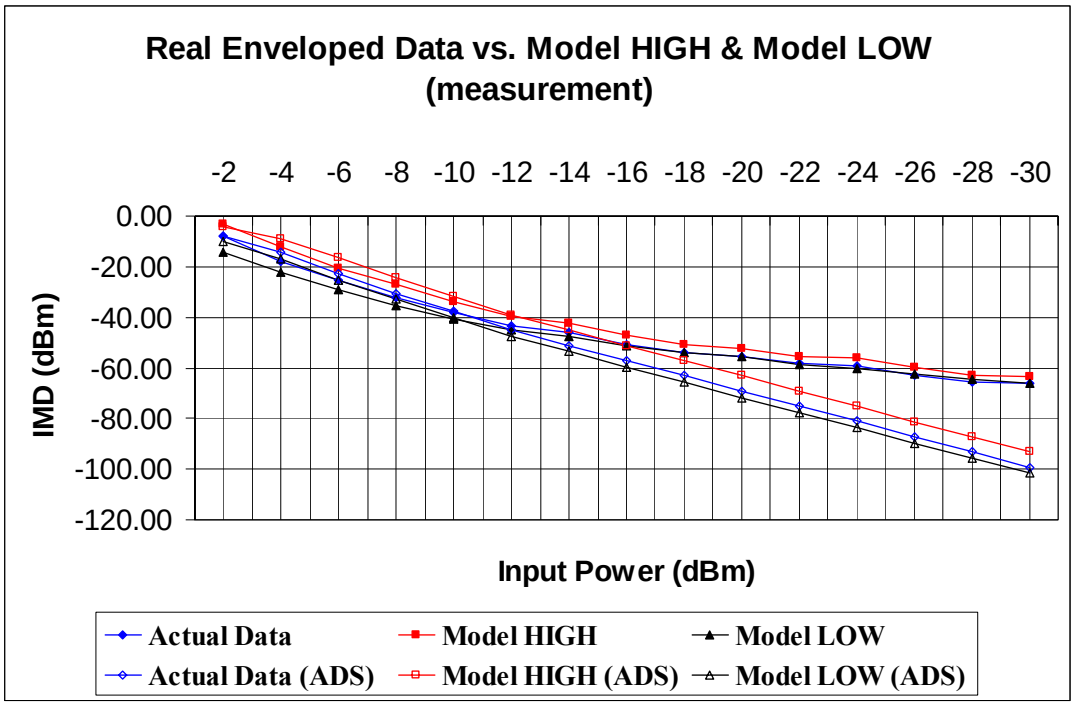

Figure 3.16: Measurement and simulation results for real envelope signal, ModelHIGH and ModelLOW for HMC481MP86. Simulation results are indicated by ADS expression in parenthesis.

3.4.2 Results for complex enveloped data

The complex enveloped signal is composed of 8192 samples with sampling frequency of 167 nsecs. The base bandwidth of this signal is 900 kHz and it has Ψ of 9.1 dB. Tables 3.7 and 3.8 tabulate the selection parameters for complex enveloped signal and its multi-tone models for HMC481MP86 and HMC372LP3 respectively. Note that one of the fundamental parameters, F, has to be modified by scaling the F values for complex enveloped data in order to be able to equate the F values of the actual signal and models. Calculation procedure of F parameter for complex enveloped signal is a problem to be solved. Tables 3.9 and 3.10, and Figures 3.17 and 3.18 display the IMD results for both measurement and simulation. We can easily observe that complex enveloped signal and multi-tone models are consistent, indicating that multi-tone modeling concept is suitable for complex

enveloped signals too. The measurement and simulation results for all the signals tabulated in Tables 3.7 and 3.8 are tabulated and illustrated in more detail in Appendix A.

Table 3.7: Important parameters of the actual and multi-tone signals for HMC481MP86 amplifier. Crest factor (Ψ), K, M and F parameters indicate whether the selected model is suitable or not.

	STIMULI G=19.3, IP3=30.8			**Ψ**	**K (x10^5)**	**F (x10^8)**	**M**
	m_1	m_2	m_3				
	Complex enveloped data			9.1	1.33	3.85	16.3
Model 1	1	0.4	0.1	5.9	1.31	1.88	16.0
Model 2	0.2	0.9	0.1	5.2	1.42	1.77	17.3
ModelHIGH	0.8	1	1	7.7	0.96	12.1	11.6
ModelLOW	0.1	1	0.05	4.2	1.42	1.18	17.3

Table 3.8: Important parameters of the actual and multi-tone signals for HMC372LP3 amplifier. Crest factor (Ψ), K, M and F parameters indicate whether the selected model is suitable or not.

	STIMULI G=15.6, IP3=35			**Ψ**	**K (x10^4)**	**F (x10^6)**	**M**
	m_1	m_2	m_3				
	Complex enveloped data			9.1	1.66	4.31	2.0
Model 1	1	0.4	0.1	5.9	1.80	2.11	2.2
Model 2	0.2	0.9	0.1	5.2	1.58	1.99	1.9
ModelHIGH	0.8	1	1	7.7	2.70	13.7	3.3
ModelLOW	0.1	1	0.05	4.2	1.40	1.33	1.7

Table 3.9: Measurement and ADS simulation results for actual and model signals for complex enveloped data for HMC481MP86. The parameters of Model 1 are m_1=1, m_2=0.4, m_3=0.1.

Input Power (dBm)	Complex Enveloped Data & Model 1 (measurement and simulation results in dBm)							
	Actual Signal				Model 1			
	Output Power		IMD		Output Power		IMD	
	Meas.	ADS	Meas.	ADS	Meas.	ADS	Meas.	ADS
-2	15.48	14.36	-9.70	-11.00	15.55	14.27	-8.50	-10.09
-6	12.32	11.72	-25.80	-25.35	12.34	11.81	-26.10	-24.60
-10	8.61	8.12	-38.60	-40.26	8.75	8.24	-38.50	-39.52
-14	4.66	4.22	-47.55	-53.87	4.59	4.34	-47.50	-53.11
-18	0.71	0.25	-57.10	-65.83	0.71	0.37	-56.55	-65.13
-22	-3.29	-3.75	-61.30	-77.64	-2.93	-3.63	-60.85	-77.16
-26	-7.14	-7.76	-65.70	-88.60	-7.12	-7.64	-65.30	-89.20
-30	-11.12	-11.73	-69.00	-96.85	-11.05	-11.60	-68.65	-101.11

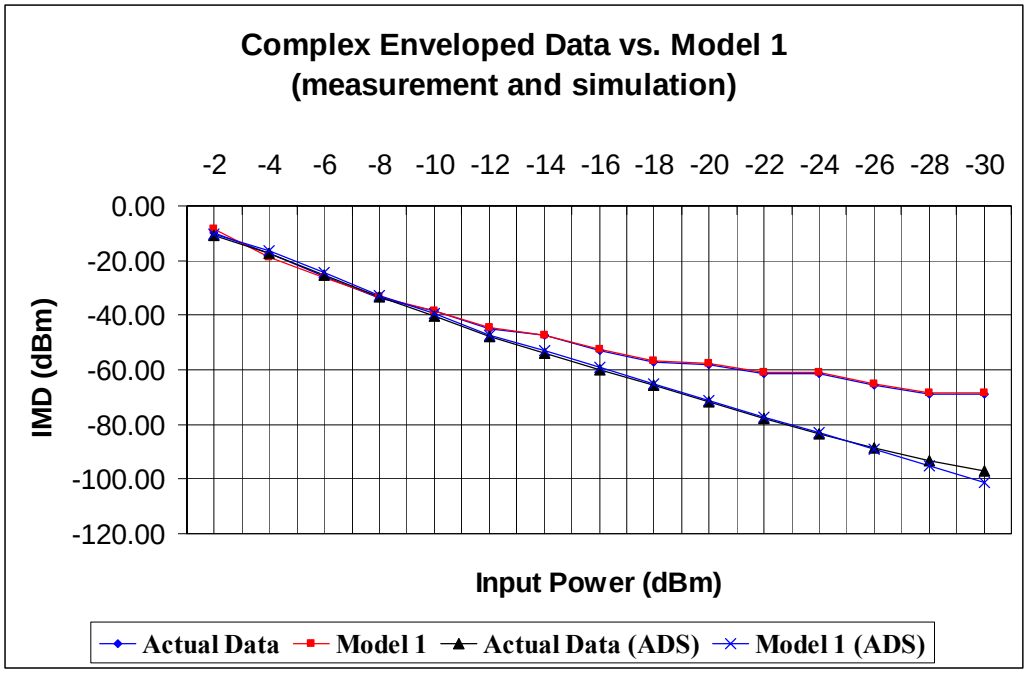

Figure 3.17: Measurement and simulation results for complex envelope signal and one of its multi-tone models (Model 1) for HMC481MP86. Simulation results are indicated by ADS expression in parenthesis.

Table 3.10: Measurement and ADS simulation results for actual and model signals for complex enveloped data for HMC372LP3. The parameters of Model 1 are m_1=1, m_2=0.4, m_3=0.1.

Input Power (dBm)	Real Enveloped Data & Model 1 (measurement and simulation results in dBm)							
	Actual Signal				Model 1			
	Output Power		IMD		Output Power		IMD	
	Meas.	ADS	Meas.	ADS	Meas.	ADS	Meas.	ADS
2	16.46	15.87	-14.18	-18.38	16.46	15.93	-13.35	-17.63
-2	13.02	12.42	-29.70	-36.41	13.11	12.53	-31.65	-35.66
-6	11.09	10.48	-39.65	-43.40	11.03	10.60	-41.75	-42.65
-10	7.18	6.51	-52.00	-55.47	6.93	6.63	-50.55	-54.73
-14	3.11	2.56	-56.50	-67.29	3.27	2.68	-56.00	-66.62
-18	-0.96	-1.44	-59.75	-78.79	-0.87	-1.32	-59.70	-78.64
-22	-4.92	-5.44	-63.20	-88.37	-4.75	-5.31	-63.00	-90.64
-26	-9.16	-9.44	-66.65	-94.62	-9.16	-9.32	-66.30	-102.64
-30	-13.16	-13.46	-73.20	-99.12	-13.21	-13.34	-72.80	-114.72

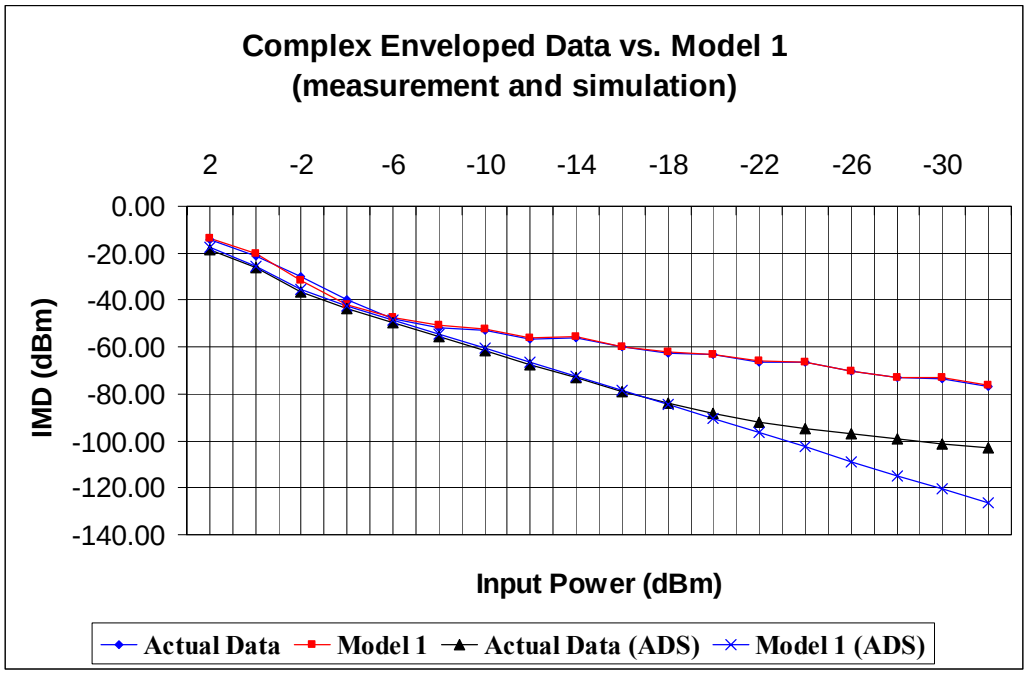

Figure 3.18: Measurement and simulation results for complex envelope signal and one of its multi-tone models (Model 1) for HMC372LP3. Simulation results are indicated by ADS expression in parenthesis.

CHAPTER 4

APPLICATION OF MULTI-TONE MODELING TO THE ANALYSIS OF A FEEDFORWARD SYSTEM

Feedforward systems are inherently complex and difficult to analyze analytically. Even if order of nonlinearity of both amplifiers is limited to three, the order of analysis is nine at the output of the error amplifier. In [7, 49], a feedforward system is analyzed for a CDMA signal assuming that CDMA signal can be replaced by Additive White Gaussian Noise (AWGN) under certain conditions. Not all signals, however, can be replaced by noise or suchlike equivalent signal. A general but simple model signal is required in order to analyze and estimate the final regime of the feedforward system under the stimulus of not well defined arbitrary signals. In this manner, application of multi-tone modeling to a feedforward system is also proposed by [7] as a simple and flexible way of analyzing complex systems like feedforward especially when stimulus is an arbitrary signal. Coskun [7] modeled feedforward system using multi-tone modeling concept without including phase mismatches in carrier cancellation and error cancellation loops. The proposed model has also been applied to real time signals and simulation results presented. In this work, we extend the analysis such that phase mismatches in both loops are included and apply this extended model to several real time signals. Moreover, parameter selection criteria, which are used to decide on the multi-tone models, are proposed. These criteria are defined and explained in detail in Chapter 3.

4.1 Modeling the feedforward system with phase mismatches

This section briefly describes the equations used to model the feedforward system with phase mismatches. Detailed derivation of the following equations is also presented in Appendix C. Figure 4.1 illustrates a generic feedforward system which will be used to track the derivation process of the equations used to model the feedforward system with phase mismatches. Coupler couplings are indicated by C_i, coupler losses by l_i, delay and phase in the first and second loops as τ_1, ϕ_1 and τ_2, ϕ_2 respectively. First loop will be referred to as carrier cancellation loop and the second loop as error cancellation loop throughout the text. The nonlinearities of the amplifiers are restricted to third order degree of nonlinearity.

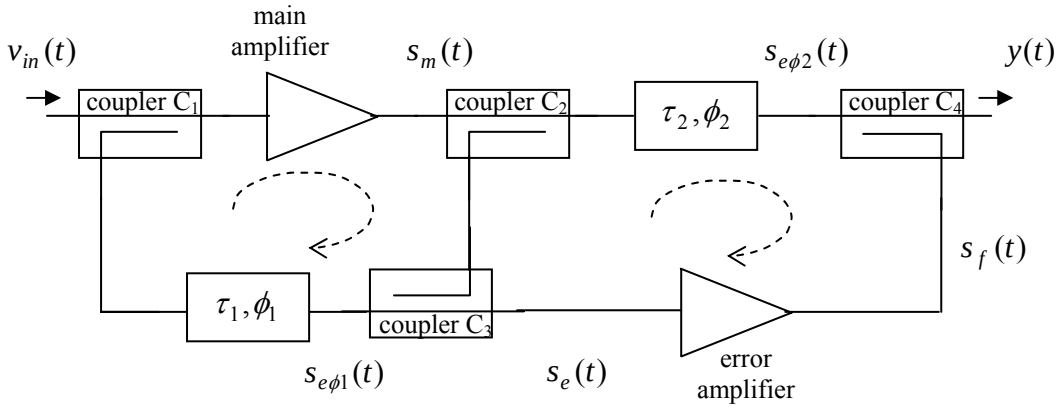

Figure 4.1: A generic feedforward system with components labeled as used in the derivation of the equations for feedforward system with phase mismatches.

A double-side banded signal with an arbitrary crest factor can be represented by a number of tones as explained in Chapter 3:

$$v_{in}(t) = v\left[\sum_{n=1}^{p} m_n \cos(n\omega_m t)\right]\cos(\omega t) \tag{4.1}$$

where ω_m and ω are the angular frequencies of the fundamental tone and the carrier, respectively. In this work, we assume that the multi-tone model is composed of in-phase evenly spaced tones and the amplitude of each tone (m_n) is a parameter that can be varied to control the properties of the multi-tone signal. The peak power,

mean power and crest factor of the signal specified in (4.1) can be found by using (3.10), (3.13) and (3.14) in Chapter 3 respectively.

V_{out} – V_{in} characteristic of a memoryless amplifier with third order nonlinearity can be expressed as a combination of linear and nonlinear terms as follows:

$$v_{out} = a_1 v_{in} + a_3 v_{in}^3 \tag{4.2}$$

In order to be able to compute v_{out}, we have to compute v_{in}^3 for the signal of the form (4.1). The resulting expression will again be in the form of (4.1) but now the number of tones will be three times as much as that of the input signal. Hence, the following expression can be written:

$$\left[\sum_{n=1}^{p} m_n \cos(n\omega_m t)\right]^3 = \left[\sum_{n=0}^{3p} m_n' \cos(n\omega_m t)\right] \tag{4.3}$$

Therefore, the expression at the output of the main amplifier with third order nonlinearity assumption can be expressed in terms of multitones as follows:

$$s_m(t) = \left[\sum_{n=0}^{3p} d_n \cos(n w_m t)\right] \cos(wt) \tag{4.4}$$

where

$$d_n = a_1 l_1 v m_n + \frac{3}{4} a_3 l_1^3 v^3 m_n^{(3)} \tag{4.5}$$

where power series coefficients a_1 and a_3 can be computed from gain and IP3 using equation (3.22). l_1 is the loss of the first coupler and is directly related to the coupling coefficient C_1. It can be computed using the following equality:

$$l_i = 10 * \log(1 - 10^{-C_i/10}) \tag{4.6}$$

$m_n^{(3)}$ in equation (4.5) can be computed using the generalization of (4.3):

$$\left[\sum_{n=1}^{p} m_n \cos(nw_m t)\right]^q = \sum_{n=0}^{pq} m_n^{(q)} \cos(nw_m t) \tag{4.7}$$

The output of the phase unit in the carrier cancellation loop (labeled as τ_1, ϕ_1) can be expressed as follows:

$$s_{e\phi 1}(t) = \frac{v}{C_1}\left[\sum_{n=1}^{p} m_n \cos(nw_m t)\right]\cos(wt + \phi_1) \tag{4.8}$$

Note that C_1 is the coupling of the coupler at the input of the feedforward system and also that the phase shift ϕ_1 is introduced to the carrier term.

The output of the main amplifier is sampled and subtracted from the output of the phase unit in the carrier cancellation loop and the following simplified expression is obtained at the input of the error amplifier:

$$s_e(t) = \left[\sum_{n=0}^{3p} (\alpha m_n + \beta m_n^{(3)})\cos(nw_m t)\right]\cos(wt) + \left[\sum_{n=0}^{3p} \mu m_n \cos(nw_m t)\right]\sin(wt) \tag{4.9}$$

where

$$\alpha = \frac{a_1 l_1 v}{C_2 C_3} - \frac{l_3 v \cos(\phi_1)}{C_1} \qquad \beta = \frac{3a_3 l_1^3 v^3}{4C_2 C_3} \qquad \mu = \frac{l_3 v \sin(\phi_1)}{C_1} \tag{4.10}$$

Note that the expression is still third order however contrary to the output of the single amplifier mentioned above it includes quadrature terms because of the phase mismatch introduced to the carrier (4.8).

The expression in (4.9) is applied to a third order nonlinear error amplifier. The resulting expression is ninth order and can be expressed as follows:

$$s_f(t) = b_1 s_e(t) + b_3 s_e^3(t) \tag{4.11}$$

where b_1 and b_3 are the power series coefficients defining the nonlinearity of the error amplifier. Like a_1 and a_3, they can be found from gain and IP3 of the error amplifier using using equation (3.22). which can be extracted and organized as follows:

$$s_f(t) = \left\{ \sum_{n=0}^{3p} (A_1 m_n + A_3 m_n^{(3)} + A_5 m_n^{(5)} + A_7 m_n^{(7)} + A_9 m_n^{(9)}) \cos(n w_m t) \right\} \cos(wt)$$

$$+ \left\{ \sum_{n=0}^{3p} (B_1 m_n + B_3 m_n^{(3)} + B_5 m_n^{(5)} + B_7 m_n^{(7)}) \cos(n w_m t) \right\} \sin(wt) \tag{4.12}$$

where

$$A_1 = b_1 \alpha$$

$$A_3 = b_1 \beta + \frac{3}{4} b_3 \left[\alpha^3 + \alpha \mu^2 \right]$$

$$A_5 = \frac{3}{4} b_3 \left[3\alpha^2 \beta + \beta \mu^2 \right]$$

$$A_7 = \frac{9}{4} b_3 \alpha \beta^2$$

$$A_9 = \frac{3}{4} \beta^3$$

$$B_1 = b_1 \mu$$

$$B_3 = \frac{3}{4} b_3 \left[\alpha^2 \mu + \mu^3 \right]$$

$$B_5 = \frac{3}{2} \alpha \beta \mu$$

$$B_7 = \frac{3}{4} b_3 \beta^2 \mu \tag{4.13}$$

The output of the main amplifier (4.4) is applied to a phase unit (labeled as τ_2, ϕ_2) and the following expression is obtained:

$$s_{e\phi 2}(t) = l_2 \left[\sum_{n=0}^{3p} d_n \cos(n w_m t) \right] \cos(wt + \phi_2) \tag{4.14}$$

where l_2 is the loss of the second coupler. Note that the phase term ϕ_2 is introduced to the carrier term. The output of the error amplifier (s_f) is subtracted from the output of the second phase unit ($s_{e\phi 2}$) at the coupler C_4 and the output of the feedforward system can be expressed as follows:

$$y(t) = l_4 s_{e\phi 2}(t) - \frac{s_f(t)}{C_4} \tag{4.15}$$

where l_4 is the loss and C_4 is the coupling of the output coupler. Note that the expression is of ninth order.

When $\phi_1 = \phi_2 = 0$, the equations describing the feedforward system with phase mismatches reduce to the following expressions:

$$s_m(t) = \sum_{n=0}^{3p} d_n \cos(n\omega_m t) \tag{4.16}$$

$$s_e(t) = \sum_{n=0}^{3p} e_n \cos(n\omega_m t) \tag{4.17}$$

$$s_f(t) = \sum_{n=0}^{3p} f_n \cos(n\omega_m t) \tag{4.18}$$

$$y(t) = \sum_{n=0}^{3p} y_n \cos(n\omega_m t) \tag{4.19}$$

where

$$d_n = a_1 l_1 v m_n + \frac{3}{4} a_3 l_1^3 v^3 m_n^{(3)} \tag{4.20}$$

$$e_n = \left[\frac{a_1 l_1}{C_2 C_3} - \frac{l_3}{C_1} \right] v m_n + \frac{3 a_3 l_1^3}{4 C_2 C_3} v^3 m_n^{(3)} \tag{4.21}$$

$$f_n = b_1 e_n + \frac{3}{4} b_3 e_n^3 \tag{4.22}$$

$$y_n = l_2 l_4 d_n - \frac{f_n}{C_4} \tag{4.23}$$

Calculation of $m_n^{(q)}$ in (4.7) requires calculation of very high orders depending on the order of nonlinearity of amplifiers. If order of nonlinearity is restricted to three, for instance, the expression at the output of the feedforward system requires the calculation of $m_n^{(q)}$ coefficients for q = 3, 5, 7 and 9. The

maximum value of q increases with the square of nonlinearity. In order to calculate these new coefficients a smart indexing technique is developed and used. This technique makes use of well known equalities in (4.24) and (4.25) to find the terms falling to multiples of Δw, the difference between fundamental tones.

$$\cos 2\theta = 2\cos^2 \theta - 1 \tag{4.24}$$

$$\cos\theta \cos\phi = 0.5\cos(\theta + \phi) + 0.5\cos(\theta - \phi) \tag{4.25}$$

In order to evaluate $m_n^{(3)}$, we first evaluate square of the expression of a baseband multi-tone signal:

$$\left[\sum_{n=1}^{p} m_n \cos(nw_m t)\right]^2 = \sum_{n=0}^{2p} m_n^{(2)} \cos(nw_m t) \tag{4.26}$$

then we multiply the result with the signal itself to get $m_n^{(3)}$:

$$\left[\sum_{n=1}^{p} m_n \cos(nw_m t)\right]^3 = \left(\sum_{n=0}^{2p} m_n^{(2)} \cos(nw_m t)\right)\left[\sum_{n=1}^{p} m_n \cos(nw_m t)\right] = \sum_{n=0}^{3p} m_n^{(3)} \cos(nw_m t) \tag{4.27}$$

Similarly, $m_n^{(5)}$ can be evaluated by simply multiplying (4.26) with (4.27). This procedure can be extended to find higher orders by simply multiplying the previously obtained multi-tone expression with (4.26) to obtain the next order provided that q is an odd number greater than one.

An m-file is used to calculate $m_n^{(2)}$ in MATLAB. This program (see Appendix B) makes use of (4.24) and (4.25) and calculates the coefficients at each $k.\Delta w$ frequency where k is a positive integer and Δw is the difference between frequencies of fundamental tones of a multi-tone signal. To find which fundamental tones contribute to the creation of which tones emerging after the multiplication process. To explain further, let's assume a generic four tone signal:

$$A\cos\theta + B\cos 2\theta + C\cos 3\theta + D\cos 4\theta \tag{4.28}$$

and multiply by itself:

$$(A\cos\theta + B\cos 2\theta + C\cos 3\theta + D\cos 4\theta)(A\cos\theta + B\cos 2\theta + C\cos 3\theta + D\cos 4\theta) \tag{4.29}$$

Multiplication process of the first term is illustrated above. First term is multiplied with each term inside second parenthesis. As a result of first multiplication a DC term and a term at 2θ frequency emerge. As a result of second multiplication a term at θ and a term at 3θ frequencies appear. With the same reasoning, each term in first parenthesis is multiplied by each term in the second parenthesis and finally contributions at each emerging frequency are summed up to form the amplitude value at that frequency. As a result, (4.26) is evaluated and then used to evaluate (4.27) in the similar way. Once more each term in (4.26) is multiplied by each term in the second parenthesis in (4.27) and final contributions at each frequency are summed up to find $m_n^{(3)}$. This method can be simply extended to find higher orders of $m_n^{(q)}$ provided that q is an odd number greater than one. We assumed a third order nonlinearity throughout this work, hence evaluated only $m_n^{(3)}$, $m_n^{(5)}$, $m_n^{(7)}$ and $m_n^{(9)}$. The m-files used to calculate these coefficients can be found in Appendix B.

4.2 Application of the model to real time signals

The multi-tone model proposed for feedforward system is applied to a feedforward circuit designed in Agilent Technologies Advanced Design System (ADS) and simulations for actual signals are carried in ADS environment. Multi-tone models, on the other hand, are formed in The MathWorks MATLAB and results for simulations with these model signals are obtained in MATLAB environment. The simulation setup and the properties of signals used are explained in the following discussion. Then, the results are presented.

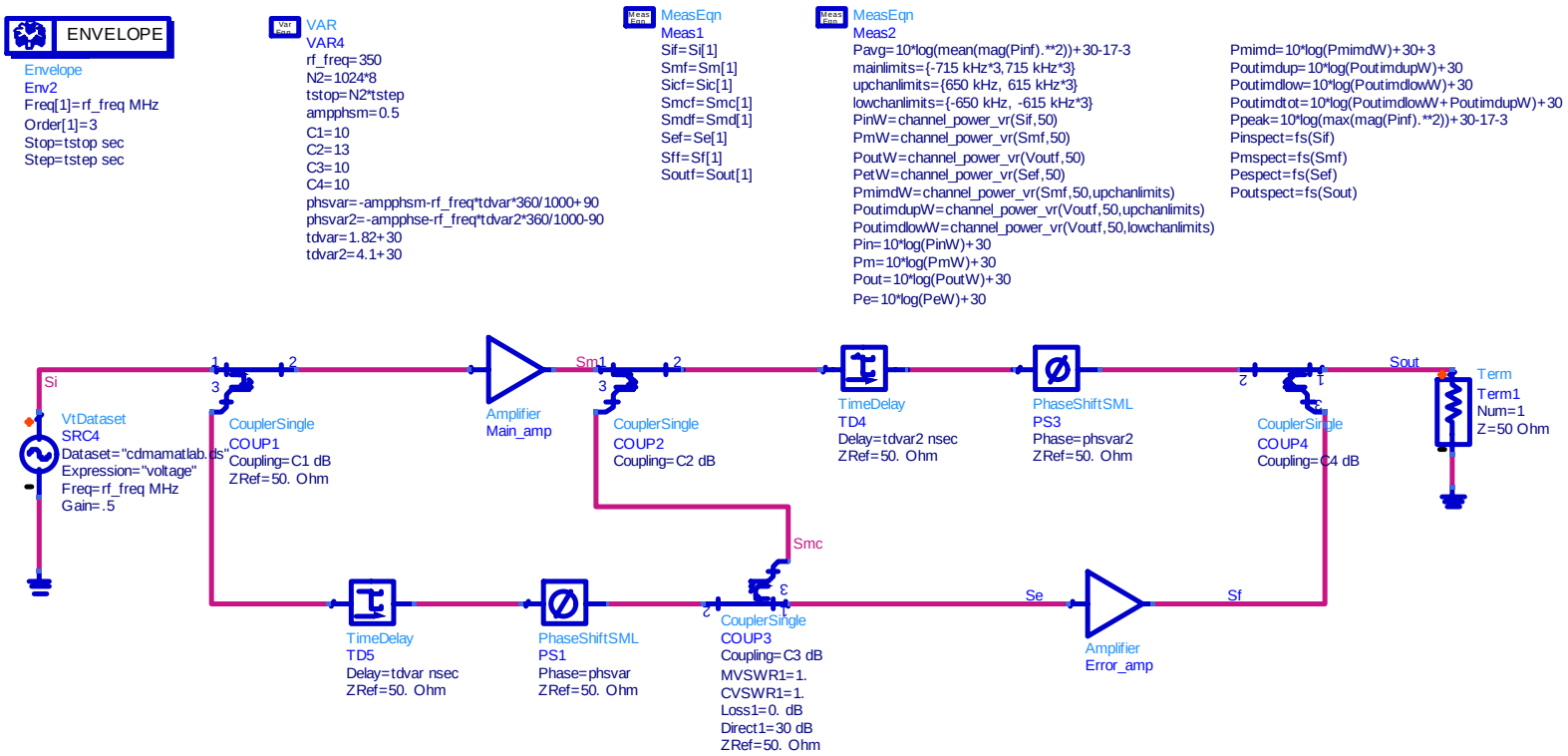

Figure 4.2: Schematic of the feedforward system in ADS envelope simulation environment.

4.2.1 Simulation setup

In this work, two programs are employed for verification of the model: Agilent Technologies' Advanced Design System (ADS) and The MathWorks' MATLAB. A feedforward circuit shown in Figure 4.2 is formed in ADS environment. This circuit is used in two different configurations. In the first configuration, main and error amplifiers are real amplifiers designed using SPICE models. The main amplifier is designed using SEMELAB D2001UK RF power transistor. Its linear gain (G_m), IP3 ($IP3^m$) and delay are measured to be 13.1 dB, 32 dBm and 1.8 nsec, respectively, for a gate voltage of 2.6V at 350 MHz. The error amplifier is a two stage amplifier, designed using SEMELAB D2019UK RF power transistors, such that it's linear gain (G_e), IP3 ($IP3^e$) and delay are 33.4 dB, 36 dBm and 4.1 nsec, respectively, for a gate voltage of 2.6V at 350 MHz. The AM-AM and AM-PM curves at 350 MHz are illustrated in Figures 4.3 and 4.4 for main and error amplifiers respectively.

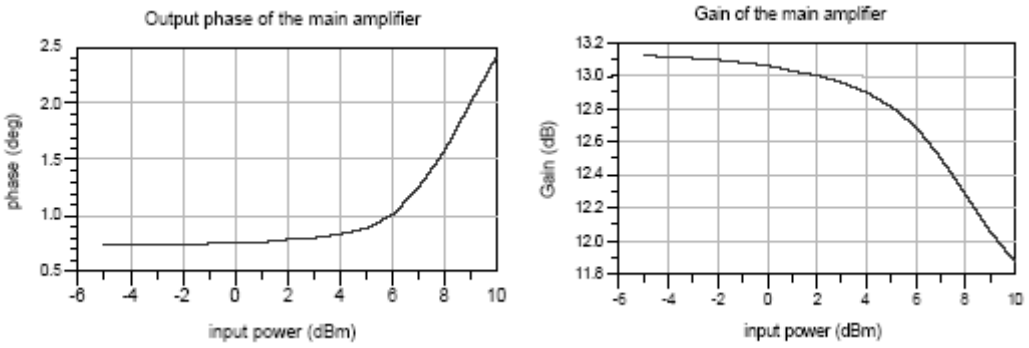

(a) **(b)**

Figure 4.3: a) AM-PM (phase) **b)** AM-AM (gain) characteristic of the main amplifier at 350 MHz.

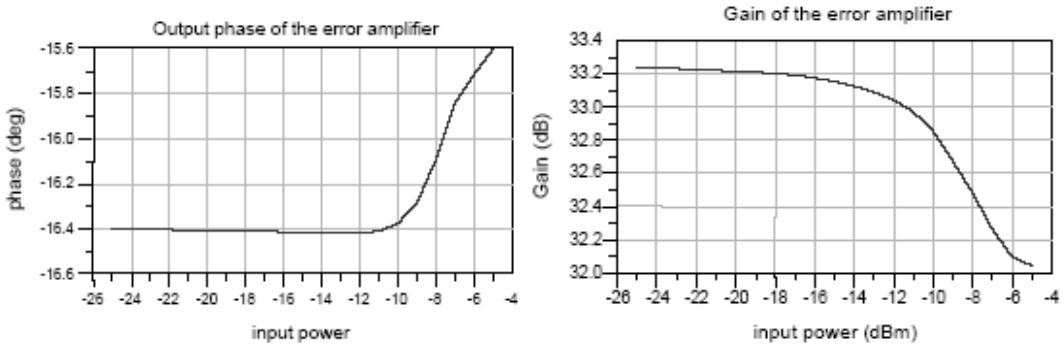

(a) **(b)**

Figure 4.4: a) AM-PM (phase) **b)** AM-AM (gain) characteristic of the error amplifier at 350 MHz.

In the second configuration, real amplifiers are replaced by system amplifiers. Gain and third order intercept point of real amplifiers are used to specify the characteristic of system amplifiers. The order of nonlinearity is limited to three; hence only gain and IP3 values are enough to fully specify the system amplifiers. Simulation results for both system and real amplifiers are obtained. Main amplifier and error amplifier subcircuits used with actual amplifier SPICE models are illustrated in Figures 4.5 and 4.6 respectively. Couplings of the couplers are chosen such that error amplifier gain is reduced and their nominal values for this configuration are 10 dB for C_1, C_3 and C_4, and 13 dB for C_2.

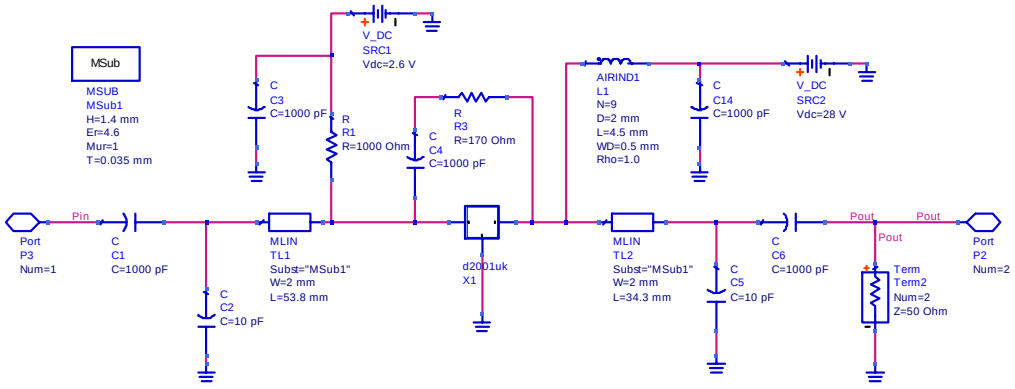

Figure 4.5: Schematic of the main amplifier subcircuit. SPICE model of SEMELAB D2001UK RF power transistor is used.

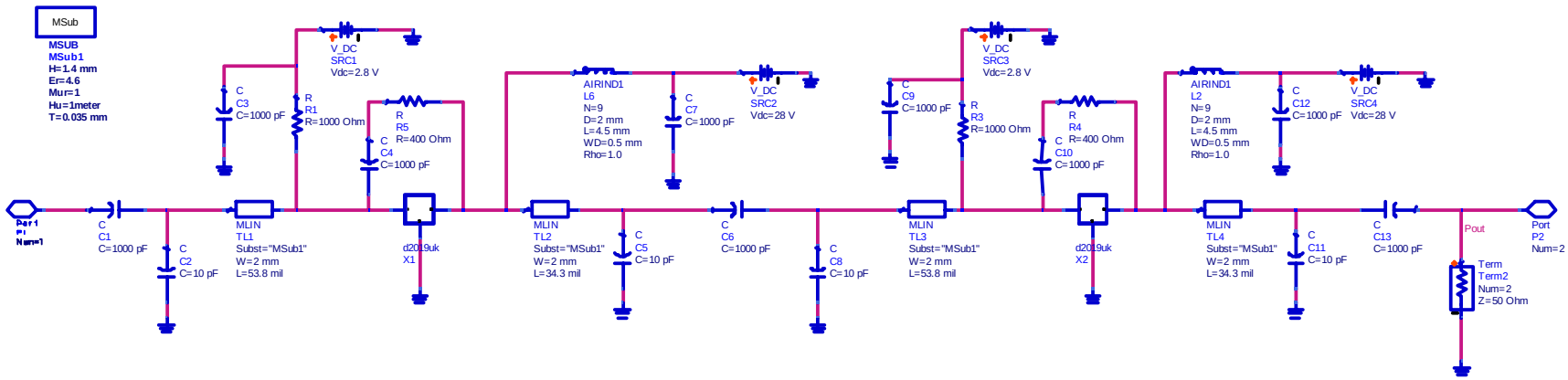

Figure 4.6: Schematic of the error amplifier subcircuit which is composed of two amplifier stages. SPICE model of SEMELAB D2019UK RF power transistor is used.

In order to measure spectral regrowth and adjacent channel power with digitally modulated RF signals at the input, ADS uses RF envelope simulation toolbox which uses some predefined functions to monitor the power spectra and calculate the main channel or adjacent channel powers. Envelope simulator requires that the center, stop and step frequencies and order of the simulation is defined by the user. The spectrum and channel power are obtained using some predifined measurement functions. The spectrum of the signal at a specified node is computed using the function *fs(node_f)* where *node_f* represents the voltage at the specified node at the fundamental frequency. Function *fs* performs time-to-frequency trnsform and can be used with different types of windowing such as rectangular, Keiser, Hanning or Hamming. In this work, we use Hanning window with a window constant of 0.5. The power of the signal at the fundamental frequency and adjacent channels is calculated in Watts using the function *channel_power_vr(node_f, 50, limits, window type)* where *node_f* is the voltage at the specified node and the load resistance is selected to be 50 Ohms. The power is calculated inside the limits specified by the index *limits*. Window type can also be defined by simply writing the name of the window. In order to measure the power of one of the adjacent channels for a third order system, limits are defined as B and 3B where B is the baseband bandwidth of the input data.

Real enveloped input signals are stored in time versus voltage format as *.tim* file. Using the File/Instrument server menu in the schematic, .tim formatted file is converted to a different format, namely *.mdif*. The new dataset (.ds) is used in the component palette *VtDataset* as a source file for our system. Complex enveloped signals, on the other hand, are stored in *.ascsig* format as complex voltage (I+jQ) and converted to (.ds) files using the same palette.

The same feedforward system is adapted to MATLAB environment using the equations describing feedforward system (see APPENDIX B). Then, we computed output power and adjacent channel power at each node of the circuit for multi-tone models used as stimuli and compared the results to the actual signal results obtained in ADS environment. MATLAB results are scaled by adding 26.5 dB (10xlog10(451.8)) in order to compensate for resolution bandwidth (RBW) of 451.8 Hz used in ADS measurements. The RBW is specified by the sampling

period (T_s) and the number of samples (N_{points}) used in calculation of the FFT in simulation environment. The RBW of the power spectrum is $1/(N_{points} \times T_s)$ = 1/(8192 x 0.27 usec) which is equal to 451.8 Hz. Actual signal results obtained in ADS environment and multi-tone model signals' results obtained in MATLAB environment are compared in order to verify the multi-tone model and expressions derived for feedforward circuit.

4.2.2 Simulation results

There are four different stimuli used to verify multi-tone modeling in feedforward system. The basic properties of these signals are tabulated in table 4.1. Signal 1 is a real enveloped signal generated using *rand* function in MATLAB. Signal 2 is a narrowband complex enveloped signal generated in a similar way. Signals 3 and 4 are respectively narrowband and wideband CDMA signals generated by ADS CDMA design file.

Table 4.1: The basic properties of the actual signals used in simulation are shown.

Label	**Type**	**Form**	**# of samples**	**Bandwidth (MHz)**	**Ψ (dB)**
Signal1	Real enveloped	Random	8192	5	7.55
Signal2	Complex enveloped	Random	8192	1.8	9.10
Signal3	Complex enveloped	IS-95	8192	1.23	6.12
Signal4	Complex enveloped	Widecdma	16384	16	6.50

The actual signals are used as input to the feedforward system in ADS environment and results are compared to the results obtained for multi-tone models in MATLAB. ADS simulation results for both system amplifiers and actual amplifiers are included. Multi-tone models are selected by considering the peak-to-average and parameter selection criteria proposed in Chapter 3. The F parameter for

complex enveloped actual signals is scaled such that it becomes equal to the F parameter of an empirically found multi-tone model. Hence, whenever a new multi-tone model is required for a complex enveloped signal, F parameter can be directly used to decide.

I. Signal 1

Signal 1 is a real enveloped signal which has been generated at a sampling rate of 60 nsec using *rand* function in MATLAB. It consists of 8192 samples and has a bandwidth of 5 MHz. The peak-to-average ratio of the signal is 7.55 dB. The instantaneous peak power waveform and the envelope histogram are illustrated in Figure 4.7. Note that the peaks in the instantaneous peak power plot occur randomly and rarely. The peak-to-average values in the histogram plot of the signal have an almost uniform distribution up to around 5.5 dB where a peak occurs. However, the number of samples drastically decreases as the peak-to-average value is increased. Although there are few samples with such a high peak-to-average value, these are well enough to drive the amplifier into nonlinearity. Multi-tone signals, on the other hand, are periodic deterministic signals whose maximum peaks occur periodically. Hence, a multi-tone signal will potentially drive the amplifier more than the actual signal with the same peak-to-average value. Ideally, a designer's aim is to model the signal with another signal of the same peak-to-average histogram; however, this is nothing but creating the signal itself. Instead, we employ easy to generate signals such as multi-tone signals which imitate the response of the actual signal. As a result of periodicity, however, a multi-tone model will always have a lower peak-to-average value than that of the actual signal. Peak-to-average value of signal 1 is 7.55 dB and simulation results for P_{main}, $P_{mainacp}$, P_{out} and P_{outacp} are 17.08 dBm, -11.18 dBm, 17.12 dBm and -30.50 dBm respectively for nominal coupler coupling values (C_1=C_3= C_4=10 dB, C_2=13 dB). K, M and F parameters for this signal are 5337, 0.65 and 6.7×10^5 respectively. Table 4.2 tabulates the model selection parameters for multi-tone signals with various

peak-to-average values ranging from 7.46 down to 4.65 dB. Results indicate that the multi-tone signal with a peak-to-average value of 6.32 dB models the actual signal well, since the parameters K, M and F match with those of Signal 1. Note that peak-to-average value of this signal is more than 1 dB lower than that of the actual signal as expected. For this multi-tone model (m_1=0.9, m_2=0.55, m_3=0.1) simulation (system and real amplifiers) and model results are compared by sweeping the system parameters C_1, C_2, C_3, C_4, ϕ_1 and ϕ_2. The results are illustrated in Figures 4.8-4.11. System and real amplifier results are indicated on the figures. Real amplifiers are formed using SPICE models supplied by the producer. Figure 4.11 illustrates phase sweep for both first phase unit (ϕ_1) and the second phase unit (ϕ_2) in one figure. Note that model and simulation results coincide with each other. Results for multi-tone model are closer to the simulation results for system amplifiers rather than the simulation results for real amplifiers. This is a consequence of the fact that the results for system amplifiers and model are obtained for constant gain and third order intercept point, whereas, the gain and IP3 of the actual amplifiers vary with amplitude and frequency leading to both phase and delay mismatch in the carrier and error cancellation loops. This phenomenon is more remarkable when the bandwidth of the signal is increased as in the case of signal 4.

Figure 4.8 illustrates the main channel and adjacent channel output power as coupling of the coupler C_1 is swept from 8-12 dB. The result indicates that the optimum coupling value in terms of IMD is around 9 dB. Note that the effect of C_1 vanishes beyond 10 dB coupling value. Figure 4.9 illustrates the sweep results for C_3 and exhibits a similar characteristic. The optimum value is reached at 10.5 dB coupling value. C_3 has a more drastic effect on the final distortion cancellation performance because error signal is formed in this coupler via subtraction. Figure 4.10 illustrates the sweep results for C_4. The optimum value is reached at 11 dB coupling. C_4 is the final component in a feedforward system and directly affects the performance of the system. Unless the coupler coupling is chosen properly, the distortion signal amplified at error amplifier cannot cancel out the distortion products added by the main amplifier. Note that, at the optimum coupler coupling values results for real amplifier configuration deviate from the results of system

amplifier configuration and multi-tone model. This indicates that around these regions, where the cancellation performance is extremely high, the main and error amplifiers shall be modeled more accurately in order to follow the real amplifier results. Figure 4.11 illustrates the adjacent channel output power results for different phase mismatches introduced into carrier and error cancellation loops. Note that up to 10˚ of phase mismatch in the first loop (ϕ_1) is tolerated by the system, whereas, a phase mismatch in the second loop directly affects the adjacent channel power. The results for real amplifiers again deviate from the results for system amplifiers and multi-tone model; however, the trends coincide with each other.

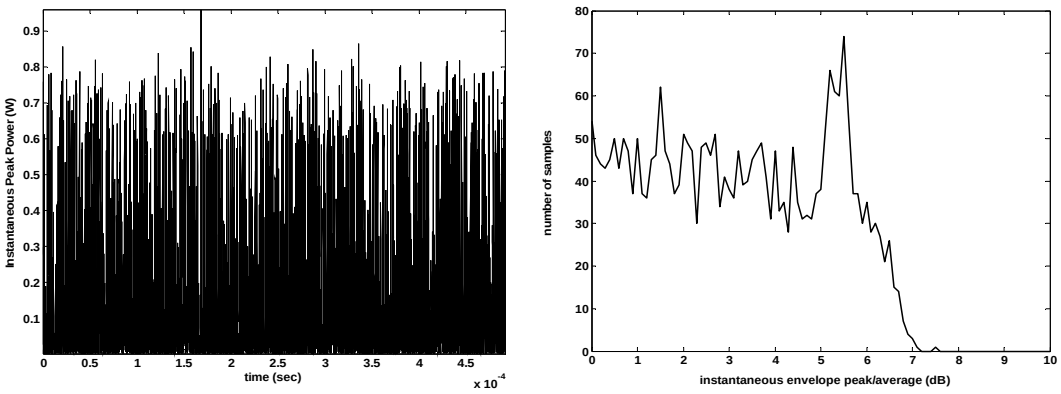

Figure 4.7: a) Instantaneous peak power waveform. **b)** Instantaneous envelope peak-to-average histogram

Table 4.2: Different multi-tone sets for signal 1 obtained for C_1=C_3=C_4=10 dB, C_2=13 dB, $IP3^m$=32 dBm, $IP3^e$=36 dBm, G_m=13.1 dB, G_e=33.4 dB.

m_1	m_2	m_3	Ψ (dB)	K	M	F ($x10^5$)	P_{main} (dBm)	$P_{mainacp}$ (dBm)	P_{out} (dBm)	P_{outacp} (dBm)
0.7	0.35	0.5	7.46	6794	0.82	18.7	16.77	-6.74	17.23	-28.68
0.55	0.35	0.15	6.93	5954	0.72	10.7	16.93	-9.17	17.23	-29.94
0.9	0.55	0.1	6.32	5168	0.63	6.1	17.08	-11.63	17.22	-31.47
0.6	0.2	0.1	5.97	4804	0.58	4.0	17.15	-13.43	17.21	-33.02
0.9	0.1	0.1	4.65	4036	0.49	0.7	17.29	-21.25	17.20	-40.21

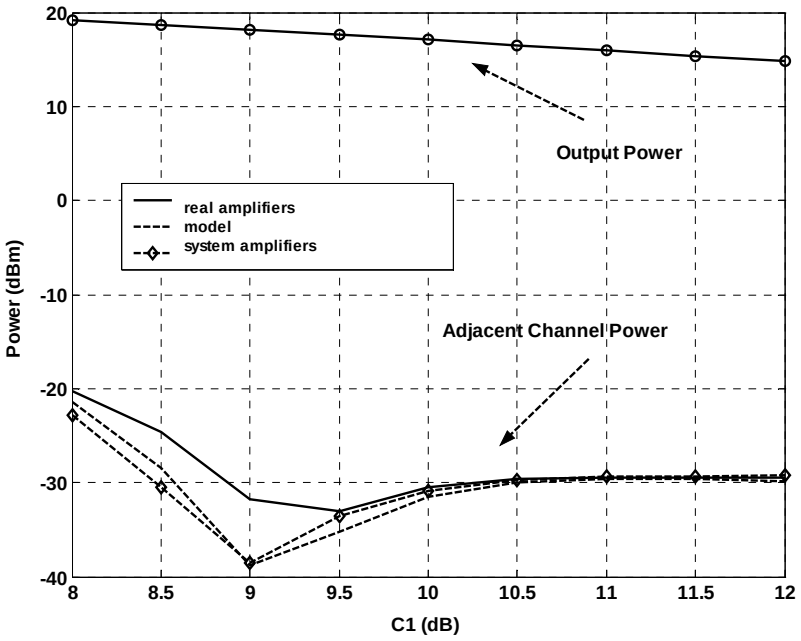

Figure 4.8: Feedforward output power and ACP for various C_1 – m_1=0.9, m_2=0.55, m_3=0.1 – C_2=13, C_3=C_4=10, G_m=13.1 dB, $IP3^m$=32 dBm, G_e=33.4 dB, $IP3^e$=36 dBm.

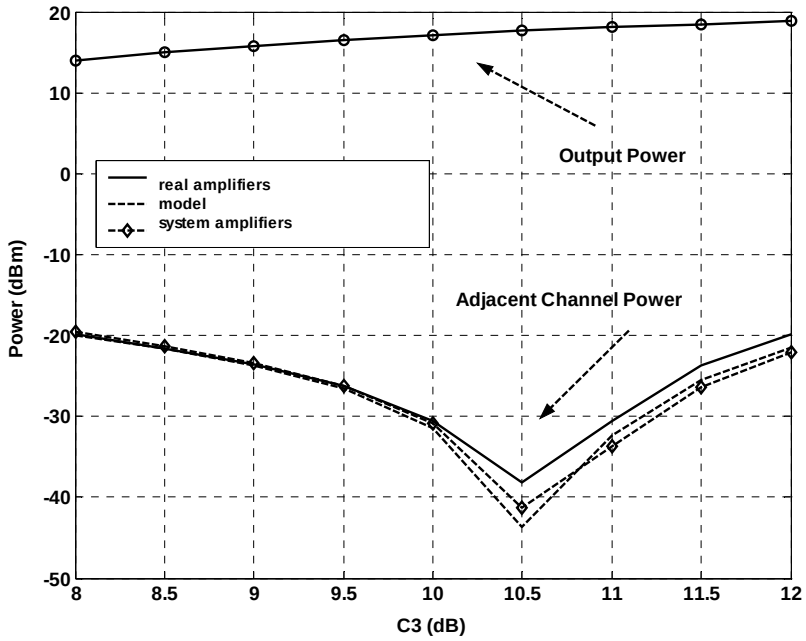

Figure 4.9: Feedforward output power and ACP for various C_3 – m_1=0.9, m_2=0.55, m_3=0.1 – C_2=13, C_1=C_4=10, G_m=13.1 dB, $IP3^m$=32 dBm, G_e=33.4 dB, $IP3^e$=36 dBm.

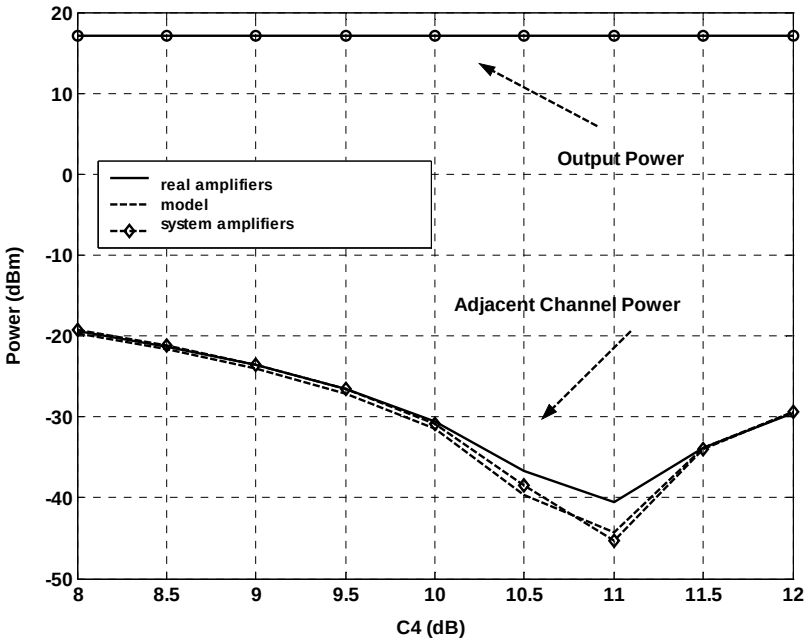

Figure 4.10: Feedforward output power and ACP for various C_4 – m_1=0.9, m_2=0.55, m_3=0.1 – C_2=13, C_1=C_3=10, G_m=13.1 dB, $IP3^m$=32 dBm, G_e=33.4 dB, $IP3^e$=36 dBm.

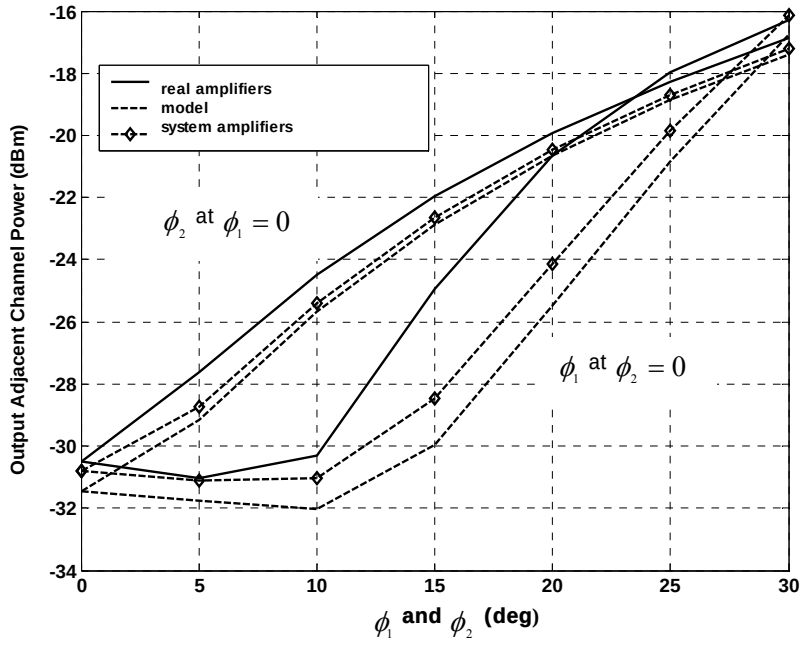

Figure 4.11: Feedforward output power and ACP for various phase mismatches ϕ_1 and ϕ_2 – m_1=0.9, m_2=0.55, m_3=0.1 – C_2=13, C_1=C_3=C_4=10, G_m=13.1 dB, $IP3^m$=32 dBm, G_e=33.4 dB, $IP3^e$=36 dBm.

II. Signal 2

Signal 2 is a complex enveloped signal which was formed using 'rand' function in Matlab. It consists of 8192 samples, has a bandwidth of 1.8 MHz and Ψ of 9.1 dBm. The instantaneous peak power waveform and the envelope histogram are illustrated in Figure 4.12. Table 4.3 tabulates multi-tone signals with various peak-to-average values from 7.01 down to 4.13 dB. Simulation results for P_{main}, $P_{mainacp}$, P_{out} and P_{outacp} are 17.28 dBm, -13.01 dBm, 17.17 dBm and -32.27 dBm respectively for nominal coupler coupling values (C_1=C_3= C_4=10 dB, C_2=13 dB). K, M and F parameters for this signal are 4666, 0.53 and $8x10^5$ respectively. For multi-tone model (m_1=1, m_2=0.4, m_3=0.1) simulation (system and real amplifiers) and model results are compared by sweeping the system parameters C_1, C_2, C_3, C_4, ϕ_1 and ϕ_2. The results are illustrated in Figures 4.13-4.16.

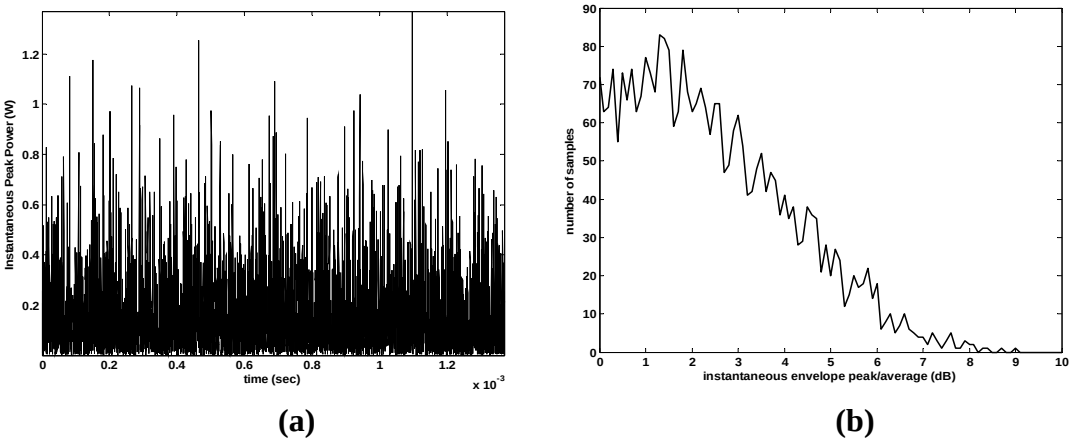

Figure 4.12: a) Instantaneous peak power waveform. **b)** Instantaneous envelope peak-to-average histogram.

Table 4.3: Different multi-tone sets for signal 2 obtained for C_1=C_3=C_4=10 dB, C_2=13 dB, $IP3^m$=32 dBm, $IP3^e$=36 dBm, G_m=13.1 dB, G_e=33.4 dB.

m_1	m_2	m_3	Ψ (dB)	K	M	F ($x10^5$)	P_{main} (dBm)	$P_{mainacp}$ (dBm)	P_{out} (dBm)	P_{outacp} (dBm)
0.5	0.7	0.2	7.01	6300	0.76	12.3	16.91	-8.79	17.23	-29.80
0.1	0.35	0.1	6.28	5132	0.62	7.1	17.12	-11.18	17.21	-30.94
1	0.4	0.1	5.85	4782	0.58	3.9	17.18	-13.76	17.21	-33.19
0.5	0.1	0.1	5.60	4815	0.58	2.7	17.18	-15.43	17.21	-34.79
0.7	0.05	0.05	4.13	3906	0.48	0.3	17.33	-25.56	17.19	-44.42

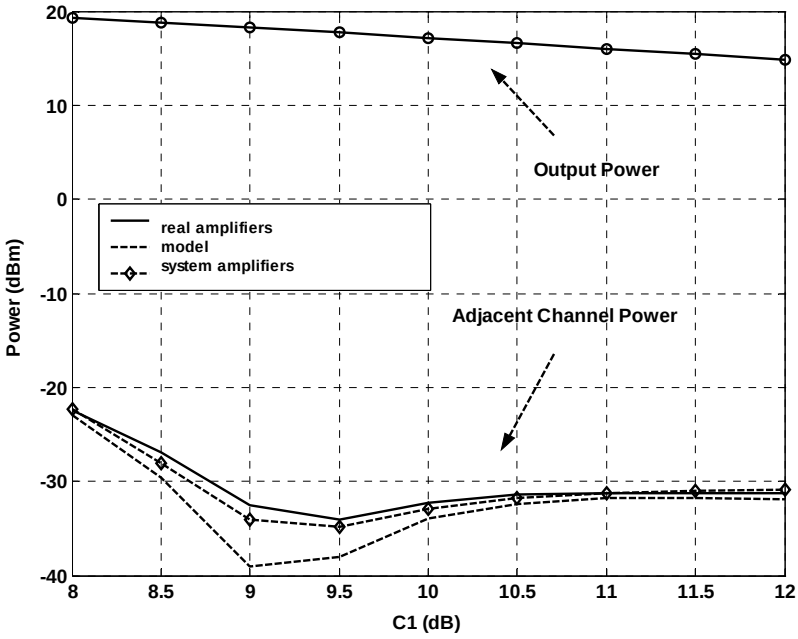

Figure 4.13: Feedforward output power and ACP for various C_1 – m_1=1, m_2=0.4, m_3=0.1 – C_2=13, C_3=C_4=10, G_m=13.1 dB, $IP3^m$=32 dBm, G_e=33.4 dB, $IP3^e$=36 dBm.

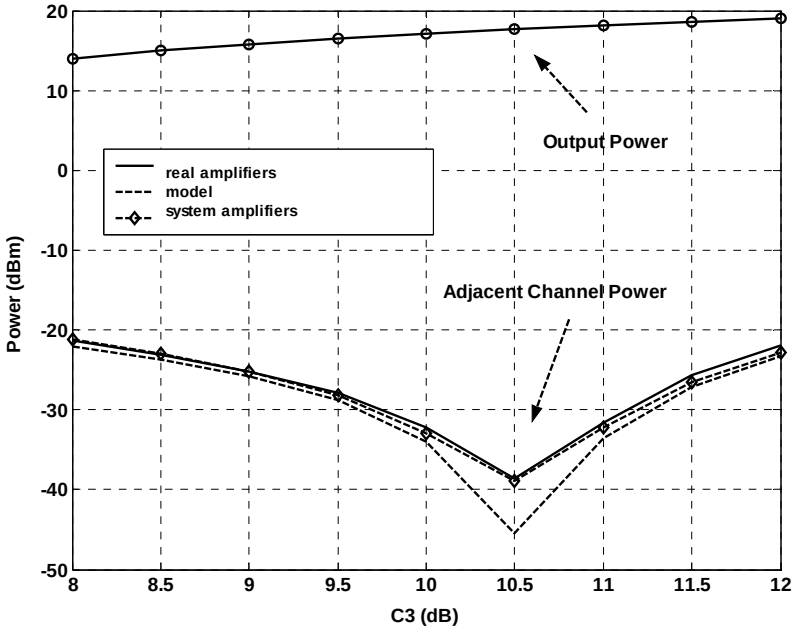

Figure 4.14: Feedforward output power and ACP for various C_3 – m_1=1, m_2=0.4, m_3=0.1 – C_2=13, C_1=C_4=10, G_m=13.1 dB, $IP3^m$=32 dBm, G_e=33.4 dB, $IP3^e$=36 dBm.

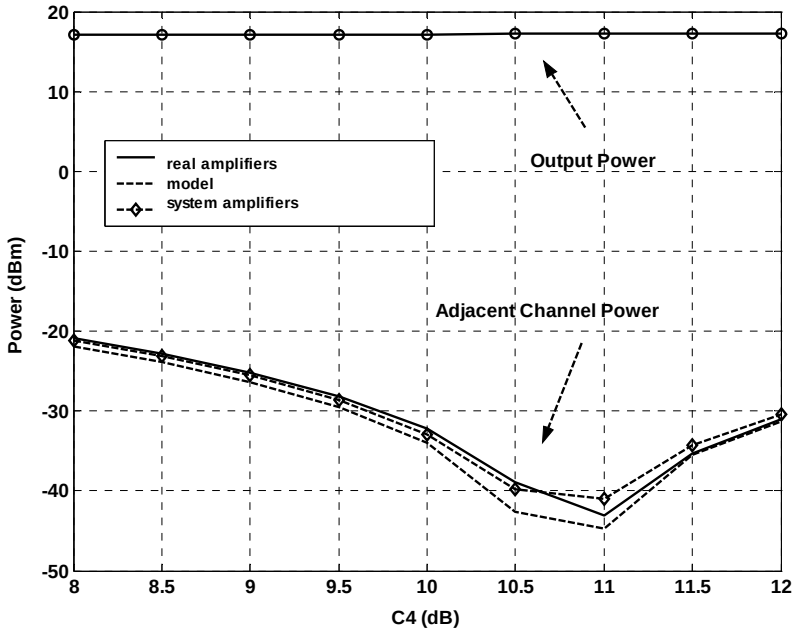

Figure 4.15: Feedforward output power and ACP for various C_4 – m_1=1, m_2=0.4, m_3=0.1 – C_2=13, C_1=C_3=10, G_m=13.1 dB, $IP3^m$=32 dBm, G_e=33.4 dB, $IP3^e$=36 dBm.

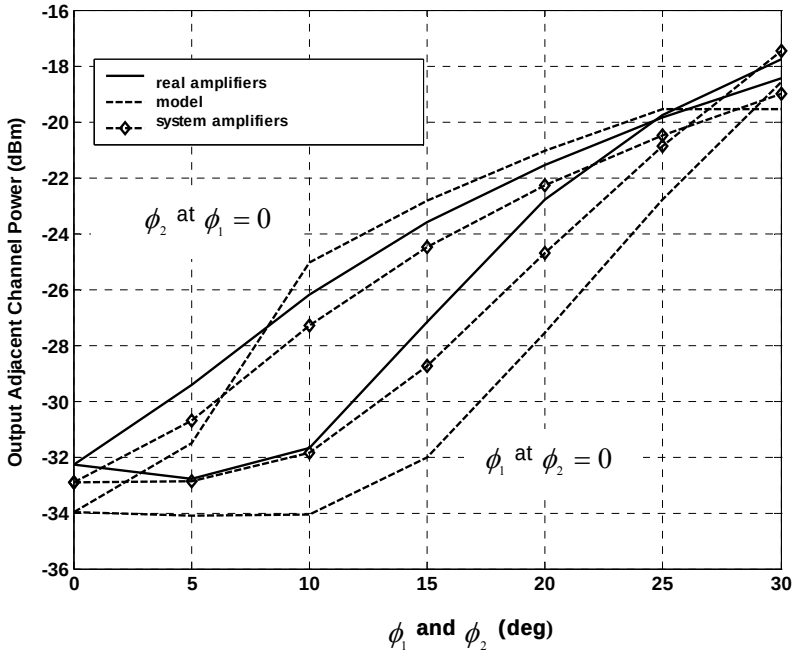

Figure 4.16: Feedforward output power and ACP for various phase mismatches ϕ_1 and ϕ_2 – m_1=1, m_2=0.4, m_3=0.1 – C_2=13, C_1=C_3=C_4=10, G_m=13.1 dB, $IP3^m$=32 dBm, G_e=33.4 dB, $IP3^e$=36 dBm.

III. Signal 3

Signal 3 is a complex enveloped signal which was formed using ADS CDMA design file. It consists of 8192 samples, has a bandwidth of 1.23 MHz and Ψ of 6.12. The instantaneous peak power waveform and the envelope histogram are illustrated in Figure 4.17. Table 4.4 tabulates multi-tone signals with various peak-to-average values from 7.07 down to 3.82 dB. Simulation results for P_{main}, $P_{mainacp}$, P_{out} and P_{outacp} are 17.47 dBm, -14.50 dBm, 17.17 dBm and -33.18 dBm respectively for nominal coupler coupling values (C_1=C_3= C_4=10 dB, C_2=13 dB). K, M and F parameters for this signal are 3301, 0.38 and 3.8×10^5 respectively. For multi-tone model (m_1=0.1, m_2=1, m_3=0.05) simulation (system and real amplifiers) and model results are compared by sweeping the system parameters C_1, C_2, C_3, C_4, ϕ_1 and ϕ_2. The results are illustrated in Figures 4.18-4.21. System and real amplifier results are indicated on the figures.

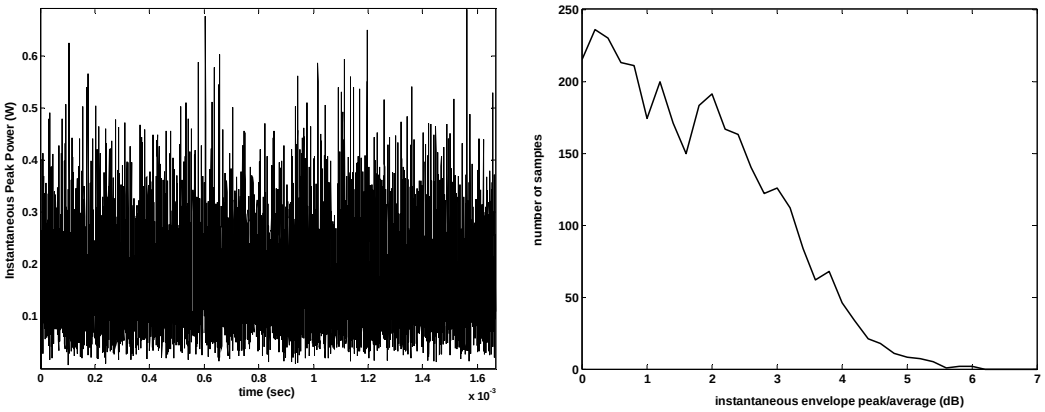

(a) **(b)**

Figure 4.17: a) Instantaneous peak power waveform. **b)** Instantaneous envelope peak-to-average histogram.

Table 4.4: Different multi-tone sets for signal 3 obtained for C_1=C_3=C_4=10 dB, C_2=13 dB, $IP3^m$=32 dBm, $IP3^e$=36 dBm, G_m=13.1 dB, G_e=33.4 dB.

m_1	M_2	m_3	Ψ (dB)	K	M	F ($x10^5$)	P_{main} (dBm)	$P_{mainacp}$ (dBm)	P_{out} (dBm)	P_{outacp} (dBm)
1	0.3	0.9	7.07	6591	0.80	16.0	16.85	-7.60	17.23	-28.27
0.1	0.4	0.7	6.40	5115	0.62	10.5	17.12	-9.45	17.21	-29.02
0.1	1	0.05	4.17	3667	0.45	2.5	17.37	-15.73	17.19	-34.18
0.05	1	0.05	3.82	3589	0.44	2.3	17.38	-16.02	17.19	-34.43
0.2	0.9	-	4.54	3795	0.46	2.8	17.34	-14.07	17.19	-32.62

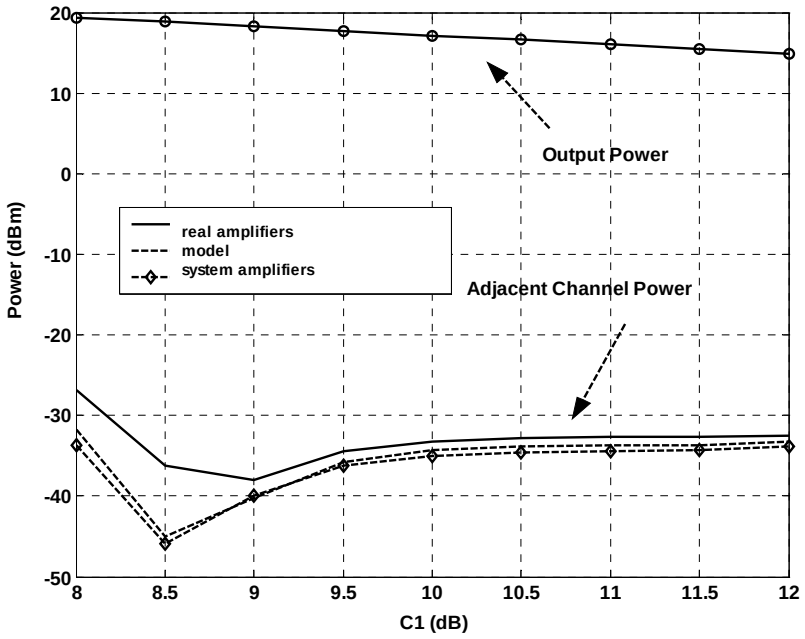

Figure 4.18: Feedforward output power and ACP for various C_1 – m_1=0.1, m_2=1, m_3=0.05 – C_2=13, C_3=C_4=10, G_m=13.1 dB, $IP3^m$=32 dBm, G_e=33.4 dB, $IP3^e$=36 dBm.

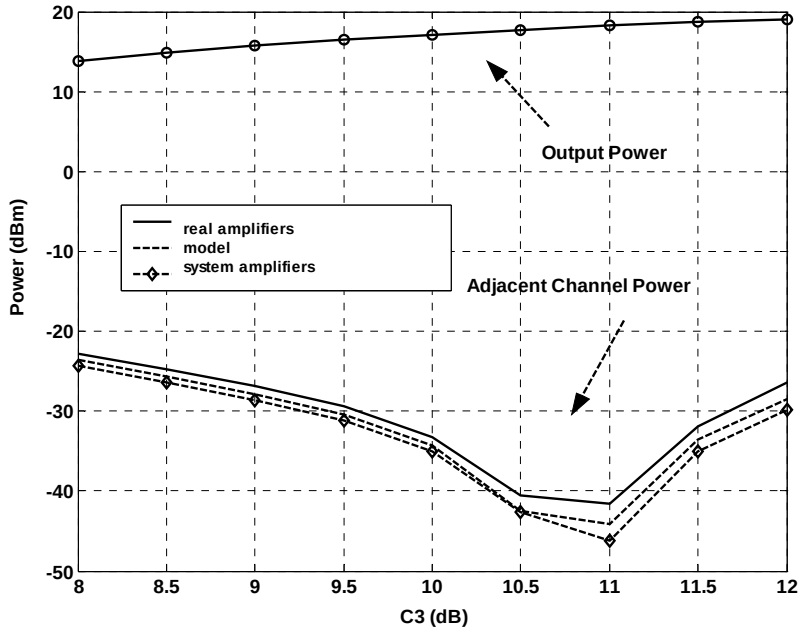

Figure 4.19: Feedforward output power and ACP for various C_3 – m_1=0.1, m_2=1, m_3=0.05 – C_2=13, C_1=C_4=10, G_m=13.1 dB, $IP3^m$=32 dBm, G_e=33.4 dB, $IP3^e$=36 dBm.

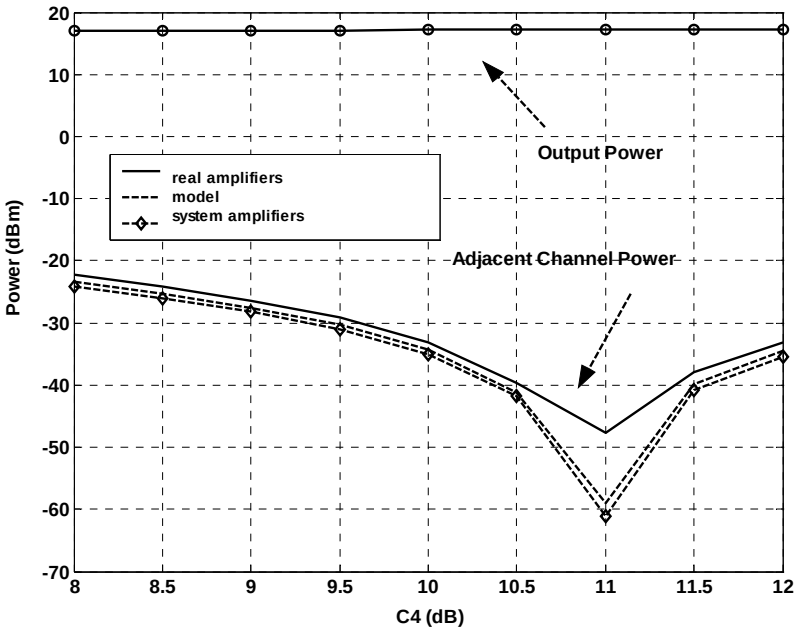

Figure 4.20: Feedforward output power and ACP for various C_4 – m_1=0.1, m_2=1, m_3=0.05 – C_2=13, C_1=C_3=10, G_m=13.1 dB, $IP3^m$=32 dBm, G_e=33.4 dB, $IP3^e$=36 dBm.

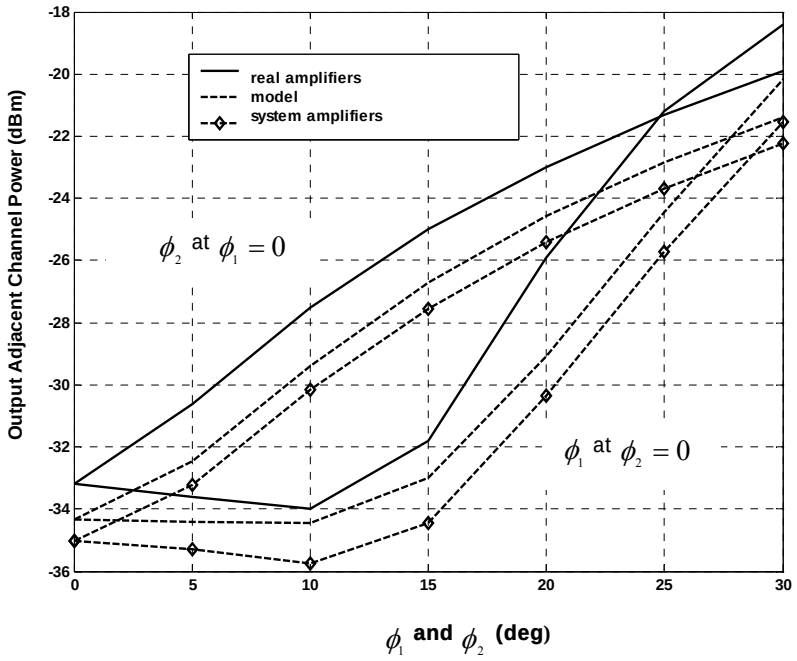

Figure 4.21: Feedforward output power and ACP for various phase mismatches ϕ_1 and ϕ_2 – m_1=0.1, m_2=1, m_3=0.05 – C_2=13, C_1=C_3=C_4=10, G_m=13.1 dB, $IP3^m$=32 dBm, G_e=33.4 dB, $IP3^e$=36 dBm.

IV. Signal 4

Signal 4 is a complex enveloped signal which was formed using ADS CDMA design file. It consists of 16384 samples, has a bandwidth of 16 MHz and Ψ of 6.5. The instantaneous peak power waveform and the envelope histogram are illustrated in Figure 4.22. Table 4.4 tabulates multi-tone signals with various peak-to-average values from 7.90 down to 4.19 dB. Simulation results for P_{main}, $P_{mainacp}$, P_{out} and P_{outacp} are 17.42 dBm, -17.10 dBm, 17.15 dBm and -35.60 dBm respectively for nominal coupler coupling values (C_1=C_3= C_4=10 dB, C_2=13 dB). K, M and F parameters for this signal are 6731, 0.39 and $1.6x10^6$ respectively. For multi-tone model (m_1=0.9, m_2=0, m_3=0, m_4=0.3) simulation (system and real amplifiers) and model results are compared by sweeping the system parameters C_1, C_2, C_3, C_4, ϕ_1 and ϕ_2. The results are illustrated in Figures 4.23-4.26. System and real amplifier results are indicated on the figures.

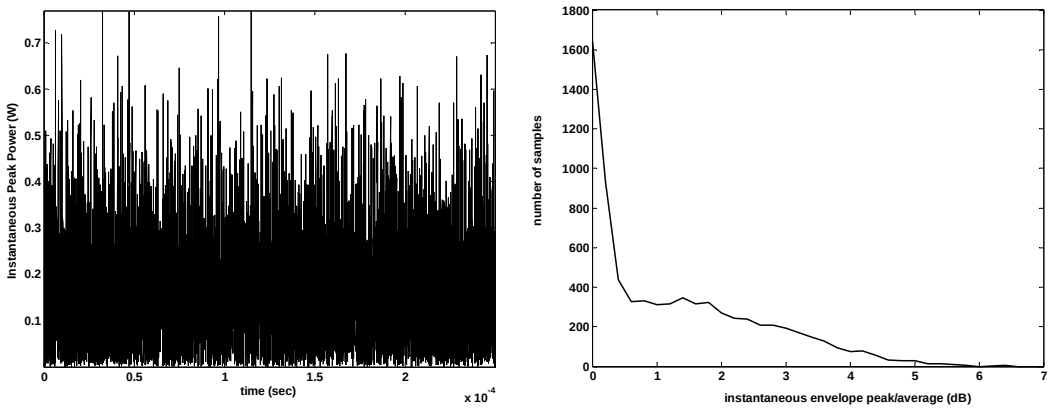

(a) **(b)**

Figure 4.22: a) Instantaneous peak power waveform. **b)** Instantaneous envelope peak-to-average histogram.

Table 4.5: Different multi-tone sets for signal 4 obtained for C_1=C_3=C_4=10 dB, C_2=13 dB, $IP3^m$=32 dBm, $IP3^e$=36 dBm, G_m=13.1 dB, G_e=33.4 dB.

m_1	m_2	m_3	m_4	Ψ (dB)	K	M	F ($x10^5$)	P_{main} (dBm)	$P_{mainacp}$ (dBm)	P_{out} (dBm)	P_{outacp} (dBm)
0.9	0.2	0.7	0.3	7.90	14733	0.89	113	16.70	-6.26	17.23	-29.40
0.8	0.1	0.2	0.2	6.66	11174	0.68	23.1	17.04	-12.02	17.22	-32.51
0.9	0	0	0.3	5.05	8223	0.50	7.7	17.29	-16.78	17.20	-35.52
1	0.05	0.05	0.05	4.19	7658	0.47	0.6	17.34	-28.14	17.19	-47.17
0.8	0.1	0.15	-	5.16	9159	0.56	6.2	17.21	-17.77	17.21	-36.88
0.1	0.9	0.2	-	5.25	8292	0.50	14.8	17.28	-13.95	17.20	-32.77

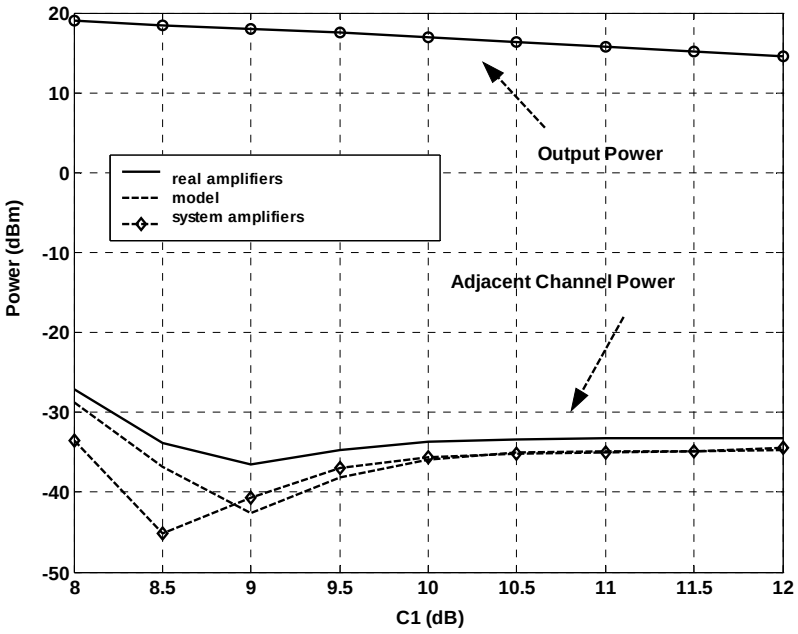

Figure 4.23: Feedforward output power and ACP for various C_1 – m_1=0.9, m_2=0, m_3=0, m_4=0.3 – C_2=13, C_3=C_4=10, G_m=13.1 dB, $IP3^m$=32 dBm, G_e=33.4 dB, $IP3^e$=36 dBm.

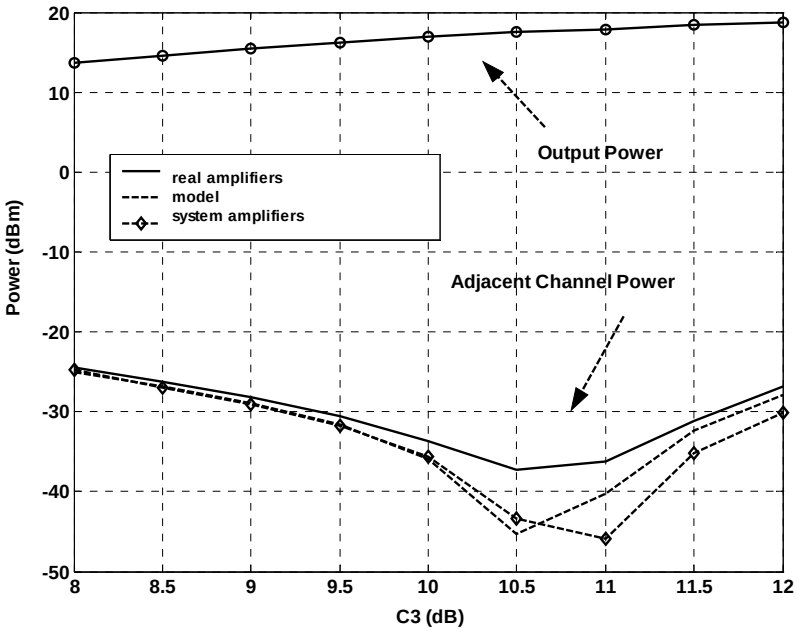

Figure 4.24: Feedforward output power and ACP for various C_3 – m_1=0.9, m_2=0, m_3=0, m_4=0.3 – C_2=13, C_1=C_4=10, G_m=13.1 dB, $IP3^m$=32 dBm, G_e=33.4 dB, $IP3^e$=36 dBm.

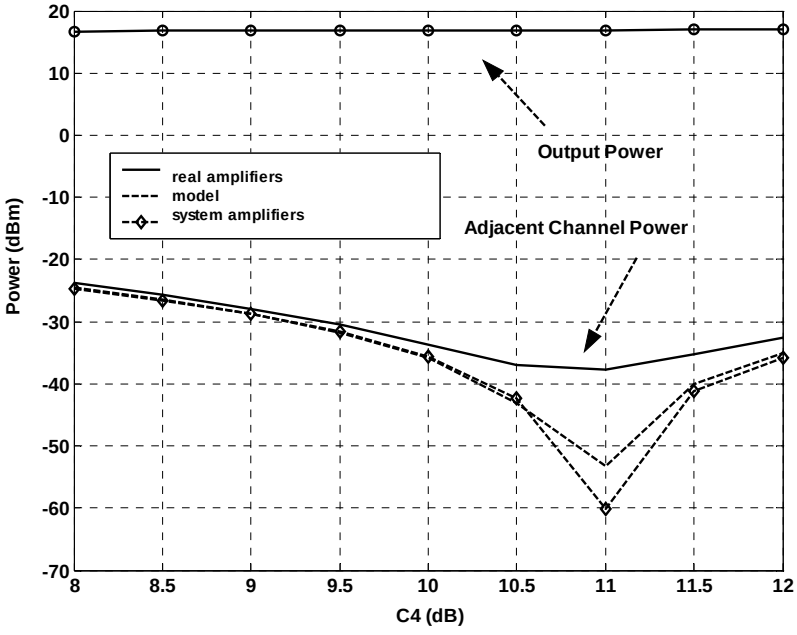

Figure 4.25: Feedforward output power and ACP for various C_4 – m_1=0.9, m_2=0, m_3=0, m_4=0.3 – C_2=13, C_1=C_3=10, G_m=13.1 dB, $IP3^m$=32 dBm, G_e=33.4 dB, $IP3^e$=36 dBm.

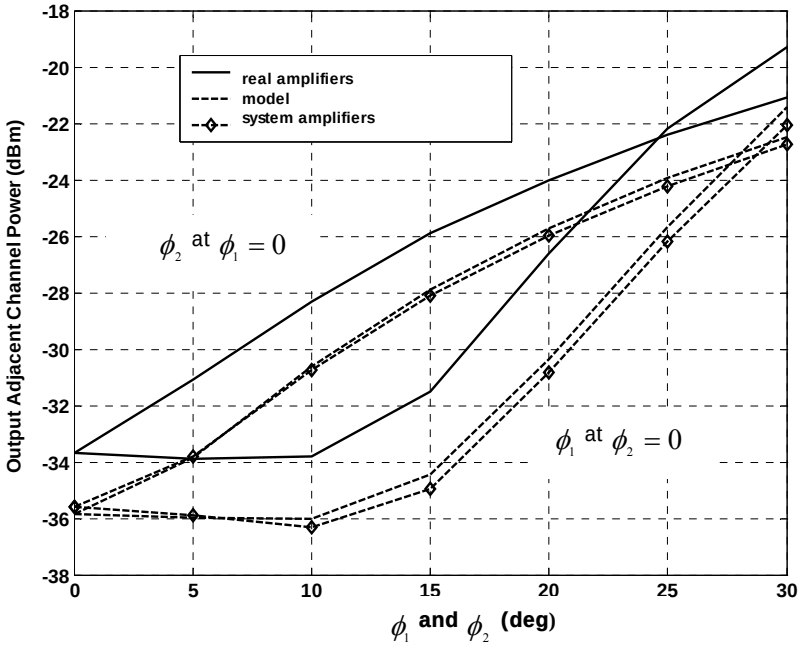

Figure 4.26: Feedforward output power and ACP for various phase mismatches ϕ_1 and ϕ_2 – m_1=0.9, m_2=0, m_3=0, m_4=0.3 – C_2=13, C_1=C_3=C_4=10, G_m=13.1 dB, $IP3^m$=32 dBm, G_e=33.4 dB, $IP3^e$=36 dBm.

CHAPTER 5

SUMMARY AND CONCLUSION

Modern communication systems are designed to transmit information including speech, multimedia and digital audio and video. Such applications, however, require high data speeds and compel utilization of complex modulation schemes, which exhibit both amplitude and phase variation. Furthermore, high-speed digital communication systems, which involve symbols of very short duration, employ raised-cosine shaped filters to achieve desired spectral efficiency. As a result of filtering, however, all signals become non-constant enveloped and necessitate utilization of linear power amplifiers, which can handle peak power requirement forced by peak-to-average ratio of the stimulus. Linearity objective can be simply accomplished by backing off power amplifier such that it operates away from compression point even at peak power. So-called Class-A amplifiers have very good linearity performance but suffer from very low efficiency. In addition, backing off a power amplifier will reduce its output power capability, which will impose paralleling several transistors to get the required average power. In order to overcome these problems, auxiliary systems called linearizer are used.

Linearizers employ power amplifiers which operate near or in saturation region in order to increase efficiency and use the output power capability of the transistors effectively. Among several techniques, feedforward linearization is popular for its superior distortion performance, relatively broadband operation and stability. However, this technique suffers from poor efficiency. In order to overcome the efficiency problem, several methods including hybrid usage of feedforward and predistortion [3] are proposed. In order to achieve a good

distortion performance in a feedforward system, amplitude, phase and delay matching need to be maintained within the carrier and error cancellation loops. To accomplish this task, directional couplers, variable attenuators, phase shifters, delay units and linear error amplifiers are integrated into the system. Hence, in order to obtain and maintain a good distortion performance, many component values should be controlled simultaneously. This task, however, is challenging and it is essential to develop an analytical model which would help the designer in parameter optimization. In general, it is desired to predict the final response of any nonlinear system to an arbitrary signal by using simple test signals. This task has been accomplished by single tone and two tone tests which have been the industry standards for years. However, these tests turned out to be insufficient for characterization of nonlinear systems excited by digitally modulated complex enveloped signals with high crest factors and new techniques need to be developed.

In literature there has been various work to characterize nonlinear systems in closed form for stochastically well defined signals such as n-coded CDMA which can be represented with an Additive White Gaussian Noise [49, 50]. However, similar methodology may not be applied to an arbitrarily modulated signal, which is usually the case in practice. In literature, multi-tone representation has been used to examine nonlinear systems excited by arbitrarily modulated signals. In [51], analysis for the output of a third order nonlinear system with a multi-tone excitation is provided. In [6], an analytical approach for a fifth order nonlinear memoriless system excited with n equally spaced tones with constant amplitude and with correlated and uncorrelated phases is presented. In [5], phase and magnitude of multi-tone signals are modified to represent adjacent channel power of digitally modulated QPSK signal. The number of tones is varied from 3 to 65 and simulation results for digitally modulated signal and its multi-tone models are compared. In [7], Coskun proposed an alternative multi-tone representation, which is composed of minimum number of equally spaced, in-phase tones with variable amplitudes. This representation has also been applied to a feedforward system, which is composed of main and error amplifiers with third order nonlinearity, and closed form expressions relating main and adjacent channel power at any point of the circuit to system parameters derived. In this thesis, these expressions are extended

to include phase mismatches in both carrier and error cancellation loops of a feedforward system. In addition, parameter selection criteria, which are used as guide to select potential multi-tone models, are introduced. Apart from the multi-tone modeling studies in the literature, in this study, multi-tone representation mentioned above is used to find the distortion at the output of real life amplifiers excited by arbitrarily modulated real/complex enveloped digital signals. The measurement results are also verified by RF simulations.

Multi-tone concept has been firstly verified by applying real/complex enveloped arbitrary and multi-tone signals to real amplifiers in single amplifier configuration. In this experiment, two amplifiers from Hittite Microwave Corporation namely, HMC481MP86 and HMC372LP3, have been used. Real and complex enveloped stimuli have been created in MATLAB. In order to create RF signals, these stimuli have been scaled in MATLAB and then downloaded via an interface program into Agilent E4433B ESG-D Option-UND signal generator, which involves arbitrary waveform signal generation utility to create RF signals from I and Q data supplied by the user. RF signals at the output of the signal generator then have been applied to real amplifiers and output power of main and adjacent channels have been measured using ACPR measurement utility of Agilent E4402B ESA-E series spectrum analyzer. Real/complex enveloped signals have been represented using equally spaced, in-phase and variable amplitude multi-tone signals with minimum number of tones. A similar procedure has been carried out to generate multi-tone RF signals, which have been formed in MATLAB, and measure the distortion generated by these signals. Results for multi-tone signals and for real/complex enveloped arbitrary signals are consistent and indicate that properly chosen multi-tone signals model the arbitrary stimuli successfully. Number of tones, amplitude of each tone and spacing between tones can be varied in order to find a correct multi-tone model. The closer the multi-tone signal is to the actual signal, the closer is the final response of the nonlinear system. In practice, the ultimate goal is to find a handy test signal which produces distortion as much as generated by the actual signal at the output of the system. Parameter selection criteria have been defined to predict the level of distortion at the output of a nonlinear system for third order nonlinearity. Certain parameters (K, M and F) have been derived from

nonlinear power expression in time and frequency domains. K and M parameters have been calculated from nonlinear power expression in time domain and include both in-band and side-band distortion, whereas, F parameter has been obtained by taking FFT of nonlinear part of power expression and contains side-band distortion only. These criteria have been used as guide to select potential multi-tone models. A similar single amplifier circuit has also been built in ADS and the same stimuli have been transferred to this environment. System amplifiers, which are characterized by gain and IP3, have been used in place of real amplifiers in simulation environment. The order of nonlinearity of the system has been confined to three and IP3 of the system amplifier has been modified for input power levels driving the system into strong nonlinearity, where higher order intermodulation products become effective and third order assumption deteriorates. The simulation results for multi-tone models and real/complex enveloped arbitrary signals coincide, confirming the validity of multi-tone modeling concept. Therefore, characterization of complex systems using multi-tone signals is a feasible task.

The multi-tone concept has been, thereafter, applied to the analysis of feedforward system, which is a rather complex system calling for simultaneous control of several circuit parameters. In this thesis, relations derived in [7] have been generalized to include phase mismatches in carrier and error cancellation loops. Moreover, the number and variety of stimuli have been increased in order to observe the potential problems for signals with different crest factors, bandwidths and statistics. In addition to the real/complex enveloped stimuli used in single amplifier case, a narrowband IS-95 signal and a wideband CDMA signal have been created using CDMA generation tool in ADS. Since the implementation of a feedforward circuit is elaborate, the experiment has been performed in ADS environment. Two similar feedforward circuits have been built in ADS environment: one utilizing real amplifier SPICE models, and the other one using system amplifiers in place of the main and error amplifiers. Order of nonlinearity of system amplifiers has been confined to three and characteristics of system amplifiers have been specified by gain and IP3. In contrast to the single amplifier case, IP3 value of the system amplifiers has been kept constant throughout the experiment to avoid troubles of controlling additional circuit parameters. Using the

equations relating the main and adjacent channel power to the system parameters, a program simulating feedforward system has been created in MATLAB. Results for multi-tone models have been obtained with this program and compared to the simulation results obtained for real and system amplifiers in ADS. Multi-tone models have been formed considering parameter selection criteria. The results are consistent within a few dB and verify the success of multi-tone concept in predicting the final response of complex systems to real/complex enveloped arbitrary signals. Because of the requirement of strict component matching, the distortion performance of the system depends on coupler couplings and phase mismatches in two loops. Sweeping coupling values of couplers, for instance, illustrates notches where distortion performance is optimum. It has been observed that any change in the coupling value of C_4 affects the performance directly because the elimination process of distortion products at the output of the main amplifier takes place in C_4. Phase mismatch introduced into first loop has been tolerated up to 10°, whereas distortion increases monotonically with increasing phase mismatch in the second loop.

In summary, multi-tone representation is employed in this thesis to predict the final response of nonlinear systems excited by arbitrarily generated real or complex enveloped signals. Multi-tone modeling concept is applied to the analysis and characterization of real amplifiers and feedforward systems. As a result, the potential of multi-tone modeling in nonlinear system characterization has been revealed and the results indicate that multi-tone representation is a strong candidate to replace widely used single-tone and two-tone signals in system characterization. In addition, a flexible tool taking phase mismatches into account has been achieved to make rapid parameter optimizations for optimum efficiency and linearity in a feedforward system. Such a tool will decrease the design durations for complex systems like feedforward and give the designer insight about the effect of components used in the system.

Possible future research topics can be summarized as follows.

The expressions relating output main and adjacent channel power to system parameters in feedforward system have been derived assuming the system is delay matched. Delay introduced into the system modifies both the carrier and envelope

terms of a multi-tone signal. Delay introduced into the carrier term can be represented by phase; hence, the extended expressions in this thesis can be used without any modification. The delay component in the envelope, however, compels new set of equations in order to include delay effects.

Another subject of research may be the order of nonlinearities of main and error amplifiers, which is confined to three in this work. Although third order approximation is enough in weakly nonlinear region of amplifiers, higher order distortion terms become effective in highly nonlinear region and the results deviate from expected. Considering the fact that the order of feedforward system increases as the square of the order of main and error amplifiers, expressions for feedforward system can be expanded to take into account higher order terms.

Memory effect is another contemporary research topic; characterization, formulation and considering the memory effects in the circuit design by utilizing the techniques developed in this study may yield fruitful results.

In the formulations nonlinearity of the amplifiers is represented with a power series with real coefficients. Although this is very handy, using this representation only AM/AM distortion can be explored. AM/PM distortion, together with memory effects, is the missing part. Alternative representations, such as power series with complex coefficients, can be considered. The accuracy of the multi-tone representation and the parameter selection criteria for tone coefficient determination can be improved; feedforward linearizer analysis can be extended to include the AM/PM distortion and memory effects.

REFERENCES

[1] N. Pothecary, *Feedforward Linear Power Amplifiers*, Artech House, 1999

[2] S. C. Cripps, *RF Power Amplifiers for Wireless Communications*, Artech House, 1999.

[3] P. B. Kenington, *High-Linearity RF Amplifier Design*, Artech House, 2000.

[4] N. B. Carvalho and J. C. Pedro, "Multi-tone intermodulation distortion performance of 3rd order microwave circuits," in *IEEE MMT-S Digest*, pp. 763-766, 1999.

[5] K. A. Remley, "Multisine excitation for ACPR measurements," in *IEEE MMT-S Digest*, pp. 2141-2144, 2003.

[6] N. Boulejfen, A. Harguem, and F. M. Ghannouchi, "New closed-form expressions for the prediction of multitone intermodulation distortion in fifth-order nonlinear RF circuits/systems," *IEEE Transactions on Microwave Theory and Tech.*, vol. 52, no. 1, pp. 121-132, January 2004.

[7] A. H. Coskun, *Stochastic Characterization and Mathematical Analysis of Feedforward Linearizers*, A thesis submitted to the Middle East Technical University, September 2003.

[8] C. Fager, J. C. Pedro, N. B. Carvalho, H. Zirath, F. Fortes, and M. J. Rosario, "A comprehensive analysis of IMD behavior in RF CMOS power amplifiers," *IEEE Journal of Solid-State Circuits*, vol. 39, no. 1, pp. 24-34, January 2004.

[9] N. B. Carvalho and J. C. Pedro, "Large- and small-signal IMD behavior of microwave power amplifiers," *IEEE Transactions on Microwave Theory and Tech.*, vol. 47, no. 12, pp. 2364-2374, December 1999.

[10] J. F. Sevic and M. B. Steer, "On the significance of envelope peak-to-average ratio for estimating the spectral regrowth of an RF/microwave power amplifier,"

IEEE Transactions on Microwave Theory and Tech., vol. 48, no. 6, pp. 1068-1071, June 2000.

[11] J. Vuolevi and T. Rahkonen, *Distortion in RF Power Amplifiers*, Artech House, 2003.

[12] J. H. K. Vuolevi, T. Rahkonen, and J. P. A. Manninen, "Measurement technique for characterizing memory effects in RF power amplifiers," *IEEE Transactions on Microwave Theory and Tech*., vol. 49, no. 8, pp. 1383-1389, August 2001.

[13] P. B. Kenington, "Efficiency of feedforward amplifiers," *IEE Proceedings-G*, vol. 139, no. 5, pp. 591-593, October 1992.

[14] K. J. Parsons, P. B. Kenington, and J. P. McGeehan, "Efficient linearization of RF power amplifiers for wideband applications," *Technical Paper*.

[15] K. J. Parsons, R. J. Wilkinson, and P. B. Kenington, "A highly-efficient linear amplifier for satellite and cellular applications," in *IEEE Vehicular Technology Conference*, pp. 203-207, 1995.

[16] D. Myer, "Ultra linear/feedforward amplifier design," in *IEEE MMT-S Digest*, 1998.

[17] K. Horiguchi, M. Nakayama, Y. Sakai, K. Totani, H. Senda, Y. Ikeda, and O. Ishıda, "A high efficiency feedforward amplifier with a series diode linearizer for cellular base stations," in *IEEE MMT-S Digest*, pp. 797-800, 2001.

[18] Y. Suzuki, T. Hirota, and T. Nojima, "Highly efficient feed-forward amplifier using a Class-F Doherty amplifier," in *IEEE MMT-S Digest*, pp. 77-80, 2003.

[19] K. J. Parsons and P. B. Kenington, "The efficiency of a feedforward amplifier with delay loss," *IEEE Transactions on Vehicular Tech*., vol. 43, no. 2, pp. 407-412, 1994.

[20] E. G. Jeckeln, F. M. Ghannouchi, M. Sawan, and F. Beauregard, "Efficient baseband/RF feedforward linearizer through a mirror power amplifier using software-defined radio and quadrature digital up-conversion," in *IEEE MMT-S Digest*, pp. 789-792, 2001.

[21] P. B. Kenington, R. J. Wilkinson, and J. D. Marvill, "Broadband linear amplifier design for a PCN base-station," in *IEEE Vehicular Technology Conference*, pp. 155-159, 1991.

[22] S. J. Grant, J. K. Cavers, and P. A. Goud, “A DSP controlled adaptive feedforward amplifier linearizer,” in *IEEE International Conference on Universal Personal Communications*, pp. 788-792, Cambridge, MA, Sept. 29-Oct. 2, 1996.

[23] Y. K. G. Hau, V. Postoyalko, and J. R. Richardson, “A microwave feedforward amplifier with improved phase compensation and wideband distortion cancellation,” in *IEEE MTT-S International Topical Symposium on Technologies for Wireless Applications Digest*, pp. 75-78, Vancouver, Canada, 1997.

[24] S. Kang, U. Park, K. Lee, and S. Hong, “Adaptive feedforward amplifier using pilot signal,” in *IEEE International Conference on Telecommunications*, pp. 677-680, Feb. 23-March 1, Tahiti, 2003.

[25] S. Kang, U. Park, K. Lee, and S. Hong, “Adaptive feedforward amplifier using digital controller,” in *IEEE Vehicular Technology Conference*, pp. 2076-2079, Florida, USA, 2003.

[26] Y. Yang, Y. Kim, J. Yi, J. Nam, B. Kim, W. Kang, and S. Kim, “Digital controlled adaptive feedforward amplifier for IMT-2000 band,” in *IEEE MMT-S Digest*, pp. 1487-1490, 2000.

[27] J. Presa, J. Legarda, H. Solar, J. Melendez, A. Munoz, and A. G. Alonso, “An adaptive feedforward power amplifier for UMTS transmitters,” in *IEEE International Symposium on Personal, Indoor and Mobile Radio Communications*, pp. 2715-2719, Barcelona, September 5-8, 2004.

[28] G. Hau, T. B. Nishimura, and N. Iwata, “A highly efficient linearized wide-band CDMA handset power amplifier based on predistortion under various bias conditions,” *IEEE Transactions on Microwave Theory and Tech*., vol. 49, no. 6, pp. 1194-1201, June 2001.

[29] A. Ahmed, S. M. Endalkachew, and G. Kompa, “Power amplifier linearization using memory polynomial predistorter with non-uniform delay taps,” in *IEEE MMT-S Digest*, pp. 1871-1874, 2004.

[30] A. N. D’Andrea, V. Lottici, and R. Reggiannini, “RF power amplifier linearization through amplitude and phase predistortion,” *IEEE Transactions on Communications*, vol. 44, no. 11, pp. 1477-1484, 1996.

[31] C. W. Park, F. Beauregard, G. Carangelo, and F. M. Ghannouchi, “An independently controllable AM/AM and AM/PM predistortion linearizer for cdma2000 multi-carrier applications,” in *IEEE RAWCON*, pp. 53-56, Boston, USA, August 19-22, 2001.

[32] K. Morris and P. Kenington, “Power amplifier linearisation using predistortion techniques,” in *IEEE RF and Microwave Components for Communication Systems*, pp. 1-6, Bradford, UK, 1997.

[33] S. Y. Lee, Y. S. Lee, S. H. Hong, H. S. Choi, and Y. H. Jeong, “An adaptive predistortion RF power amplifier with a spectrum monitor for multicarrier WCDMA applications,” *IEEE Transactions on Microwave Theory and Tech*., vol. 53, no. 2, pp. 786-793, February 2005.

[34] W. Woo, E. Park, K. U-yen, and S. Kenney, “Wideband predistortion linearization system for RF power amplifiers using an envelope modulation technique,” in *IEEE RAWCON*, pp. 401-404, Boston, USA, August 10-13, 2003.

[35] W. Woo, M. Miller, and J. S. Kenney, “Predistortion linearization system for high power amplifiers,” in *IEEE MMT-S Digest*, pp. 677-680, 2004.

[36] W. Woo, M. D. Miller, and J. S. Kenney, “A hybrid digital/RF envelope predistortion linearization system for power amplifiers,” *IEEE Transactions on Microwave Theory and Tech*., vol. 53, no. 1, pp. 229-237, January 2005.

[37] C. Potter, “System analysis of a W-CDMA base-station PA employing adaptive digital predistortion,” in *IEEE MMT-S Digest*, pp. 21-24, 2002.

[38] A. Springer, A. Gerdenitsch, Z. Li, A. Stelzer, and R. Weigel, “Adaptive predistortion for amplifier linearization for UMTS terminals,” in *IEEE Int. Symp. on Spread-Spectrum Tech. & Appl*., pp. 78-82, September 2-5, 2002.

[39] N. Ceylan, J. E. Mueller, T. Pittorino, and R. Weigel, “Mobile phone power amplifier linearity and efficiency enhancement using digital predistortion,” in *IEEE European Microwave Conference*, pp. 269-272, Munich, 2003.

[40] S. Im, E. J. Powers, “An application of a digital predistortion linearizer to CDMA HPA’s,” in *IEEE Communications Society*, pp. 3907-3910, 2004.

[41] N. Naskas and Y. Papananos, “Baseband predistorter for radio frequency power amplifiers based on a non-iterative, fast adaptation method,” in *IEEE International Conference on Electronics, Circuits and Systems*, pp. 117-120, Dubrovnik, Croatia, September 15-18, 2002.

[42] T. H. Vo and T. Le-Ngoc, “Baseband predistortion techniques for M-QAM transmission using non-linear power amplifiers,” in *IEEE Vehicular Technology Conference*, Florida, USA, October 6-9, 2003.

[43] P. Asbeck and C. Fallesen, “A polar linearisation system for RF power amplifiers,” in *IEEE International Conference on Electronics, Circuits and Systems*, pp. 478-481, Jounieh, Lebanon, December 17-20, 2000.

[44] T. Sowlati, D. Rozenblit, R. Pullela, M. Damgaard, E. McCarthy, D. Koh, D. Ripley, F. Balteanu, and I. Gheorghe, “Quad-band GSM/GPRS/EDGE polar loop transmitter,” *IEEE Journal of Solid-State Circuits*, vol. 39, no. 12, pp. 2179-2189, December 2004.

[45] S. Mann, M. Beach, P. Warr, and J. McGeehan, “Increasing the talk-time of mobile radios with efficient linear transmitter architectures,” in *Electronics & Communication Engineering Journal*, pp. 65-76, April 2001.

[46] Y. Y. Woo, J. Yi, Y. Yang, and B. Kim, “SDR transmitter based on LINC amplifier with bias control,” in *IEEE MMT-S Digest*, pp. 1703-1706, 2003.

[47] P. Garcia, A. Ortega, J. Mingo, and A. Valdovinos, “Nonlinear distortion cancellation using LINC transmitters in OFDM systems,” *IEEE Transactions on Broadcasting*, vol. 51, no. 1, pp. 84-93, March 2005.

[48] P. Colantonio, J. A. Garcia, F. Giannini, E. Limiti, E. Malaver, and J. C. Pedro, “High linearity and efficiency microwave Pas,” in *IEEE GAAS Symposium*, pp. 183-186, Amsterdam, 2004.

[49] A. H. Coskun and S. Demir, “A mathematical characterization and analysis of a feedforward circuit for CDMA applications,” *IEEE Transactions on Microwave Theory and Tech.*, vol. 51, no. 3, pp. 767-777, March 2003.

[50] Q. Wu, H. Xiao, and F. Li, “Linear RF power amplifier design for CDMA signals: A spectrum analysis approach,” *Microwave J.*, pp. 22-40, December 1998.

[51] J. C. Pedro and N. B. Carvalho, “On the use of multitone techniques for assessing RF components’ intermodulation distortion,” *IEEE Transactions on Microwave Theory and Tech.*, vol. 47, no. 12, pp. 2393-2402, December 1999.

APPENDIX A

DETAILED RESULTS FOR CHAPTER 3

Detailed measurement and simulation results for real and complex enveloped arbitrary signals and their multi-tone models are presented for both amplifiers, separately. First, the results for real enveloped data then the results for complex enveloped data are tabulated and illustrated. Tables A.1, A.4, A.7 and A.10 tabulate the important parameters for actual data and respective multi-tone models. Model 1 and Model 2 are expected to estimate the actual data, whereas Model HIGH and Model LOW are designed to overestimate and underestimate IMD results respectively. Actual signals are compared to these multi-tone signals and results obtained from measurement and simulation are separately illustrated. Tables A.2, A.5, A.8 and A.11 tabulate the results for actual signals, Model 1 and Model 2 for real and complex enveloped signals for each amplifier separately. On the other hand, Tables A.3, A.6, A.9 and A.12 tabulate the results for actual signals, Model HIGH and Model LOW for real and complex enveloped signals for each amplifier separately. The measurement and simulation results are also illustrated in figures following tables where results are tabulated. Each figure is labeled to show whether the results are obtained by simulation or measurement; belong to the actual signals or multi-tone signals. The properties of the stimuli and the amplifiers used in measurement and simulation are stated in Chapter 3 in detail. The discussions in Chapter 3 also hold for the results tabulated and illustrated in this chapter.

A.1 Results for real enveloped data

i. HMC481MP86

Table A.1: Important parameters of the real enveloped signal and multi-tone signals for HMC481MP86 amplifier.

	STIMULI G=19.3, IP3=30.8			**Ψ**	**K ($x10^5$)**	**F ($x10^9$)**	**M**
	m_1	m_2	m_3				
	Real enveloped data			7.5	4.48	2.47	54.7
Model 1	0.9	0.55	0.1	6.3	5.13	2.33	62.9
Model 2	0.2	0.55	0.1	6.1	3.78	2.28	46.3
ModelHIGH	1	0.9	0.8	7.7	14.7	8.97	179.9
ModelLOW	0.1	0.1	0.8	4.8	3.07	1.27	37.5

Table A.2: Measurement and ADS simulation results for main and adjacent channel output powers for the actual and multi-tone model signals for real enveloped data. The amplitude coefficients for Model 1 are m_1=0.9, m_2=0.55, m_3=0.1, and for Model 2 are m_1=0.2, m_2=0.55, m_3=0.1.

Input Power (dBm)	**Real Enveloped Data & Models** (measurement and simulation results in dBm)											
	Actual Signal				**Model Signals**							
					Model 1				Model 2			
	Output Power		IMD		Output Power		IMD		Output Power		IMD	
	Meas.	ADS	Meas.	ADS	Meas.	ADS	Meas.	ADS	Meas.	ADS	Meas.	ADS
-2	14.93	14.00	-8.15	-8.18	15.07	14.07	-8.20	-8.26	15.10	14.26	-8.75	-9.25
-4	13.41	13.12	-18.00	-14.53	13.53	13.11	-18.95	-14.40	13.55	13.24	-19.50	-15.93
-6	11.83	11.78	-25.60	-22.49	11.89	11.73	-25.90	-22.51	11.97	11.75	-26.00	-24.04
-8	10.18	10.10	-32.40	-30.49	10.22	10.10	-32.65	-30.33	10.19	10.06	-32.75	-31.86
-10	8.12	8.24	-38.10	-37.50	8.05	8.22	-38.40	-37.38	8.13	8.16	-38.55	-38.91
-12	6.25	6.32	-43.40	-45.10	6.30	6.31	-42.75	-44.97	6.28	6.23	-42.50	-46.50
-14	4.10	4.35	-46.25	-51.11	4.18	4.34	-46.20	-50.99	4.09	4.26	-45.65	-52.52
-16	2.27	2.36	-50.60	-57.13	2.33	2.35	-50.55	-57.01	2.27	2.26	-50.10	-58.54
-18	0.38	0.38	-54.10	-63.12	0.42	0.37	-53.90	-63.00	0.40	0.28	-53.20	-64.53
-20	-1.85	-1.60	-55.40	-69.10	-1.63	-1.61	-55.10	-68.97	-1.86	-1.70	-54.90	-70.50
-22	-3.57	-3.60	-58.40	-75.10	-3.40	-3.61	-58.15	-74.97	-3.62	-3.73	-57.65	-76.61
-24	-5.75	-5.60	-59.40	-81.12	-5.60	-5.61	-59.30	-81.00	-5.84	-5.71	-59.10	-82.53
-26	-7.61	-7.59	-62.90	-87.10	-7.66	-7.65	-62.70	-87.11	-7.70	-7.74	-62.05	-88.64
-28	-9.47	-9.59	-65.40	-93.10	-9.25	-9.66	-64.95	-93.14	-9.50	-9.68	-64.30	-94.46
-30	-11.68	-11.62	-66.10	-99.18	-11.57	-11.60	-65.85	-98.98	-11.73	-11.70	-65.45	-100,51

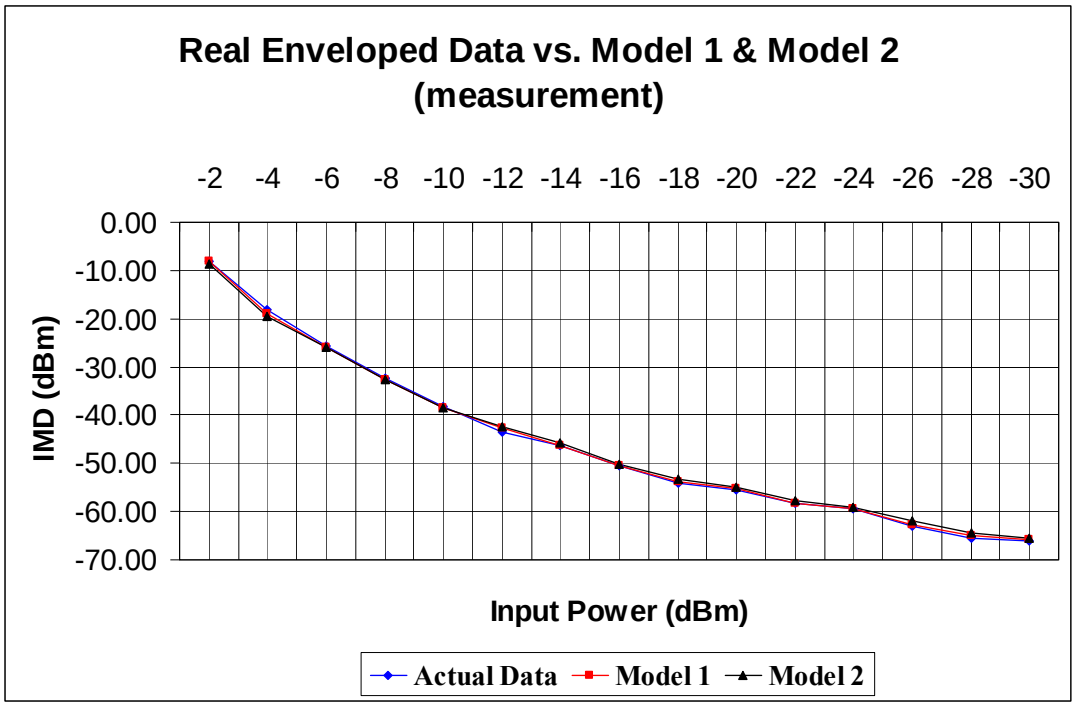

Figure A.1: Measured IMD results for real enveloped signal, Model 1 and Model 2 for HMC481MP86 amplifier.

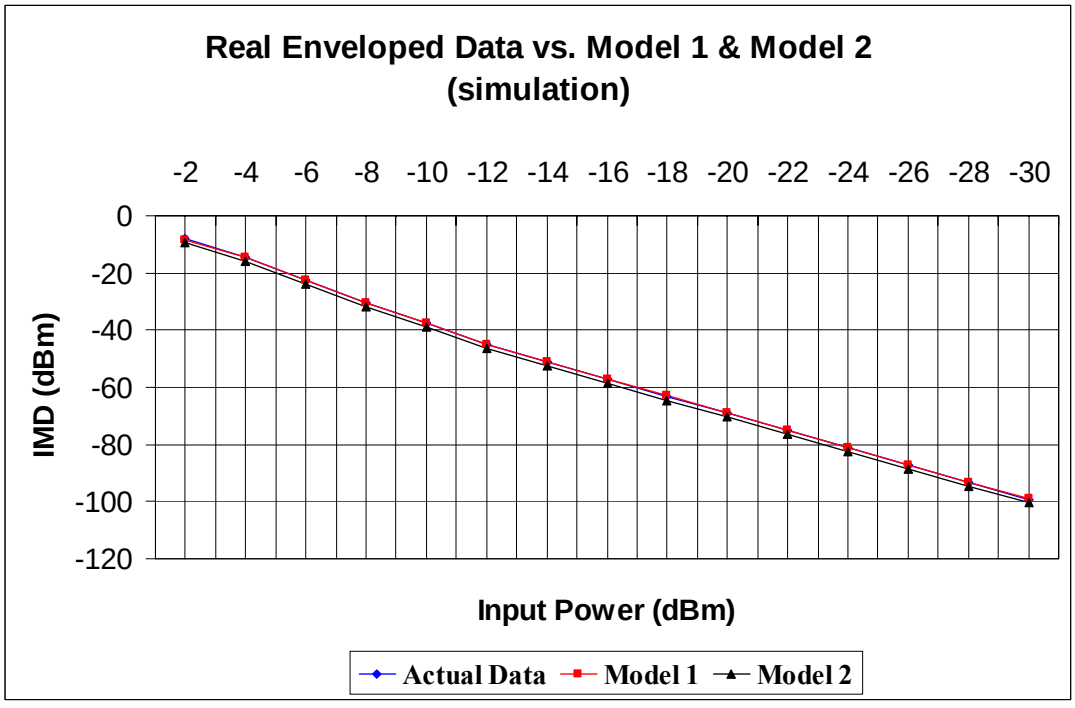

Figure A.2: Simulated IMD results for real enveloped signal, Model 1 and Model 2 for HMC481MP86 amplifier.

Table A.3: Measurement and ADS simulation results for main and adjacent channel output powers for the actual and multi-tone model signals for real enveloped data. The amplitude coefficients for Model HIGH are m_1=1, m_2=0.9, m_3=0.8, and for Model LOW are m_1=0.1, m_2=0.1, m_3=0.8.

Input Power (dBm)	**Real Enveloped Data & Models** (measurement and simulation results in dBm)											
	Actual Signal				**Model Signals**							
					Model HIGH				Model LOW			
	Output Power		IMD		Output Power		IMD		Output Power		IMD	
	Meas.	ADS	Meas.	ADS	Meas.	ADS	Meas.	ADS	Meas.	ADS	Meas.	ADS
-2	14.93	14.00	-8.15	-8.18	14.37	13.29	-3.15	-4.09	15.44	14.67	-14.10	-9.85
-4	13.41	13.12	-18.00	-14.53	13.14	12.55	-12.40	-8.94	13.57	13.52	-22.30	-17.06
-6	11.83	11.78	-25.60	-22.49	11.79	11.45	-20.65	-16.65	11.90	11.93	-29.10	-25.17
-8	10.18	10.10	-32.40	-30.49	10.07	9.96	-27.15	-24.46	10.24	10.20	-35.20	-32.99
-10	8.12	8.24	-38.10	-37.50	7.98	8.14	-34.05	-31.51	8.01	8.28	-40.45	-40.04
-12	6.25	6.32	-43.40	-45.10	6.17	6.27	-39.40	-39.11	6.24	6.34	-44.80	-47.63
-14	4.10	4.35	-46.25	-51.11	3.94	4.31	-42.30	-45.12	4.02	4.35	-47.65	-53.65
-16	2.27	2.36	-50.60	-57.13	2.28	2.33	-46.85	-51.15	2.20	2.36	-51.05	-59.68
-18	0.38	0.38	-54.10	-63.12	0.38	0.36	-50.80	-57.14	0.43	0.37	-53.85	-65.66
-20	-1.85	-1.60	-55.40	-69.10	-1.92	-1.62	-52.45	-63.10	-1.84	-1.61	-55.60	-71.63
-22	-3.57	-3.60	-58.40	-75.10	-3.80	-3.65	-55.60	-69.21	-3.53	-3.64	-58.55	-77.74
-24	-5.75	-5.60	-59.40	-81.12	-5.93	-5.62	-56.10	-75.13	-5.89	-5.61	-60.00	-83.66
-26	-7.61	-7.59	-62.90	-87.10	-7.66	-7.65	-59.95	-81.25	-7.66	-7.65	-62.60	-89.77
-28	-9.47	-9.59	-65.40	-93.10	-9.53	-9.66	-62.90	-87.27	-9.47	-9.59	-64.60	-95.59
-30	-11.68	-11.62	-66.10	-99.18	-11.81	-11.61	-63.50	-93.11	-11.75	-11.61	-66.10	-101.64

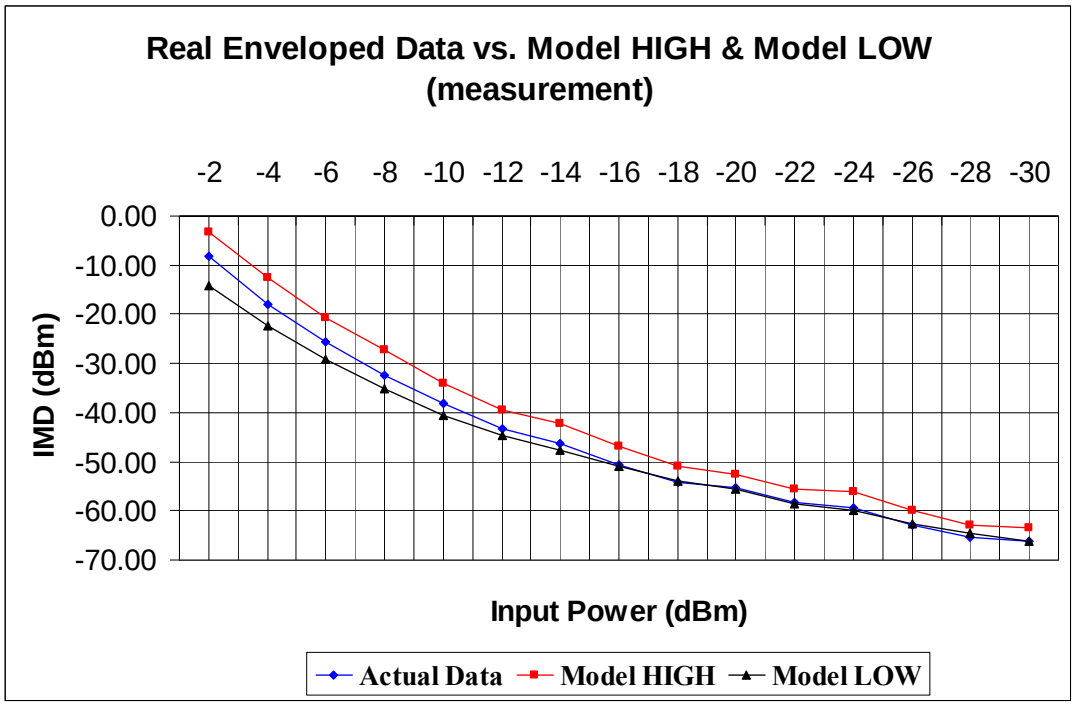

Figure A.3: Measured IMD results for real enveloped signal, Model HIGH and Model LOW for HMC481MP86 amplifier.

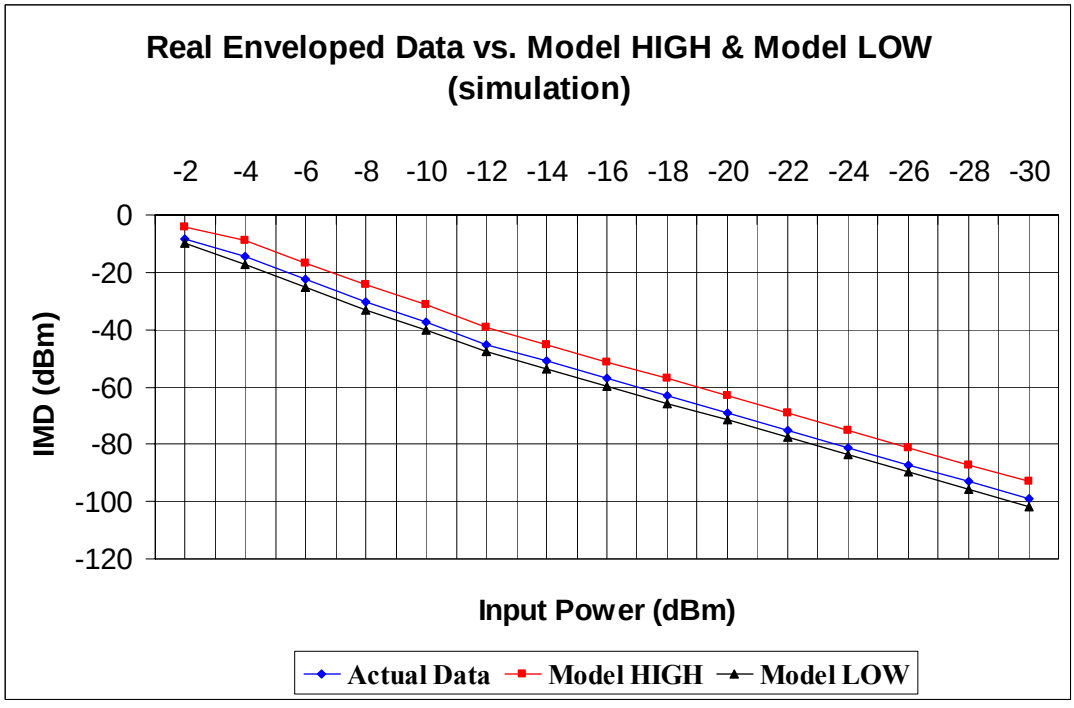

Figure A.4: Simulated IMD results for real enveloped signal, Model HIGH and Model LOW for HMC481MP86 amplifier.

ii. HMC372LP3

Table A.4: Important parameters of the real enveloped signal and multi-tone signals for HMC372LP3 amplifier.

	STIMULI G=15.6, IP3=35			**Ψ**	**K** **(x10^4)**	**F** **(x10^7)**	**M**
	m_1	m_2	m_3				
	Real enveloped data			7.5	7.03	2.78	8.6
Model 1	0.9	0.55	0.1	6.3	6.90	2.62	8.4
Model 2	0.2	0.55	0.1	6.1	6.60	2.56	8.1
ModelHIGH	1	0.9	0.8	7.7	8.94	10.1	10.9
ModelLOW	0.1	0.1	0.8	4.8	5.19	1.42	6.4

Table A.5: Measurement and ADS simulation results for main and adjacent channel output power for the actual and multi-tone model signals for real enveloped data. The amplitude coefficients for Model 1 are m_1=0.9, m_2=0.55, m_3=0.1, and for Model 2 are m_1=0.2, m_2=0.55, m_3=0.1.

Input Power (dBm)	**Real Enveloped Data & Models** (measurement and simulation results in dBm)											
	Actual Signal				**Model Signals**							
					Model 1				Model 2			
	Output Power		IMD		Output Power		IMD		Output Power		IMD	
	Meas.	ADS	Meas.	ADS	Meas.	ADS	Meas.	ADS	Meas.	ADS	Meas.	ADS
2	15.72	15.85	-13.15	-15.62	16.00	15.84	-13.90	-15.50	15.82	15.89	-13.90	-17.03
0	14.31	14.29	-19.50	-23.59	14.47	14.28	-20.10	-23.50	14.31	14.26	-21.20	-25.00
-2	12.57	12.51	-29.30	-33.70	12.82	12.50	-30.80	-33.58	12.64	12.44	-32.60	-35.11
-4	10.59	10.61	-40.10	-40.62	10.61	10.60	-39.85	-40.50	10.43	10.52	-40.75	-42.03
-6	8.76	8.61	-45.30	-46.73	8.78	8.60	-44.90	-46.61	8.69	8.51	-44.60	-48.14
-8	6.74	6.62	-48.90	-52.76	6.85	6.61	-48.00	-52.64	6.72	6.52	-47.75	-54.17
-10	4.54	4.69	-50.60	-58.60	4.70	4.67	-50.05	-58.48	4.53	4.59	-49.80	-60.01
-12	2.70	2.70	-53.60	-64.59	2.70	2.69	-53.00	-64.47	2.66	2.60	-52.60	-66.00
-14	0.47	0.70	-53.80	-70.61	0.53	0.69	-53.65	-70.49	0.41	0.60	-53.40	-72.02
-16	-1.49	-1.31	-57.30	-76.64	-1.32	-1.32	-56.85	-76.51	-1.50	-1.41	-56.40	-78.04
-18	-3.25	-3.30	-59.80	-82.62	-3.33	-3.31	-59.20	-82.50	-3.37	-3.41	-58.70	-84.03
-20	-5.42	-5.30	-60.85	-88.59	-5.30	-5.30	-60.40	-88.47	-5.41	-5.39	-60.15	-90.00
-22	-7.32	-7.33	-63.80	-94.70	-7.21	-7.34	-63.20	-94.58	-7.22	-7.43	-62.65	-96.11
-24	-9.80	-9.30	-64.60	-100.62	-9.49	-9.31	-64.20	-100.50	-9.77	-9.40	-63.95	-102.03
-26	-11.71	-11.34	-67.75	-106.73	-11.50	-11.35	-67.20	-106.61	-11.64	-11.44	-66.70	-108.14
-28	-13.29	-13.34	-69.80	-112.76	-13.04	-13.36	-69.30	-112.64	-13.17	-13.45	-68.45	-114.17
-30	-15.36	-15.29	-70.90	-118.59	-15.18	-15.30	-70.65	-118.48	-15.34	-15.39	-70.10	-120.01
-32	-17.23	-17.29	-73.70	-124.59	-17.20	-17.30	-73.40	-124.38	-17.19	-17.39	-72.55	-126.00

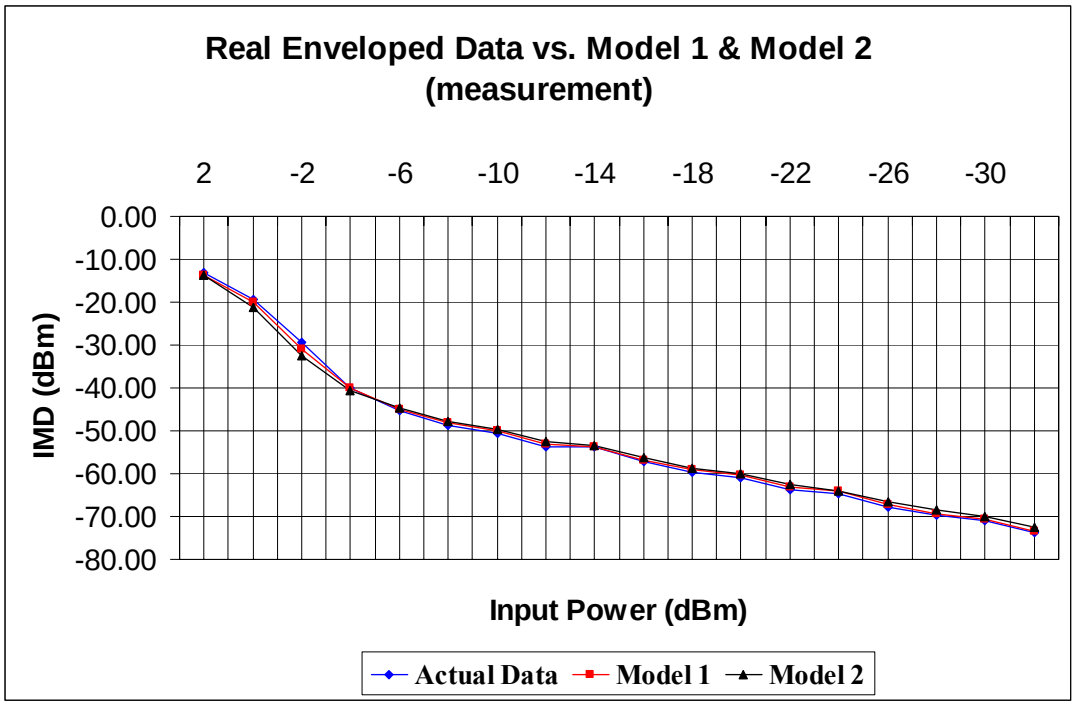

Figure A.5: Measured IMD results for real enveloped signal, Model 1 and Model 2 for HMC372LP3 amplifier.

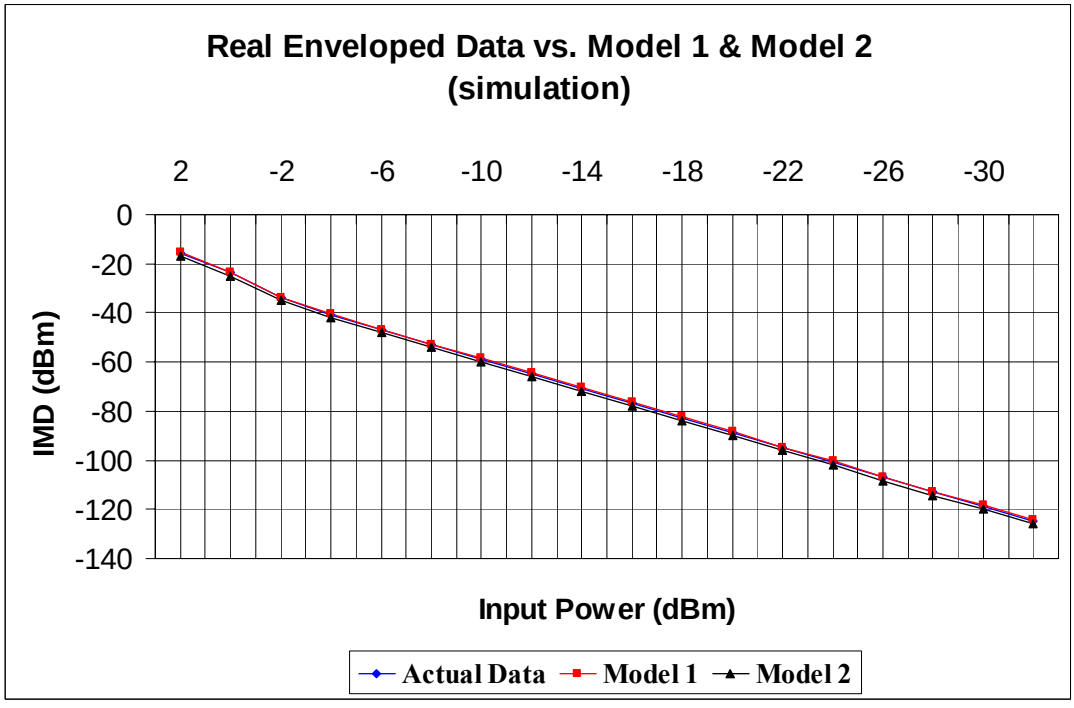

Figure A.6: Simulated IMD results for real enveloped signal, Model 1 and Model 2 for HMC372LP3 amplifier.

Table A.6: Measurement and ADS simulation results for main and adjacent channel output powers for the actual and multi-tone model signals for real enveloped data. The amplitude coefficients for Model HIGH are m_1=1, m_2=0.9, m_3=0.8, and for Model LOW are m_1=0.1, m_2=0.1, m_3=0.8.

Input Power (dBm)	**Real Enveloped Data & Models** (measurement and simulation results in dBm)											
	Actual Signal				**Model Signals**							
					Model HIGH				Model LOW			
	Output Power		IMD		Output Power		IMD		Output Power		IMD	
	Meas.	ADS	Meas.	ADS	Meas.	ADS	Meas.	ADS	Meas.	ADS	Meas.	ADS
2	15.72	15.85	-13.15	-15.62	15.30	15.44	-10.05	-9.64	15.99	16.11	-17.55	-18.16
0	14.31	14.29	-19.50	-23.59	13.94	14.09	-15.40	-17.60	14.47	14.41	-27.80	-26.13
-2	12.57	12.51	-29.30	-33.70	12.42	12.43	-23.60	-27.71	12.64	12.55	-38.25	-36.24
-4	10.59	10.61	-40.10	-40.62	10.32	10.56	-35.70	-34.63	10.20	10.63	-42.65	-43.16
-6	8.76	8.61	-45.30	-46.73	8.51	8.57	-41.80	-40.75	8.45	8.61	-45.85	-49.27
-8	6.74	6.62	-48.90	-52.76	6.67	6.59	-45.50	-46.77	6.53	6.62	-48.75	-55.30
-10	4.54	4.69	-50.60	-58.60	4.34	4.66	-47.20	-52.61	4.33	4.68	-50.75	-61.14
-12	2.70	2.70	-53.60	-64.59	2.49	2.68	-50.65	-58.61	2.52	2.69	-53.10	-67.13
-14	0.47	0.70	-53.80	-70.61	0.17	0.68	-50.85	-64.62	0.08	0.69	-54.60	-73.15
-16	-1.49	-1.31	-57.30	-76.64	-1.53	-1.32	-54.25	-70.65	-1.76	-1.32	-57.15	-79.18
-18	-3.25	-3.30	-59.80	-82.62	-3.49	-3.32	-57.25	-76.64	-3.35	-3.31	-59.10	-85.16
-20	-5.42	-5.30	-60.85	-88.59	-5.74	-5.30	-57.95	-82.60	-5.71	-5.30	-61.00	-91.13
-22	-7.32	-7.33	-63.80	-94.70	-7.40	-7.34	-60.85	-88.71	-7.73	-7.34	-63.35	-97.24
-24	-9.80	-9.30	-64.60	-100.62	9.80	-9.31	-61.45	-94.63	-9.86	-9.31	-64.90	-103.16
-26	-11.71	-11.34	-67.75	-106.73	-11.85	-11.35	-64.85	-100.75	-11.81	-11.35	-67.40	-109.27
-28	-13.29	-13.34	-69.80	-112.76	-13.68	-13.36	-67.60	-106.77	-13.30	-13.36	-69.20	-115.30
-30	-15.36	-15.29	-70.90	-118.59	-15.56	-15.30	-67.80	-112.61	-15.51	-15.30	-70.95	-121.14
-32	-17.23	-17.29	-73.70	-124.59	-17.37	-17.30	-71.00	-118.61	-17.34	-17.30	-73.10	-127.15

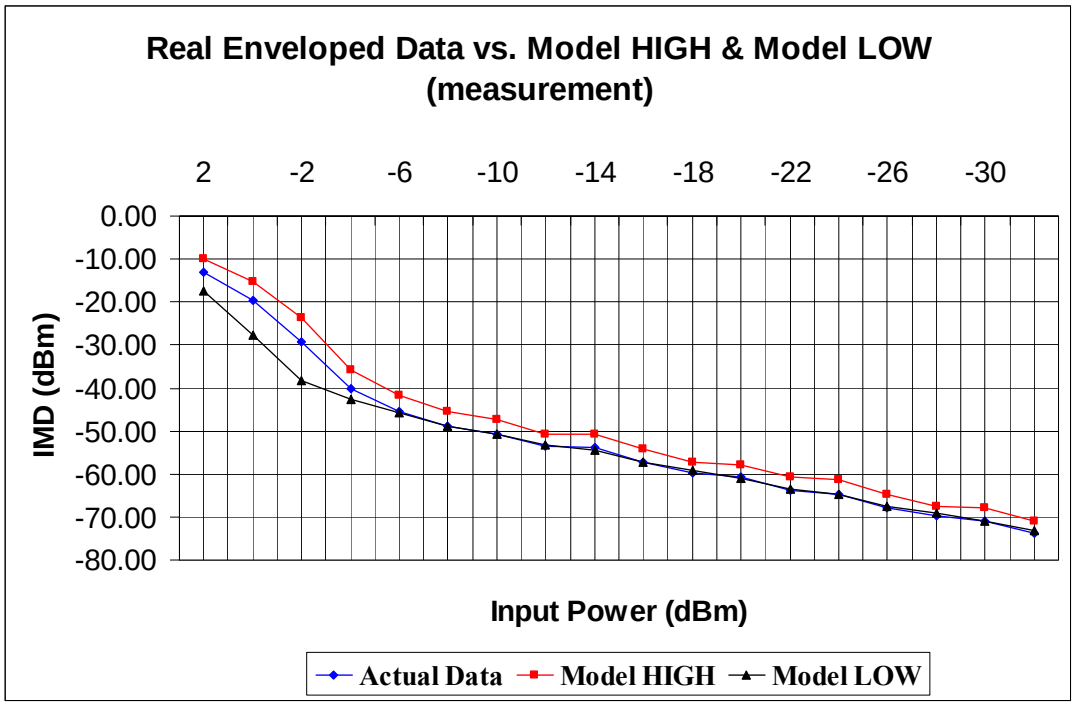

Figure A.7: Measured IMD results for real enveloped signal, Model HIGH and Model LOW for HMC372LP3 amplifier.

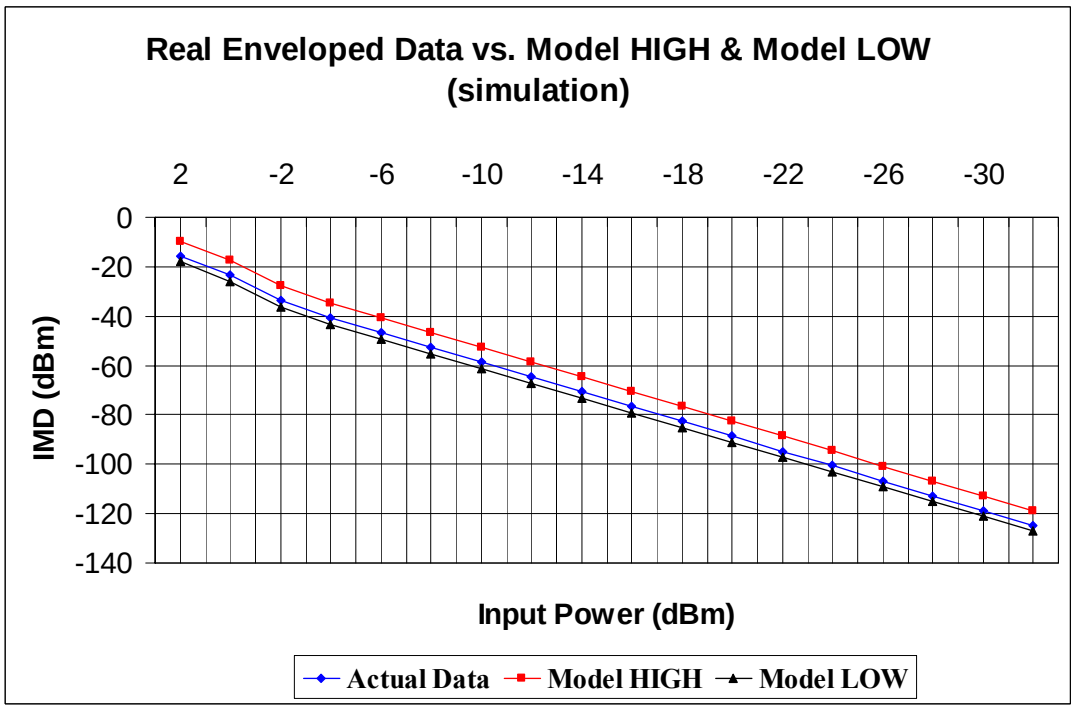

Figure A.8: Simulated IMD results for real enveloped signal, Model HIGH and Model LOW for HMC372LP3 amplifier.

A.2 Results for complex enveloped data

i. HMC481MP86

Table A.7: Important parameters of the complex enveloped signal and multi-tone signals for HMC481MP86 amplifier.

	STIMULI G=15.6, IP3=35			**Ψ**	**K (x10^5)**	**F (x10^8)**	**M**
	m_1	m_2	m_3				
	Complex enveloped data			9.1	1.33	3.85	16.3
Model 1	1	0.4	0.1	5.9	1.31	1.88	16.0
Model 2	0.2	0.9	0.1	5.2	1.42	1.77	17.3
ModelHIGH	0.8	1	1	7.7	0.96	12.1	11.6
ModelLOW	0.1	1	0.05	4.2	1.42	1.18	17.3

Table A.8: Measurement and ADS simulation results for main and adjacent channel output powers for the actual and multi-tone model signals for complex enveloped data. The amplitude coefficients for Model 1 are m_1=1, m_2=0.4, m_3=0.1, and for Model 2 are m_1=0.2, m_2=0.9, m_3=0.1.

Input Power (dBm)	**Complex Enveloped Data & Models** (measurement and simulation results in dBm)											
	Actual Signal				**Model Signals**							
					Model 1				Model 2			
	Output Power		IMD		Output Power		IMD		Output Power		IMD	
	Meas.	ADS	Meas.	ADS	Meas.	ADS	Meas.	ADS	Meas.	ADS	Meas.	ADS
-2	15.48	14.36	-9.70	-11.00	15.55	14.27	-8.50	-10.09	15.72	14.48	-10.05	-9.64
-4	14.07	13.23	-17.30	-17.40	13.90	13.26	-18.60	-16.55	14.14	13.41	-19.60	-16.79
-6	12.32	11.72	-25.80	-25.35	12.34	11.81	-26.10	-24.60	12.40	11.89	-26.75	-24.84
-8	10.51	10.02	-33.58	-33.22	10.78	10.09	-33.25	-32.63	10.70	10.13	-33.75	-32.86
-10	8.61	8.12	-38.60	-40.26	8.75	8.24	-38.50	-39.52	8.53	8.26	-38.85	-39.75
-12	6.68	6.19	-44.80	-47.86	6.84	6.31	-44.45	-47.12	6.71	6.34	-44.30	-47.36
-14	4.66	4.22	-47.55	-53.87	4.59	4.34	-47.50	-53.11	4.66	4.35	-47.10	-53.38
-16	2.71	2.24	-52.85	-59.86	2.59	2.36	-52.55	-59.14	2.67	2.36	-51.90	-59.38
-18	0.71	0.25	-57.10	-65.83	0.71	0.37	-56.55	-65.13	0.77	0.38	-55.55	-65.37
-20	-1.31	-1.75	-58.05	-71.77	-1.18	-1.62	-57.75	-71.14	-1.28	-1.62	-56.90	-71.38
-22	-3.29	-3.75	-61.30	-77.64	-2.93	-3.63	-60.85	-77.16	-3.31	-3.63	-60.00	-77.40
-24	-5.18	-5.74	-61.40	-83.28	-4.96	-5.62	-61.15	-83.15	-5.15	-5.62	-60.50	-83.39
-26	-7.14	-7.76	-65.70	-88.60	-7.12	-7.64	-65.30	-89.20	-7.14	-7.63	-64.25	-89.44
-28	-9.13	-9.76	-68.70	-93.20	-9.23	-9.64	-68.30	-95.23	-9.13	-9.64	-67.00	-95.46
-30	-11.12	-11.73	-69.00	-96.85	-11.05	-11.60	-68.65	-101.11	-11.23	-11.60	-67.85	-101.35

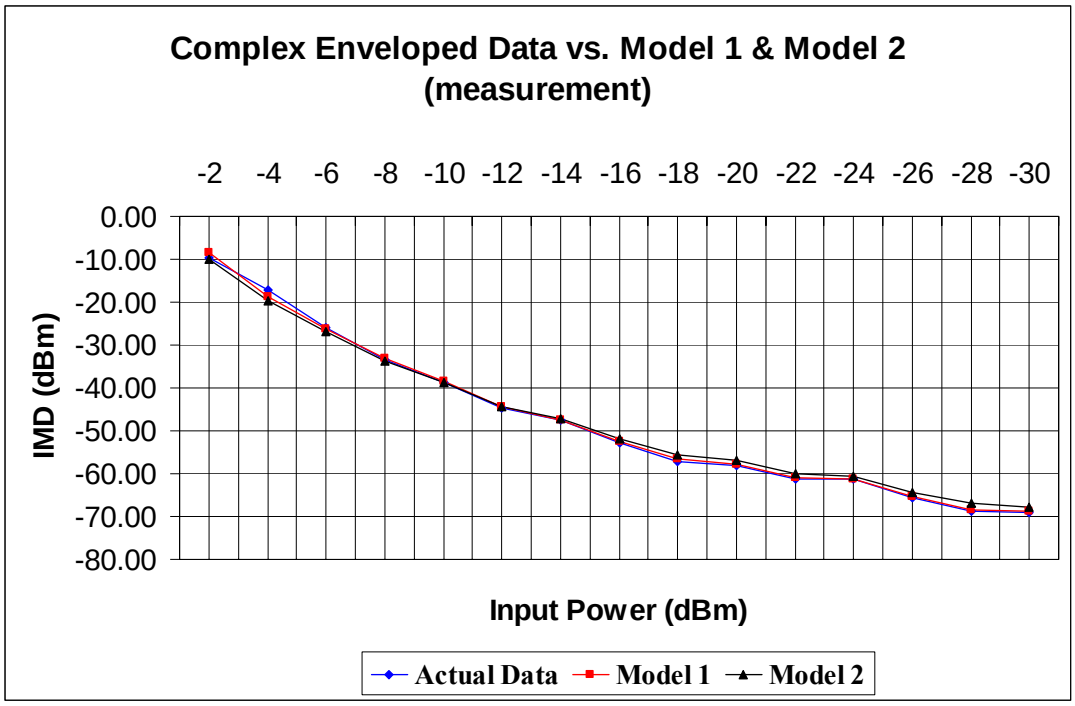

Figure A.9: Measured IMD results for complex enveloped signal, Model 1 and Model 2 for HMC481MP86 amplifier.

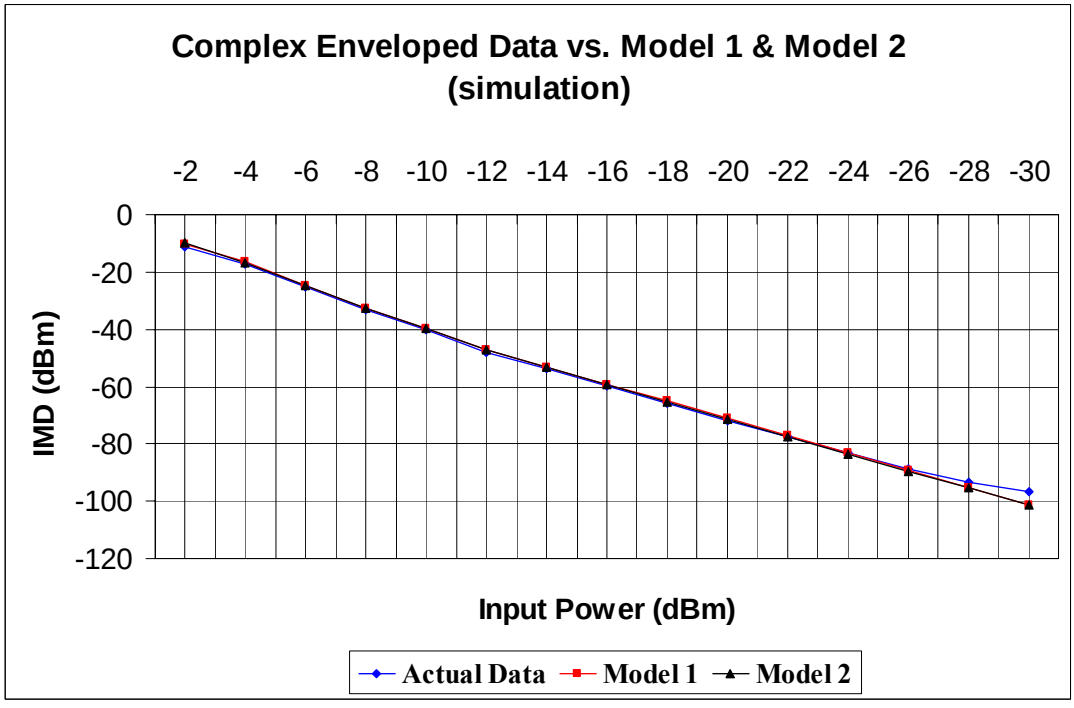

Figure A.10: Simulated IMD results for complex enveloped signal, Model 1 and Model 2 for HMC481MP86 amplifier.

Table A.9: Measurement and ADS simulation results for main and adjacent channel output powers for the actual and multi-tone model signals for complex enveloped data. The amplitude coefficients for Model HIGH are m_1=0.8, m_2=1, m_3=1, and for Model LOW are m_1=0.1, m_2=1, m_3=0.05.

Input Power (dBm)	**Complex Enveloped Data & Models** (measurement and simulation results in dBm)											
	Actual Signal				**Model Signals**							
					Model HIGH				Model LOW			
	Output Power		IMD		Output Power		IMD		Output Power		IMD	
	Meas.	ADS	Meas.	ADS	Meas.	ADS	Meas.	ADS	Meas.	ADS	Meas.	ADS
-2	15.48	14.36	-9.70	-11.00	14.49	13.37	0.00	-3.88	15.76	14.70	-14.88	-10.96
-4	14.07	13.23	-17.30	-17.40	13.43	12.59	-7.80	-8.73	14.15	13.54	-21.85	-18.52
-6	12.32	11.72	-25.80	-25.35	11.96	11.48	-17.30	-16.50	12.48	11.95	-29.15	-26.57
-8	10.51	10.02	-33.58	-33.22	10.45	9.92	-24.25	-24.53	10.65	10.15	-36.00	-34.59
-10	8.61	8.12	-38.60	-40.26	8.42	8.15	-31.00	-31.42	8.68	8.28	-40.30	-41.48
-12	6.68	6.19	-44.80	-47.86	6.64	6.27	-37.35	-39.02	6.68	6.34	-45.75	-49.09
-14	4.66	4.22	-47.55	-53.87	3.39	4.31	-41.25	-45.04	4.72	4.35	-48.30	-55.10
-16	2.71	2.24	-52.85	-59.86	2.84	2.34	-45.40	-51.04	2.84	2.37	-52.50	-61.11
-18	0.71	0.25	-57.10	-65.83	0.65	0.36	-50.45	-57.03	0.95	0.38	-55.80	-67.10
-20	-1.31	-1.75	-58.05	-71.77	-1.15	-1.63	-51.15	-63.04	-1.21	-1.62	-57.40	-73.11
-22	-3.29	-3.75	-61.30	-77.64	-3.23	-3.63	-55.90	-69.06	-3.14	-3.62	-60.15	-79.13
-24	-5.18	-5.74	-61.40	-83.28	-5.26	-5.62	-55.00	-75.05	-5.07	-5.62	-61.10	-85.12
-26	-7.14	-7.76	-65.70	-88.60	-7.16	-7.64	-59.30	-81.10	-7.02	-7.63	-64.50	-91.17
-28	-9.13	-9.76	-68.70	-93.20	-9.04	-9.64	-63.45	-87.13	-9.07	-9.64	-67.10	-97.19
-30	-11.12	-11.73	-69.00	-96.85	-11.17	-11.61	-62.90	-93.02	-11.08	-11.60	-68.00	-103.08

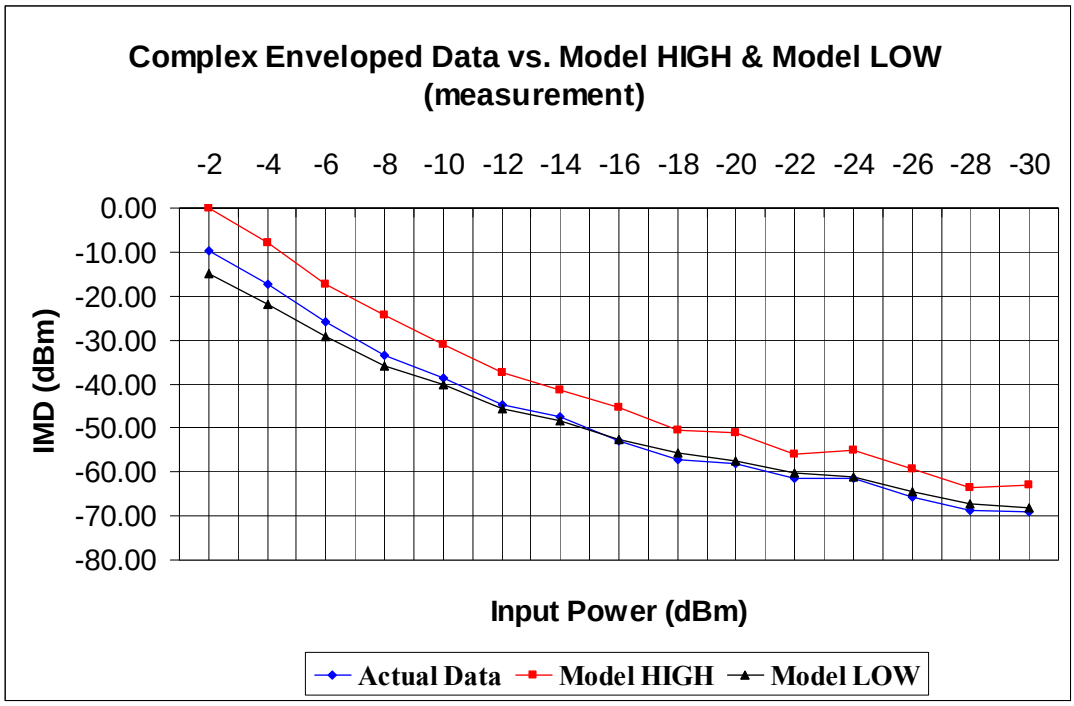

Figure A.11: Measured IMD results for complex enveloped signal, Model HIGH and Model LOW for HMC481MP86 amplifier.

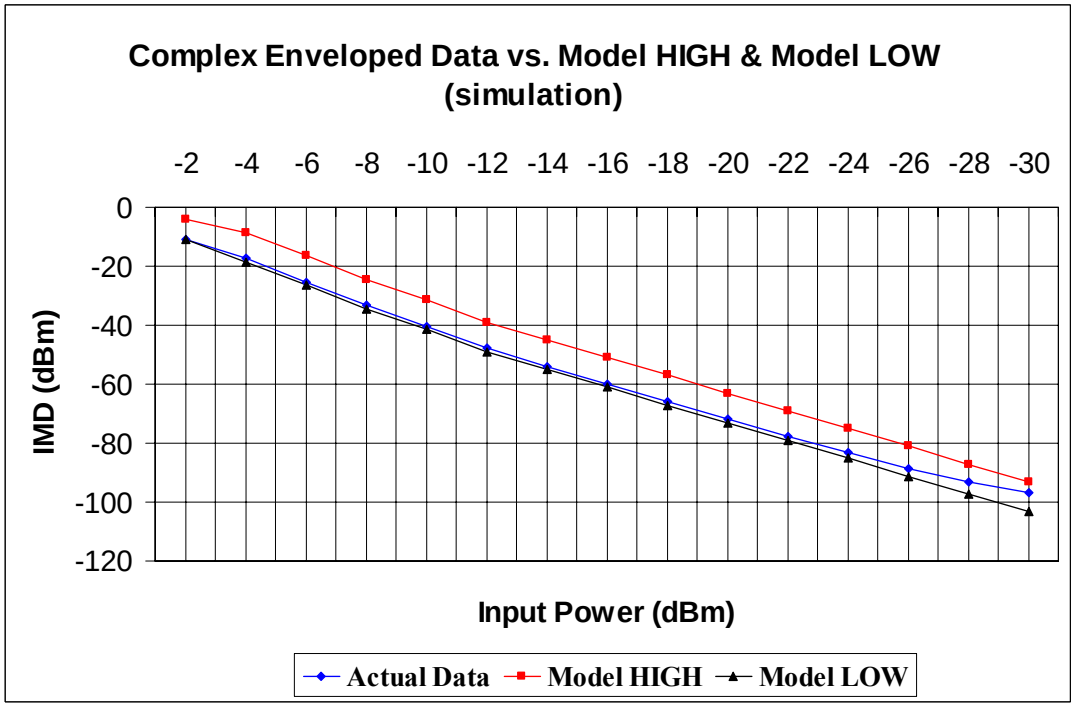

Figure A.12: Simulated IMD results for complex enveloped signal, Model HIGH and Model LOW for HMC481MP86 amplifier.

ii. HMC372LP3

Table A.10: Important parameters of the complex enveloped signal and multi-tone signals for HMC372LP3 amplifier.

	STIMULI G=15.6, IP3=35			**Ψ**	**K** **(x10^4)**	**F** **(x10^6)**	**M**
	m_1	m_2	m_3				
	Complex enveloped data			9.1	1.66	4.31	2.0
Model 1	1	0.4	0.1	5.9	1.80	2.11	2.2
Model 2	0.2	0.9	0.1	5.2	1.58	1.99	1.9
ModelHIGH	0.8	1	1	7.7	2.70	13.7	3.3
ModelLOW	0.1	1	0.05	4.2	1.40	1.33	1.7

Table A.11: Measurement and ADS simulation results for main and adjacent channel output powers for the actual and multi-tone model signals for complex enveloped data. The amplitude coefficients for Model 1 are m_1=1, m_2=0.4, m_3=0.1, and for Model 2 are m_1=0.2, m_2=0.9, m_3=0.1.

Input Power (dBm)	**Complex Enveloped Data & Models** (measurement and simulation results in dBm)											
	Actual Signal				**Model Signals**							
					Model 1				Model 2			
	Output Power		IMD		Output Power		IMD		Output Power		IMD	
	Meas.	ADS	Meas.	ADS	Meas.	ADS	Meas.	ADS	Meas.	ADS	Meas.	ADS
2	16.46	15.87	-14.18	-18.38	16.46	15.93	-13.35	-17.63	16.55	16.04	-13.80	-17.87
0	14.81	14.21	-21.05	-26.39	14.85	14.31	-19.90	-25.64	15.03	14.37	-22.10	-25.88
-2	13.02	12.42	-29.70	-36.41	13.11	12.53	-31.65	-35.66	13.13	12.56	-35.35	-35.90
-4	11.09	10.48	-39.65	-43.40	11.03	10.60	-41.75	-42.65	11.11	10.62	-42.30	-42.89
-6	9.11	8.50	-47.80	-49.45	8.95	8.62	-47.45	-48.70	9.11	8.63	-47.00	-48.94
-8	7.18	6.51	-52.00	-55.47	6.93	6.63	-50.55	-54.73	7.20	6.63	-49.20	-54.96
-10	5.05	4.55	-53.00	-61.34	5.04	4.68	-52.30	-60.62	5.15	4.68	-51.55	-60.85
-12	3.11	2.56	-56.50	-67.29	3.27	2.68	-56.00	-66.62	3.09	2.69	-54.70	-66.86
-14	1.11	0.56	-56.00	-73.15	1.07	0.68	-55.70	-72.64	0.96	0.68	-54.90	-72.88
-16	-0.96	-1.44	-59.75	-78.79	-0.87	-1.32	-59.70	-78.64	-0.99	-1.31	-58.45	-78.88
-18	-2.92	-3.44	-62.85	-83.96	-3.21	-3.31	-62.30	-84.63	-3.03	-3.31	-61.10	-84.87
-20	-4.92	-5.44	-63.20	-88.37	-4.75	-5.31	-63.00	-90.64	-4.83	-5.31	-61.75	-90.88
-22	-6.79	-7.44	-66.60	-91.87	-7.00	-7.32	-66.15	-96.66	-6.91	-7.32	-64.90	-96.90
-24	-9.16	-9.44	-66.65	-94.62	-9.16	-9.32	-66.30	-102.64	-9.13	-9.31	-65.55	-102.89
-26	-11.13	-11.45	-70.50	-96.98	-11.42	-11.33	-70.00	-108.69	-11.21	-11.33	-68.85	-108.94
-28	-13.16	-13.46	-73.20	-99.12	-13.21	-13.34	-72.80	-114.72	-13.18	-13.34	-71.30	-114.96
-30	-14.84	-15.43	-73.30	-101.13	-14.16	-15.30	-72.80	-120.59	-14.73	-15.30	-71.85	-120.85
-32	-16.79	-17.47	-76.60	-103.20	-16.70	-17.30	-76.30	-126.58	-16.67	-17.30	-74.80	-126.86

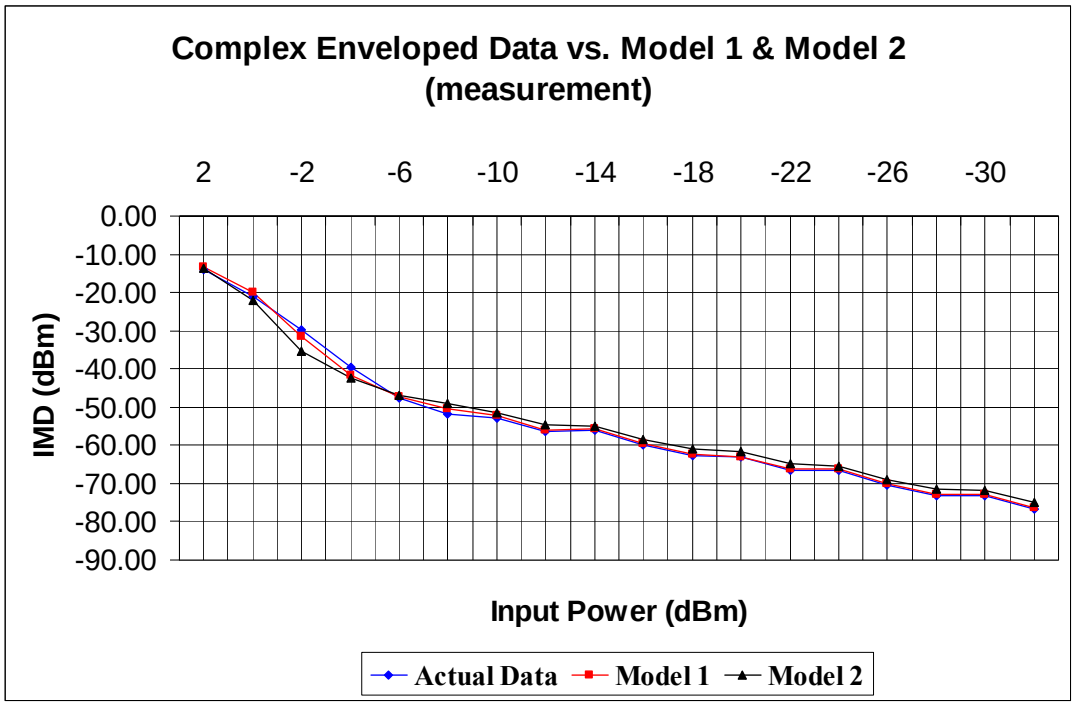

Figure A.13: Measured IMD results for complex enveloped signal, Model 1 and Model 2 for HMC372LP3 amplifier.

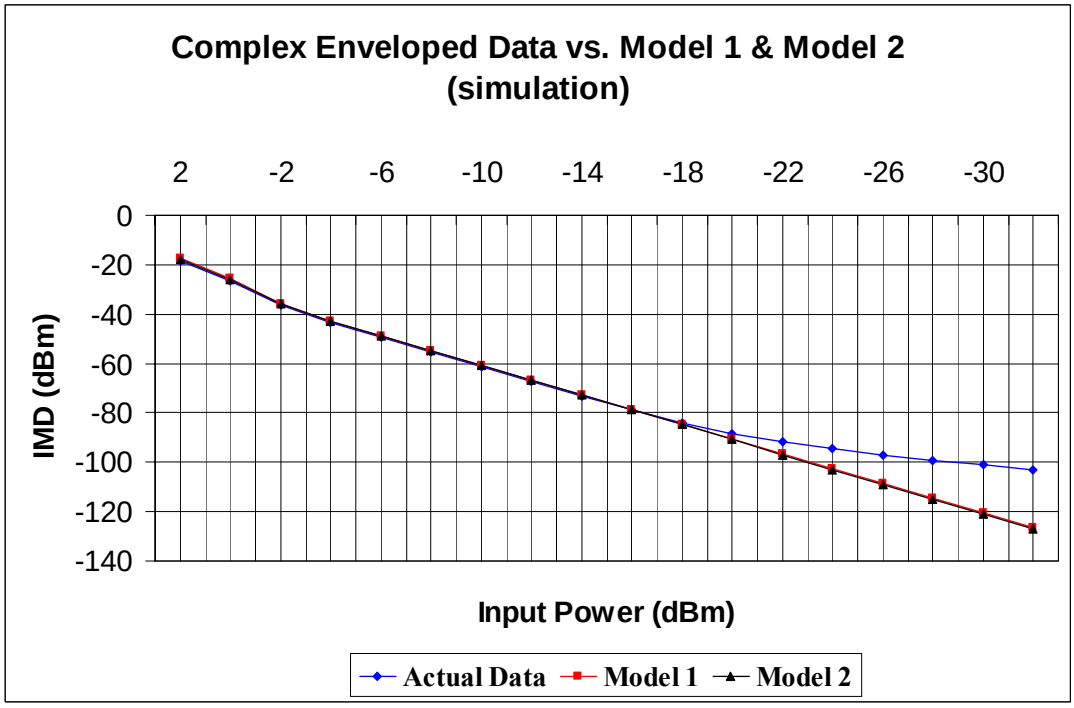

Figure A.14: Simulated IMD results for complex enveloped signal, Model 1 and Model 2 for HMC372LP3 amplifier.

Table A.12: Measurement and ADS simulation results for main and adjacent channel output powers for the actual and multi-tone model signals for complex enveloped data. The amplitude coefficients for Model HIGH are m_1=0.8, m_2=1, m_3=1, and for Model LOW are m_1=0.1, m_2=1, m_3=0.05.

Input Power (dBm)	**Complex Enveloped Data & Models** (measurement and simulation results in dBm)											
	Actual Signal				**Model Signals**							
					Model HIGH				Model LOW			
	Output Power		IMD		Output Power		IMD		Output Power		IMD	
	Meas.	ADS	Meas.	ADS	Meas.	ADS	Meas.	ADS	Meas.	ADS	Meas.	ADS
2	16.46	15.87	-14.18	-18.38	15.75	15.47	-6.45	-9.53	16.85	16.12	-16.70	-19.60
0	14.81	14.21	-21.05	-26.39	14.37	14.09	-12.00	-17.54	14.95	14.41	-28.30	-27.61
-2	13.02	12.42	-29.70	-36.41	12.88	12.45	-19.50	-27.56	13.11	12.57	-40.00	-37.63
-4	11.09	10.48	-39.65	-43.40	11.02	10.55	-31.30	-34.55	11.21	10.63	-43.90	-44.62
-6	9.11	8.50	-47.80	-49.45	9.10	8.59	-41.00	-40.60	9.07	8.63	-47.65	-50.67
-8	7.18	6.51	-52.00	-55.47	7.14	6.61	-45.90	-46.63	7.05	6.64	-49.60	-56.69
-10	5.05	4.55	-53.00	-61.34	5.00	4.66	-45.90	-52.52	5.07	4.68	-51.88	-62.58
-12	3.11	2.56	-56.50	-67.29	3.06	2.68	-50.40	-58.52	2.95	2.69	-54.90	-68.59
-14	1.11	0.56	-56.00	-73.15	1.00	0.68	-49.20	-64.54	0.79	0.68	-55.60	-74.60
-16	-0.96	-1.44	-59.75	-78.79	-0.95	-1.32	-54.00	-70.54	-1.24	-1.31	-58.80	-80.61
-18	-2.92	-3.44	-62.85	-83.96	-3.02	-3.31	-57.75	-76.53	-3.00	-3.31	-61.15	-86.60
-20	-4.92	-5.44	-63.20	-88.37	-5.15	-5.31	-57.70	-82.54	-5.10	-5.31	-62.15	-92.61
-22	-6.79	-7.44	-66.60	-91.87	-6.92	-7.32	-60.85	-88.56	-6.97	-7.32	-64.85	-98.63
-24	-9.16	-9.44	-66.65	-94.62	-9.29	-9.32	-59.70	-94.55	-9.31	-9.31	-66.30	-104.62
-26	-11.13	-11.45	-70.50	-96.98	-11.25	-11.33	-64.50	-100.60	-11.14	-11.33	-69.25	-110.67
-28	-13.16	-13.46	-73.20	-99.12	-13.23	-13.34	-68.35	-106.63	-13.33	-13.34	-71.50	-116.70
-30	-14.84	-15.43	-73.30	-101.13	-15.29	-15.30	-67.90	-112.52	-15.07	-15.30	-72.35	-122.59
-32	-16.79	-17.47	-76.60	-103.20	-16.88	-17.31	-70.90	-118.52	-16.99	-17.30	-75.20	-128.60

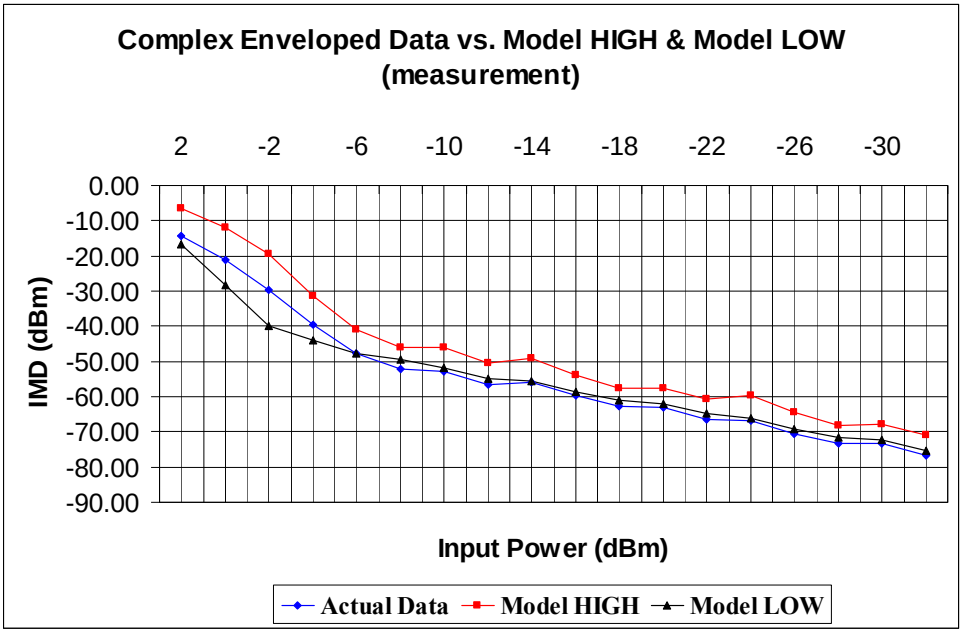

Figure A.15: Measured IMD results for complex enveloped signal, Model HIGH and Model LOW for HMC372LP3 amplifier.

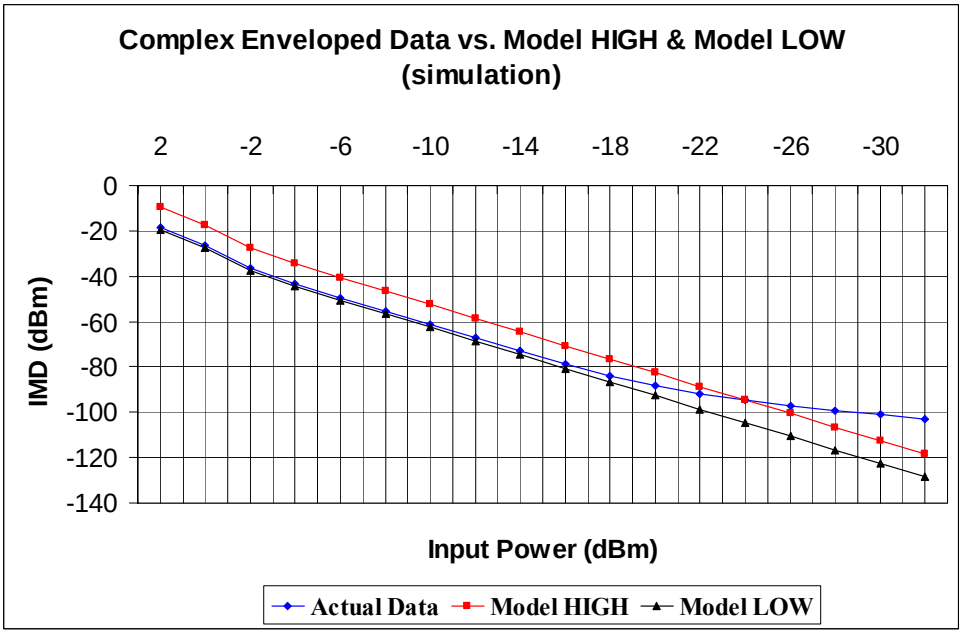

Figure A.16: Simulated IMD results for complex enveloped signal, Model HIGH and Model LOW for HMC372LP3 amplifier.

APPENDIX B

MATLAB PROGRAMS

This appendix includes the programs used in MATLAB at different phases of the simulation procedure. In order to follow easily, there is a short introduction before all programs. Also, descriptions are attached inside the programs whenever needed.

The following is the program mentioned in Chapter 3.4.3, which is used to prepare the signal for download into the signal generator. Program is supplied by Agilent.

arbsave.m

```
function arbsave(v,mkr1,mkr2,scale)
% arbsave(v,mkr1,mkr2,scale)
%
% Converts the vector v into I and Q. Scales these
% two vectors into integers lying between 0 and
% +16383 for 14 bit dac values.
%
% Activates markers 1 and 2, based on mkr1 and mkr2
states.
%
```

```
% Scales data to maximum range by 'scale'
%
% After conversion, the I values are stored in i.bin, % and the
Q values are stored in q.bin.
i = real(v);
q = imag(v);
mx = max([max(abs(i)) max(abs(q))]);
scaleint = round(8192*scale)-1;
i = i/mx*scaleint + 8191; % Make 14 bit unsigned
integers
q = q/mx*scaleint + 8191;
i = round(i);
q = round(q);
i = min(i,16383); % Just to be safe
i = max(i,0);
q = min(q,16383);
q = max(q,0);
i(1)=i(1)+mkr1*16384+mkr2*32768; % Set markers to begin
segment
fid = fopen('i.bin','w');
num = fwrite(fid,i,'unsigned short');
fclose(fid);
fid = fopen('q.bin','w');
num = fwrite(fid,q,'unsigned short');
fclose(fid);
```

The following program is used to compute output power and adjacent channel power at the output of the main amplifier and feedforward system when the stimulus is a multi-tone signal.

```
……..……Gain, IP3, input power and phase mismatches are
Gm=13.1;                    specified in this section of the program
IP3m=32;
IP3m=IP3m-30;
pindbm=5.27;
Ge=33.4;
IP3e=36;
IP3e=IP3e-30;
thetadeg=0;
theta2deg=0;
theta=thetadeg*pi/180;
theta2=theta2deg*pi/180;
.....……Coupler couplings, losses and a1, a3, b1 and b3 are
C1p=10;                     defined
l1p=-10*log10(1-10^(-C1p/10));
C2p=13;
l2p=-10*log10(1-10^(-C2p/10));
C3p=10;
l3p=-10*log10(1-10^(-C3p/10));
C4p=10;
l4p=-10*log10(1-10^(-C4p/10));
R=50;
a1=10^(Gm/20);
a3=(1/R)*(3/4)*(-2/3)*10^(3*Gm/20-IP3m/10);
b1=10^(Ge/20);
b3=(1/R)*(3/4)*(-2/3)*10^(3*Ge/20-IP3e/10);
C1=10^(C1p/20);
l1=10^(-l1p/20);
C2=10^(C2p/20);
l2=10^(-l2p/20);
C3=10^(C3p/20);
```

```
l3=10^(-l3p/20);
C4=10^(C4p/20);
l4=10^(-l4p/20);
pin=10.^((pindbm-30)/10)
```
.....Multi-tone coefficients are specified. Coefficients defined in 4.10 are calculated

```
m(1)=0;m(2)=0.9;m(3)=0;m(4)=0; m(5)=0.3;
pk_av_db=10*log10(2*sum(m)^2/sum(m.^2));
wm=1;
v=sqrt(4*50*pin/(sum(m.^2)));
alpha=a1*l1*v/(C2*C3)-(l3*v*cos(theta))/C1;
beta=a3*(l1^3)*(v^3)/(C2*C3);%YENI%
ep=a3*(l1^3)*(v^3)/(3*C2*C3);
mu=(l3*v*sin(theta))/C1;
ni=length(m);
nf=3*(ni-1)+1;
```
..... $m_n^{(q)}$ coefficients are calculated

```
mmcub=coefcalc_third(m);
mmfive=coefcalc_fifth(m);
mmseven=coefcalc_seventh(m);
mmnine=coefcalc_nineth(m);
```
.....Output power and adjacent channel power for the main and error amplifiers are calculated.

```
for n2=ni+1:nf,
  m(n2)=0;
end
mm=a1*l1*v*m + a3*l1^3*v^3*mmcub;
pm=0;pmimd=0;
for n2=2:ni,
   pm=pm+mm(n2)^2;
end
pm=pm/4/R;
pmdbm=10*log10(pm)+30;
```

```
for n2=ni+1:nf,
    pmimd=pmimd+mm(n2)^2;
end
pmimd=pmimd/4/R;
pmimddbm=10*log10(pmimd)+30;
me1=alpha*m+beta*mmcub;
me2=mu*m;
for q=1:nf;
   mme1(q)=me1(q)^2;
   mme2(q)=me2(q)^2;
end
me=mme1+mme2;
pe=0;
for n2=2:ni,
   pe=pe+me(n2);
end
pe=pe/4/R;
pedbm=10*log10(pe)+30;
M1=b1*alpha*m+(b1*beta+b3*(alpha^3)+b3*alpha*(mu^2))*mmcub+(b3*3*(al
pha^2)*beta+b3*(alpha^2)*ep+b3*beta*(mu^2)-
b3*ep*(mu^2))*mmfive+(b3*3*alpha*(beta^2)+b3*2*alpha*beta*ep+b3*2*alpha
*(ep^2))*mmseven+(b3*(beta^3)+b3*(beta^2)*ep+b3*2*beta*(ep^2))*mmnine;
M2=b1*mu*m+(b3*(alpha^2)*mu+b3*(mu^3))*mmcub+(b3*2*alpha*beta*mu-
b3*2*alpha*ep*mu)*mmfive+(b3*(beta^2)*mu-
b3*2*beta*ep*mu+b3*2*(ep^2)*mu)*mmseven;
my1=l2*l4*mm*cos(theta2)-M1/C4;
my2=-l2*l4*mm*sin(theta2)-M2/C4;
for q=1:nf;
   mmy1(q)=my1(q)^2;
   mmy2(q)=my2(q)^2;
end
my=mmy1+mmy2;
```

```
py=0;pyimd=0;
for n2=2:nf,
  py=py+my(n2);
end
py=py/4/R;
pydbm=10*log10(py)+30;
for n2=ni+1:nf,
  pyimd=pyimd+my(n2);
end
pyimd=pyimd/4/R;
pyimddbm=10*log10(pyimd)+30;

[pmdbm  pmimddbm  pedbm  pydbm  pyimddbm]
```

The following are the programs used in MATLAB to calculate $m_n^{(q)}$ coefficients indicated in 4.7. Since, we assume a third order nonlinear system, calculation of $m_n^{(3)}$, $m_n^{(5)}$, $m_n^{(7)}$ and $m_n^{(9)}$ is required. These coefficients are used in the MATLAB program given above to calculate main and adjacent channel power values at the output of the main amplifier and feedforward system.

- This program calculates $m_n^{(2)}$.

```
function[mmsquare]=coefcalc_square(m)

n=length(m)-1;
for p=1:2*n+1,
   mmsquare(p)=0;
end
for l=2:n+1,
mmsquare(1)=mmsquare(1)+m(l)*m(l)/2;
```

```
end
mmsquare(1);
for p=1:2*n,
    for q=1:n,
       for r=1:n,
         if q==r,
          if p==2*q,
            mmsquare(p+1)=mmsquare(p+1)+m(q+1)*m(q+1)/2;
          end
        elseif r>q,
          if p==r-q,
            mmsquare(p+1)=mmsquare(p+1)+m(r+1)*m(q+1);
          elseif p==r+q,
            mmsquare(p+1)=mmsquare(p+1)+m(r+1)*m(q+1);
          end
        end
      end
  end
end
  mmsquare;
```

- This program calculates $m_n^{(3)}$.

```
function[mmcub]=coefcalc_third(m)
w=length(m)-1;
mmsquare=coefcalc_square(m);
for s=w+2:3*w+1,
  m(s)=0;
end
for c=2*w+2:3*w+1,
  mmsquare(c)=0;
end
for l=1:3*w+1,
  mmcub(l)=0;
end
for p=1:2*w+1,
  for q=1:w+1
  mmcub((p-1)+(q-1)+1)=mmcub((p-1)+(q-1)+1)+0.5*mmsquare(p)*m(q);
  mmcub(abs(p-q)+1)=mmcub(abs(p-q)+1)+0.5*mmsquare(p)*m(q);
  end
end
mmcub;
```

- This program calculates $m_n^{(5)}$.

```
function[mmmfive]=coefcalc_fifth(m)
w=length(m)-1;
mmsquare=coefcalc_square(m);
mmcub=coefcalc_third(m);
for s=w+2:5*w+1,
   m(s)=0;
end
for c=2*w+2:5*w+1,
   mmsquare(c)=0;
end
for cc=3*w+2:5*w+1,
   mmcub(c)=0;
end
for ccc=1:5*w+1,
   mmfive(ccc)=0;
end
for p=1:2*w+1,
   for q=1:3*w+1
   mmfive((p-1)+(q-1)+1)=mmfive((p-1)+(q-1)+1)+0.5*mmsquare(p)*mmcub(q);
   mmfive(abs(p-q)+1)=mmfive(abs(p-q)+1)+0.5*mmsquare(p)*mmcub(q);
   end
end
mmmfive=mmfive;
```

- This program calculates $m_n^{(7)}$.

```
function[mmseven]=coefcalc_seventh(m)
w=length(m)-1;
mmsquare=coefcalc_square(m);
mmmfive=coefcalc_fifth1(m);
for s=w+2:7*w+1,
   m(s)=0;
end
for c=2*w+2:7*w+1,
   mmsquare(c)=0;
end
for cc=3*w+2:7*w+1,
   mmmfive(c)=0;
end
for l=1:7*w+1,
   mmseven(l)=0;
```

```
end
for p=1:2*w+1,
   for q=1:5*w+1
mmseven((p-1)+(q-1)+1)=mmseven((p-1)+(q-
1)+1)+0.5*mmsquare(p)*mmmfive(q);
mmseven(abs(p-q)+1)=mmseven(abs(p-q)+1)+0.5*mmsquare(p)*mmmfive(q);
   end
end
for q=1:3*w+1,
   mmmseven(q)=0;
   mmmseven(q)=mmseven(q);
end
mmseven=mmmseven;
```

- This program calculates $m_n^{(9)}$.

```
function[mmseven]=coefcalc_nineth(m)
w=length(m)-1;
mmsquare=coefcalc_square(m);
mmseven=coefcalc_seventh(m);
for s=w+2:9*w+1,
   m(s)=0;
end
for c=2*w+2:9*w+1,
   mmsquare(c)=0;
end
for cc=3*w+2:9*w+1,
   mmmfive(c)=0;
end
for l=1:9*w+1,
   mmseven(l)=0;
end
for p=1:2*w+1,
   for q=1:7*w+1
mmseven((p-1)+(q-1)+1)=mmseven((p-1)+(q-
1)+1)+0.5*mmsquare(p)*mmmfive(q);
mmseven(abs(p-q)+1)=mmseven(abs(p-q)+1)+0.5*mmsquare(p)*mmmfive(q);
   end
end
for q=1:3*w+1,
   mmmseven(q)=0;
   mmmseven(q)=mmseven(q);
end
mmseven=mmmseven;
```

APPENDIX C

DERIVATION OF EQUATIONS MODELING THE FEEDFORWARD SYSTEM WITH PHASE MISMATCHES

The derivation of the equations introduced in Chapter 4.1 is shown in detail.

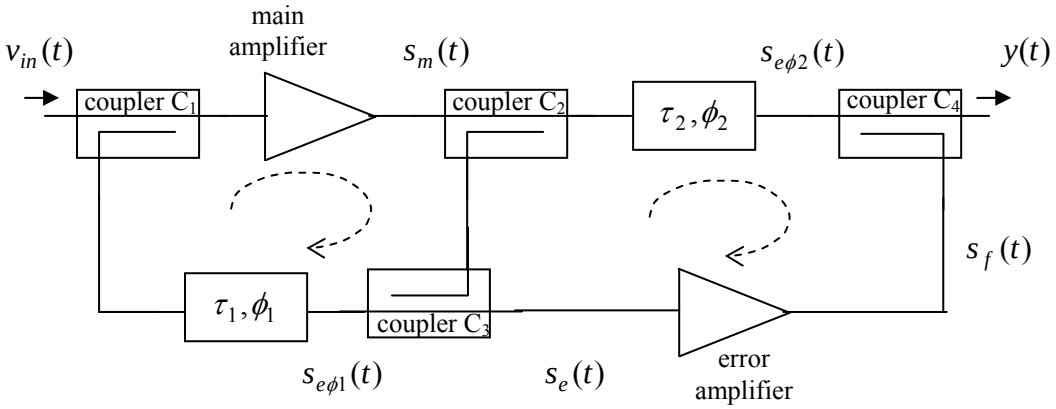

Figure C.1: A generic feedforward system. Signals at specific nodes are indicated in order to assist the following derivations.

Main and error amplifiers are assumed to be memoryless with third order nonlinearity. Their $V_{out} - V_{in}$ characteristics can be expressed as a combination of linear and nonlinear terms as follows:

$$v_{out} = a_1 v_{in} + a_3 v_{in}^3 \tag{C.1}$$

Input of the system is a multi-tone signal which can be expressed as follows:

$$v_{in}(t) = v\left[\sum_{n=1}^{p} m_n \cos(n\omega_m t)\right]\cos(\omega t) \qquad \text{(C.2)}$$

where ω_m and ω are the angular frequencies of the fundamental tone and the carrier, respectively. In this representation the tones are equi-phased, but the amplitude of each tone (m_n) is a parameter to be determined.

The output of the main amplifier is computed by inserting (C.2) into (C.1). v_{in}^3 is computed using the following equation:

$$\left[\sum_{n=1}^{p} m_n \cos(nw_m t)\right]^q = \sum_{n=0}^{pq} m_n^{(q)} \cos(nw_m t) \qquad \text{(C.3)}$$

where $m_n^{(q)}$ are the amplitude coefficients of the resulting tones. The number of input tones is p, wheras, the resultant multi-tone signal is composed of $p*q+1$ terms including the dc term. The output of the main amplifier can be expressed as follows:

$$s_m(t) = \left[\sum_{n=0}^{3p} d_n \cos(nw_m t)\right]\cos(wt) \qquad \text{(C.4)}$$

where

$$d_n = a_1 l_1 v m_n + \frac{3}{4} a_3 l_1^3 v^3 m_n^{(3)} \qquad \text{(C.5)}$$

Note that l_1 is the loss of the coupler and can be found from coupling coefficient of the coupler as follows:

$$l_i = 10 * \log(1 - 10^{-C_i/10}) \qquad \text{(C.6)}$$

The signal at the input is sampled via coupler C_1 and applied to a phase unit. The output of the phase unit in the carrier cancellation loop (labeled as τ_1, ϕ_1) can be expressed as follows:

$$s_{e\phi 1}(t) = \frac{v}{C_1}\left[\sum_{n=1}^{p} m_n \cos(nw_m t)\right]\cos(wt + \phi_1) \qquad \text{(C.7)}$$

where C_1 is the coupling coefficient of the first coupler. Note that the phase shift ϕ_1 is introduced to the carrier term.

The output of the main amplifier is sampled and subtracted from the output of the phase unit in the carrier cancellation loop to obtain the expression at the input of the error amplifier:

$$s_e(t) = \frac{s_m(t)}{C_2 C_3} - l_3 s_{e\phi 1}(t) =$$

$$\frac{1}{C_2 C_3}\left[\sum_{n=0}^{3p} d_n \cos(nw_m t)\right]\cos(wt) - \frac{l_3 v}{C_1}\left[\sum_{n=1}^{p} m_n \cos(nw_m t)\right]\cos(wt + \phi_1) =$$

$$\frac{1}{C_2 C_3}\left[\sum_{n=0}^{3p} d_n \cos(nw_m t)\right]\cos(wt) - \frac{l_3 v \cos(\phi_1)}{C_1}\left[\sum_{n=1}^{p} m_n \cos(nw_m t)\right]\cos(wt)$$

$$+ \frac{l_3 v \sin(\phi_1)}{C_1}\left[\sum_{n=1}^{p} m_n \cos(nw_m t)\right]\sin(wt) \qquad \text{(C.8)}$$

Note that the first term of the expression is composed of $p*q+1$ tones, whereas, the second term is composed of p tones yet. In order to be able to make a subtraction, two terms must have equal number of tones. Therefore, the second term is modified before subtraction by inserting zero to the position of dc term and terms between $p+1$ and $p*q+1$. The resulting expression can be written as follows:

$$s_e(t) = \frac{s_m(t)}{C_2 C_3} - l_3 s_{e\phi 1}(t) =$$

$$\left\{\left(\frac{a_1 l_1 v}{C_2 C_3} - \frac{l_3 v \cos(\phi_1)}{C_1}\right)\sum_{n=0}^{3p} m_n \cos(n w_m t) + \left(\frac{3 a_3 l_1^3 v^3}{4 C_2 C_3}\right)\sum_{n=0}^{3p} m_n^{(3)} \cos(n w_m t)\right\}\cos(wt)$$

$$+\left\{\left(\frac{l_3 v \sin(\phi_1)}{C_1}\right)\sum_{n=0}^{3p} m_n \cos(n w_m t)\right\}\sin(wt) \tag{C.9}$$

where $m_n^{(3)}$ is to be computed using equation (C.3).

This expression is simplified by defining new constants α, β and μ:

$$s_e(t) = \left[\sum_{n=0}^{3p} (\alpha m_n + \beta m_n^{(3)}) \cos(n w_m t)\right]\cos(wt) + \left[\sum_{n=0}^{3p} \mu m_n \cos(n w_m t)\right]\sin(wt) \tag{C.10}$$

where

$$\alpha = \frac{a_1 l_1 v}{C_2 C_3} - \frac{l_3 v \cos(\phi_1)}{C_1} \qquad \beta = \frac{3 a_3 l_1^3 v^3}{4 C_2 C_3} \qquad \mu = \frac{l_3 v \sin(\phi_1)}{C_1} \tag{C.11}$$

Note that the expression is still third order however, contrary to the output of the single amplifier, $s_m(t)$, it includes quadrature terms because of the phase mismatch introduced to the carrier (C.7).

The expression in (C.10) is applied to the error amplifier, which is also of third order nonlinearity. The resulting expression includes ninth order terms and can be expressed in terms of $s_e(t)$ as follows:

$$s_f(t) = b_1 s_e(t) + b_3 s_e^3(t) \tag{C.12}$$

where b_1 and b_3 are the power series coefficients defining the nonlinearity of the error amplifier. Like a_1 and a_3, they can be found from gain and IP3 of the error amplifier using equation (3.22). To simplify calculation we define:

$$M_n^{(q)} = \left[\sum_{n=1}^{p} m_n \cos(nw_m t) \right]^q = \sum_{n=0}^{pq} m_n^{(q)} \cos(nw_m t) \qquad \text{(C.13)}$$

where $q \geq 1$. Now, $s_f(t)$ can be extracted as follows:

$$s_f(t) = b_1\left(\alpha M_n + \beta M_n^{(3)}\right)\cos(wt) + b_1 \mu M_n \sin(wt) +$$

$$b_3\left[\left(\alpha M_n + \beta M_n^{(3)}\right)\cos(wt) + \mu M_n \sin(wt)\right]^3 =$$

$$b_1\left(\alpha M_n + \beta M_n^{(3)}\right)\cos(wt) + b_1 \mu M_n \sin(wt) +$$

$$\frac{3}{4} b_3\left(\alpha M_n + \beta M_n^{(3)}\right)^3 \cos(wt) + \frac{3}{4} b_3\left(\alpha M_n + \beta M_n^{(3)}\right)(\mu M_n)^2 \cos(wt) +$$

$$\frac{3}{4} b_3\left(\alpha M_n + \beta M_n^{(3)}\right)^2 (\mu M_n)\sin(wt) + \frac{3}{4} b_3 (\mu M_n)^3 \sin(wt)$$

(C.14)

After arranging terms:

$$s_f(t) = \left\{ \begin{array}{l} b_1 \alpha M_n + \left(b_1 \beta + \frac{3}{4} b_3 (\alpha^3 + \alpha \mu^2) \right) M_n^{(3)} + \\ \left(\frac{3}{4} b_3 (3\alpha^2 \beta + \beta \mu^2) \right) M_n^{(5)} + \frac{9}{4} b_3 \alpha \beta^2 M_n^{(7)} + \frac{3}{4} b_3 \beta^3 M_n^{(9)} \end{array} \right\} \cos(wt) +$$

$$\left\{ b_1 \mu M_n + \frac{3}{4} b_3 (\alpha^2 \mu + \mu^3) M_n^{(3)} + \frac{3}{2} b_3 \alpha \beta \mu M_n^{(5)} + \frac{3}{4} b_3 \beta^2 \mu M_n^{(7)} \right\} \sin(wt)$$

(C.15)

After defining new constants and expanding $M_n^{(q)}$:

$$s_f(t) = \left\{ \sum_{n=0}^{3p} (A_1 m_n + A_3 m_n^{(3)} + A_5 m_n^{(5)} + A_7 m_n^{(7)} + A_9 m_n^{(9)}) \cos(n w_m t) \right\} \cos(wt)$$

$$+ \left\{ \sum_{n=0}^{3p} (B_1 m_n + B_3 m_n^{(3)} + B_5 m_n^{(5)} + B_7 m_n^{(7)}) \cos(n w_m t) \right\} \sin(wt) \tag{C.16}$$

where

$$A_1 = b_1 \alpha \qquad B_1 = b_1 \mu$$

$$A_3 = b_1 \beta + \frac{3}{4} b_3 \left[\alpha^3 + \alpha \mu^2 \right] \qquad B_3 = \frac{3}{4} b_3 \left[\alpha^2 \mu + \mu^3 \right]$$

$$A_5 = \frac{3}{4} b_3 \left[3\alpha^2 \beta + \beta \mu^2 \right] \qquad B_5 = \frac{3}{2} b_3 \alpha \beta \mu$$

$$A_7 = \frac{9}{4} b_3 \alpha \beta^2 \qquad B_7 = \frac{3}{4} b_3 \beta^2 \mu$$

$$A_9 = \frac{3}{4} b_3 \beta^3 \tag{C.17}$$

The output of the main amplifier (C.4) is applied to a phase unit (labeled as τ_2, ϕ_2) and the following expression is obtained:

$$s_{e\phi 2}(t) = l_2 \left[\sum_{n=0}^{3p} d_n \cos(n w_m t) \right] \cos(wt + \phi_2) =$$

$$l_2 \cos(\phi_2) \left[\sum_{n=0}^{3p} d_n \cos(n w_m t) \right] \cos(wt) - l_2 \sin(\phi_2) \left[\sum_{n=0}^{3p} d_n \cos(n w_m t) \right] \sin(wt) \tag{C.18}$$

where l_2 is the loss of the second coupler. Note that the phase term ϕ_2 is introduced to the carrier term. The output of the error amplifier ($s_f(t)$) is subtracted from the

output of the second phase unit ($s_{e\phi 2}(t)$) at the coupler C_4 and the output of the feedforward system is obtained as follows:

$$y(t) = l_4 s_{e\phi 2}(t) - \frac{s_f(t)}{C_4} \tag{C.19}$$

where l_4 is the loss and C_4 is the coupling of the output coupler. Note that the expression is of ninth order.